CHAPTER IV

THE EXPERIMENTAL RESULTS AND DISCUSSION

The results of the present experiment performed to study the distribution of electron and muon components of Cosmic Ray extensive air shower (EAS) are presented in this chapter. The experiment, as mentioned earlier, was performed with NBU Air Shower array, which consisted of 21 scintillation counters and two shielded magnetic spectrographs operating in conjunction with each other.

During the performance of the present experiment over 38,000 EAS events were recorded by the array, amongst which about 36,200 events were taken for the final analysis. In all of the recorded air shower events, data carrying information about electron and muon components of the EAS were collected simultaneously. As explained in detail in Chapter III, the data collected by the array of scintillation counters and recorded in the digital form by a line printer carried the information about the density of electrons at different locations of the recorded air shower. Fitting these measured electron densities to the Hillas structure function [1] representing the distribution of electrons in an EAS the basic parameters - the shower size (Ne), the shower age (s) and the coordinates of the shower core (X_0, Y_0) characterizing each of the showers were determined by the standard method of χ^2-minimization. Similarly, the information about the muons associated with the recorded air showers regarding their energy and distributions around the shower core were obtained from the data collected by the magnetic spectrographs which recorded the trajectories of muons passing through them photographically.

The results of the measurements representing the distribution of electrons and muons for different muon energy thresholds (2.5 to 100 GeV) in EAS events of size range $\sim 10^4$ to 10^6 are presented in this chapter. Various features of muon component such as their lateral distribution, variation of their densities with size of the shower and their integral energy spectra are analyzed in detail and the results are discussed. Furthermore, from their radial distributions, the total number of muons in an EAS was calculated and the observations about their variation with shower size (Ne) and the threshold energy ($\geq E_\mu$) are presented.

Among the different other experiments being performed to study the electron and muon components of the EAS, the range of muon energy and the size of air showers being investigated in the experiments performed at Moscow State University (MSU) overlap with that of the present experiment. So, a comparative study of the measurements obtained in the present experiment with those of MSU experiments is also presented in this chapter.

Finally, the results of the present experiment are also compared with some of the theoretically calculated results obtained by different authors by simulating air shower events with Monte Carlo method assuming various models of high energy particle interaction. A brief review of different models like Scaling, Scale Breaking and the Quark Gluon String Model (QGSM), whose calculated results were taken for comparison is presented in section 2.3 of Chapter II of this thesis. The conclusions of this comparative analysis of the results of present experiment with those theoretically calculated results are presented in this chapter.

4.1 The Measurements of Size and Age Parameters of the Air Showers

The air showers recorded by the array, after determining their parameters, were grouped into nine different groups according to their sizes. The sizes of the showers ranging from 1.5 X 10^4 to 1.2 X 10^6, were grouped with an approximate width of $\Delta \log Ne=0.2$. The distribution of number of showers recorded in each of the size groups are shown in fig. 4.1 and the mean values of size for each group are shown in Table- 1. Similarly, the average age of air showers having sizes in different size groups along with their standard deviations (σ_s) are also shown in Table- 1.

The average age of the showers are seen to decrease with the size when they are grouped according to their sizes. The variation of the average age with shower size is shown in fig. 4.2(a). And, the observed distributions of shower age in each of the shower size groups are shown in fig. 4.3. It is seen from the figure that the width of the distribution decreases with the shower size. The distributions at higher size ranges are much narrower than the distributions at lower size ranges. This feature is also represented in fig. 4.2(b) which shows the observed variation of relative fluctuation of shower age (σ_s/s) with the size of showers.

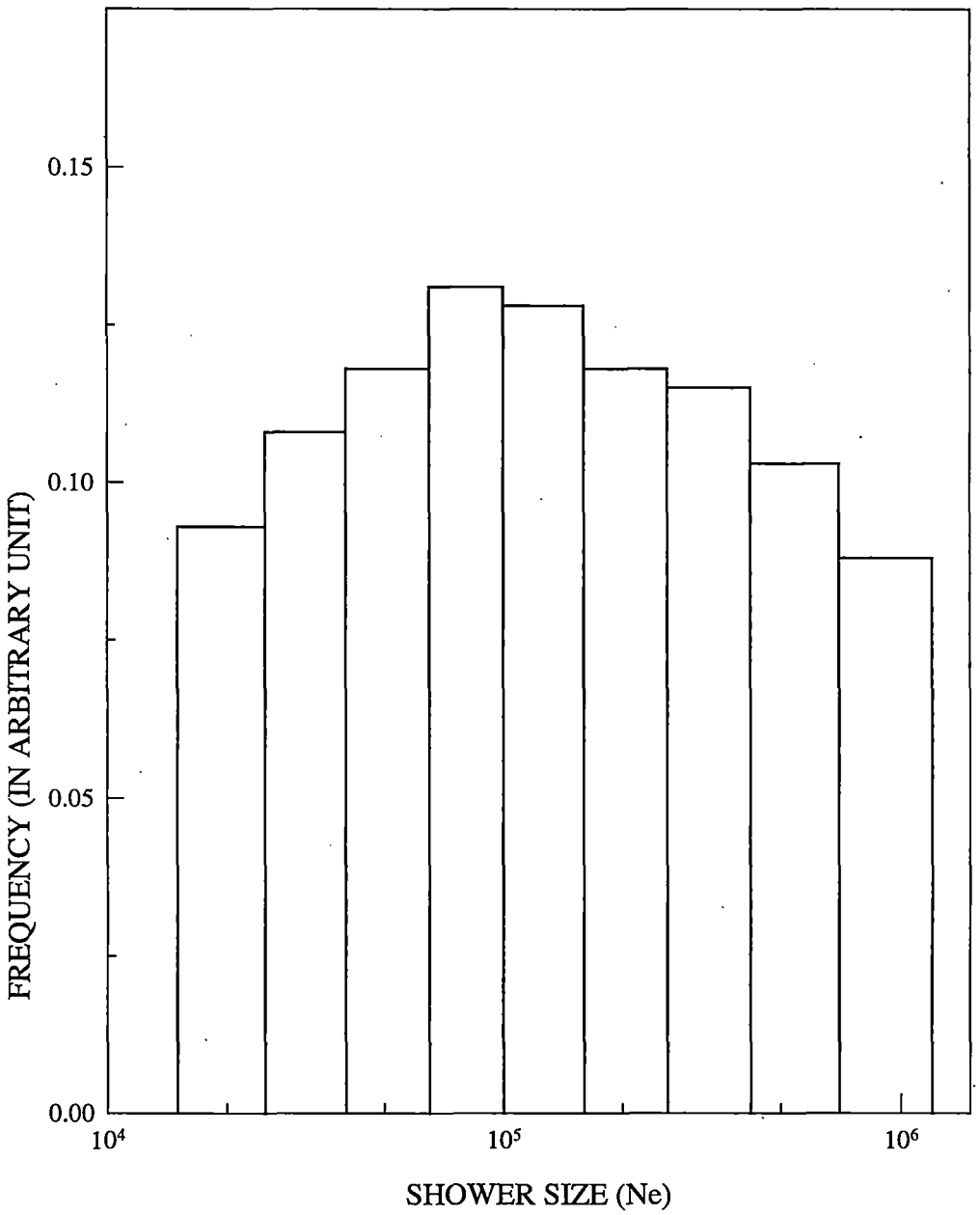

Fig. 4.1 DISTRIBUTION OF THE NUMBER OF AIR SHOWERS RECORDED IN DIFFERENT RANGES OF SHOWER SIZE

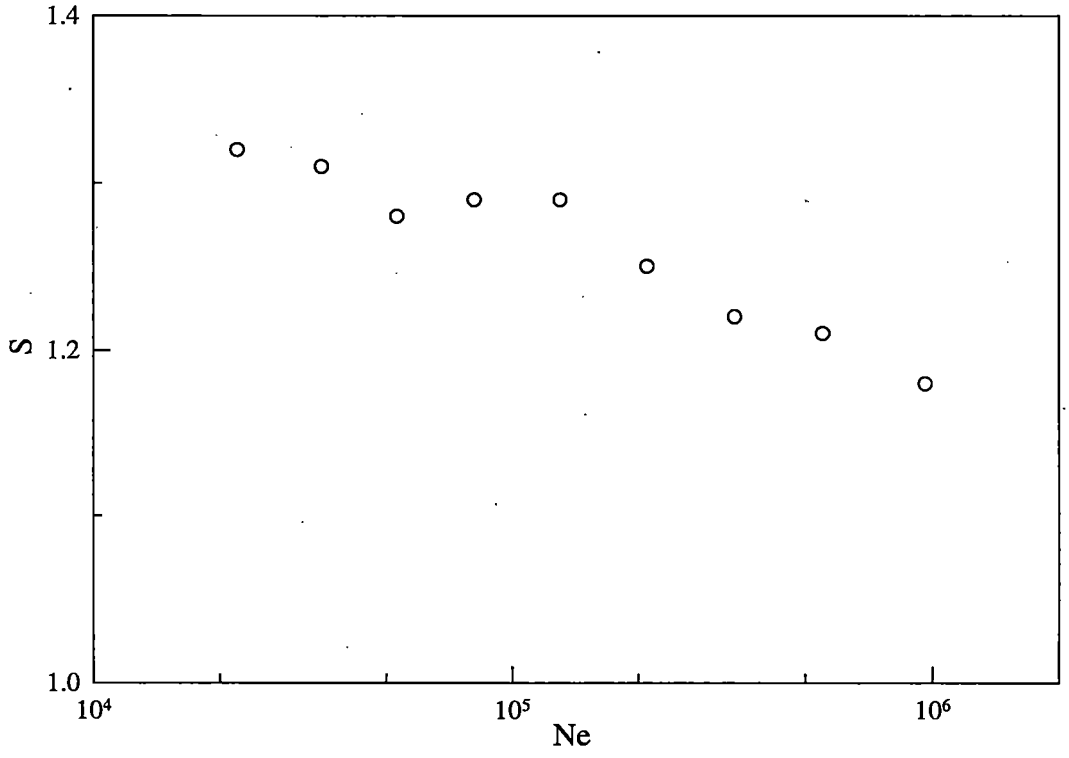

Fig. 4.2(a) THE AVERAGE AGE (S) OF THE GROUP OF AIR SHOWERS WITH AVERAGE SIZE (Ne).

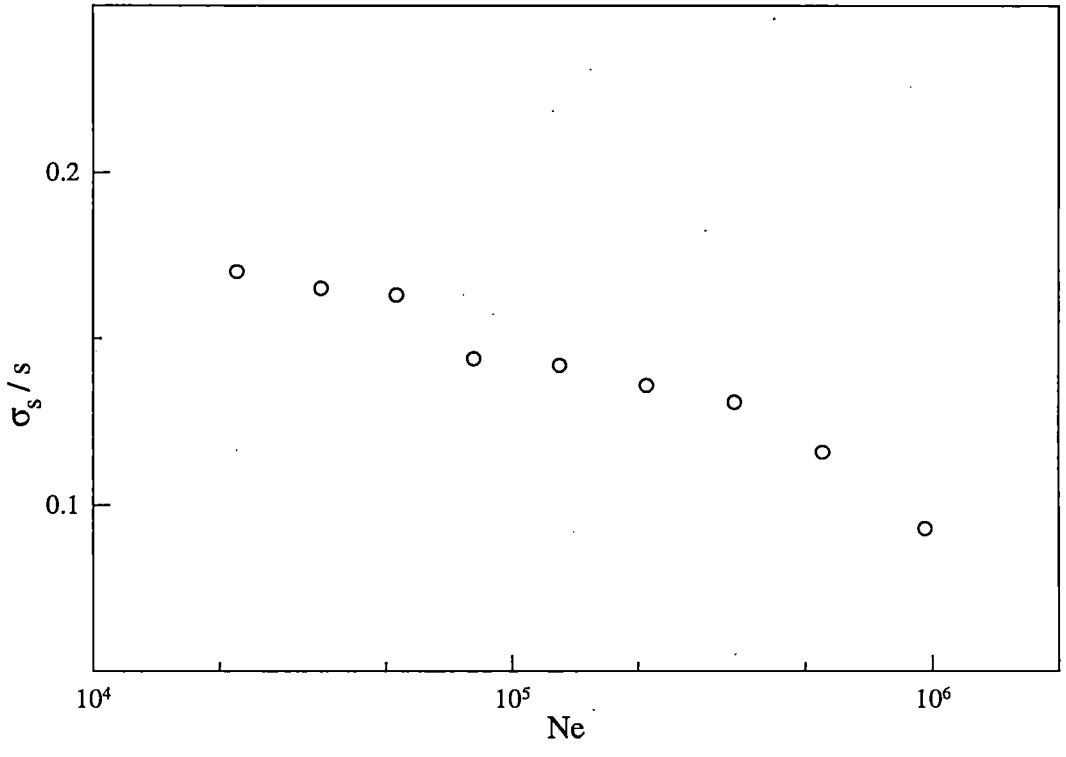

Fig. 4.2(b) THE RELATIVE FLUCTUATION OF SHOWER AGE (σ_s / s) IN THE GROUP OF AIR SHOWERS WITH AVERAGE SIZE (Ne).

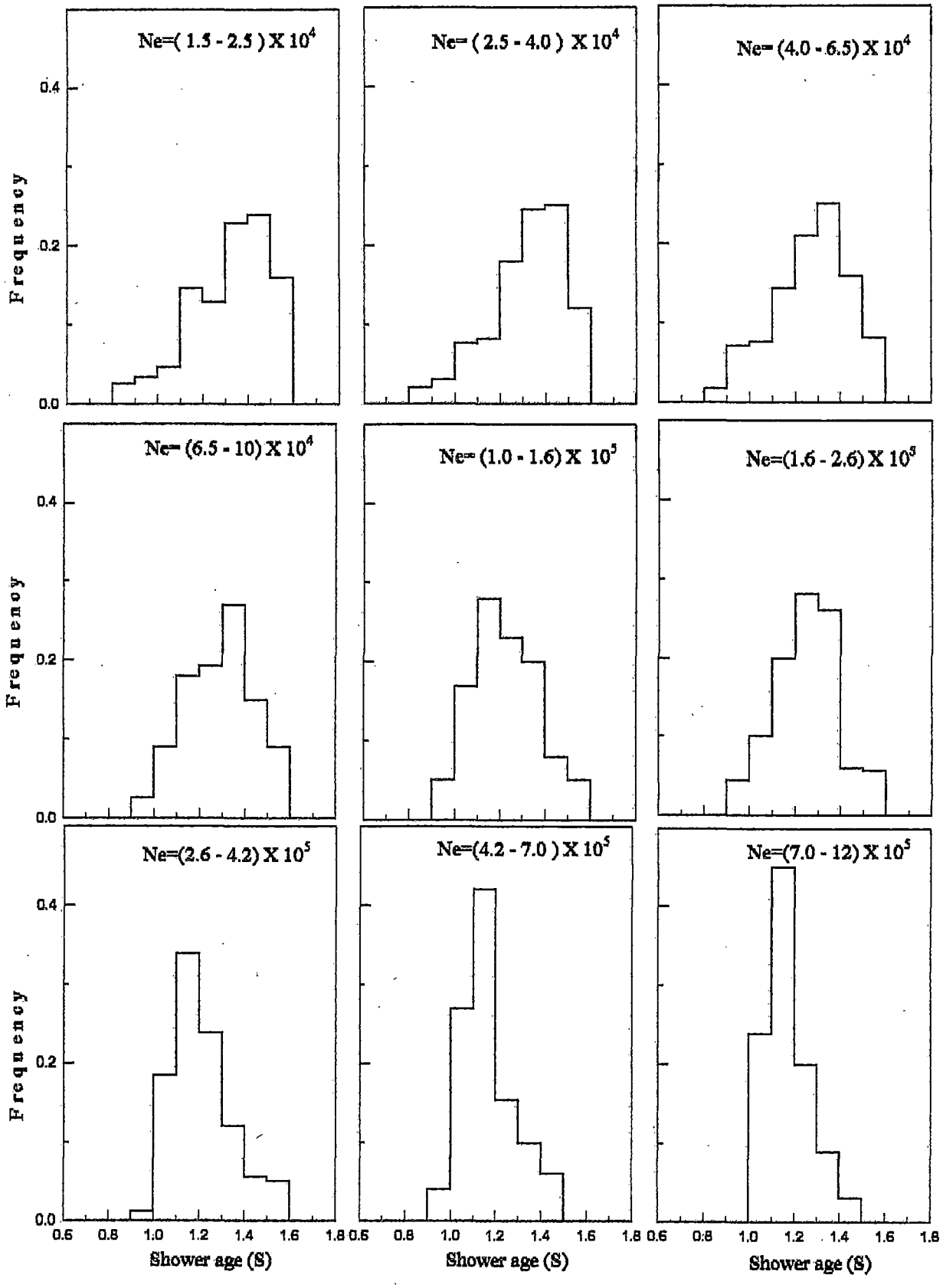

Fig. 4.3 THE DISTRIBUTION OF SHOWER AGE (S) IN DIFFERENT SHOWER SIZE GROUPS.

Table 1: The mean values of shower size and age in different size groups

Size range	Average size (Ne)	Average age (s)	σ_s
(1.5-2.5) X 10^4	2.2 X 10^4	1.32	0.22
(2.5-4.0) X 10^4	3.5 X 10^4	1.31	0.21
(4.0-6.5) X 10^4	5.3 X 10^4	1.28	0.20
(6.5-10) X 10^4	8.1 X 10^4	1.29	0.18
(1.0-1.6) X 10^5	1.3 X 10^5	1.29	0.18
(1.6-2.6) X 10^5	2.1 X 10^5	1.25	0.17
(2.6-4.2) X 10^5	3.4 X 10^5	1.22	0.16
(4.2-7.0) X 10^5	5.5 X 10^5	1.21	0.14
(7.0-12) X 10^5	9.6 X 10^5	1.18	0.11

4.2 The Measurements of Electron Densities and their Distribution in EAS

The densities of electrons at different radial points of an incident shower front were measured by the scintillation counters, each of which was calibrated for single particle pulse height. The observed densities were then corrected to take account of the transition effect in the scintillator and its covering, with the relation suggested by Asakimori et al.[2] as $\Delta_c=\Delta_o(1.192 - 0.136 \log r)$, where Δ_c and Δ_o are the corrected and observed densities respectively and r is the distance of the detector from shower core.

The distributions of these corrected densities of electrons as functions of distances from the shower core representing the 'lateral distribution of electrons' in EAS of different size groups are shown in fig. 4.4(a) to 4.4(d). The errors indicated in the figure are purely statistical. The calculated results from two different theoretically proposed structure functions viz. the NKG [3] and Hillas [1] structure functions are also shown in the figures. It can be observed from these figures that the experimentally measured electron distributions are in fairly good agreement with that calculated with Hillas function in comparison to that of NKG function up to the distances of 20-25m from the shower core.

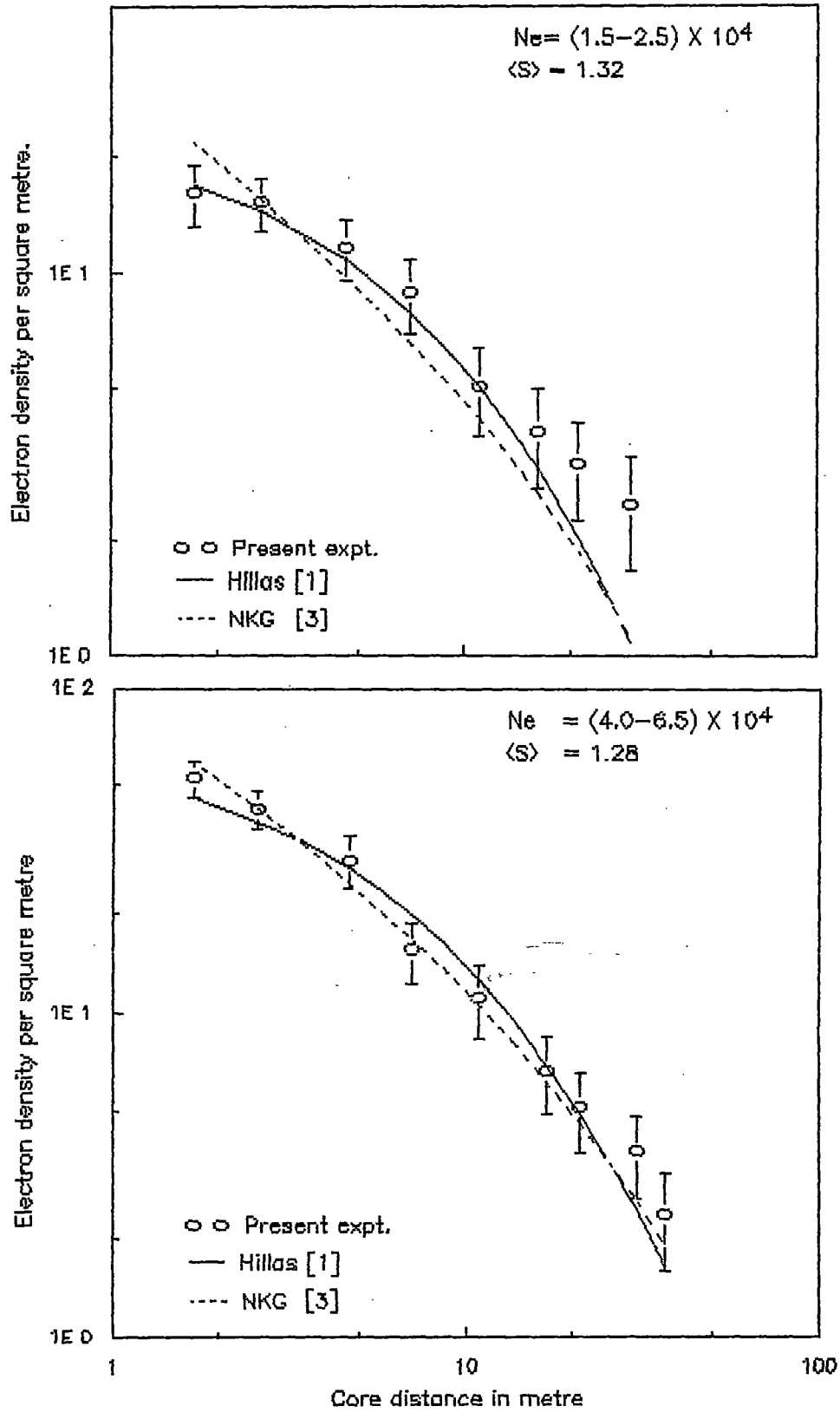

Fig. 4.4(a) THE LATERAL DISTRIBUTION OF ELECTRONS IN EAS WITH SIZES IN TWO DIFFERENT RANGES.

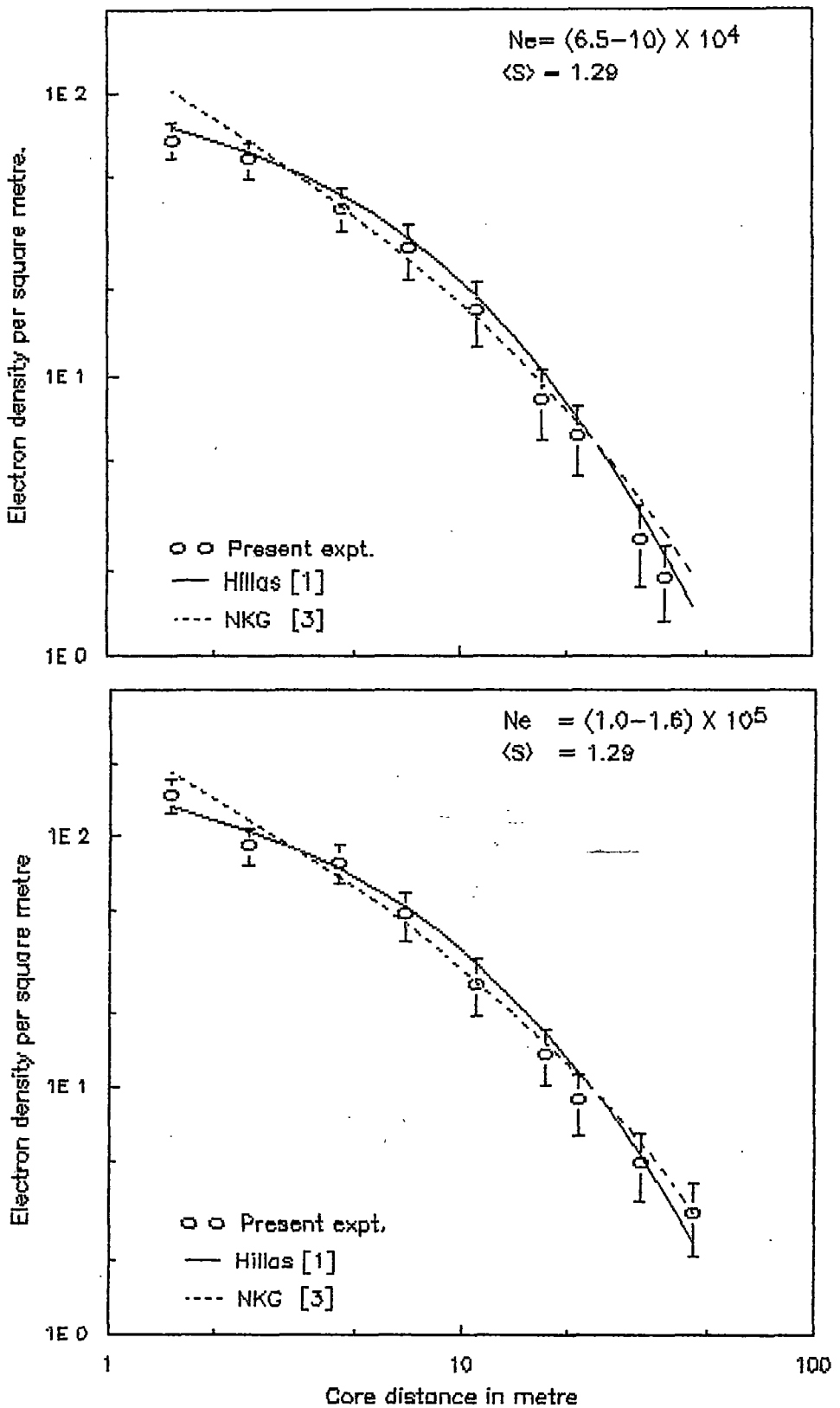

Fig. 4.4(b) THE LATERAL DISTRIBUTION OF ELECTRONS IN EAS WITH SIZES IN TWO DIFFERENT RANGES.

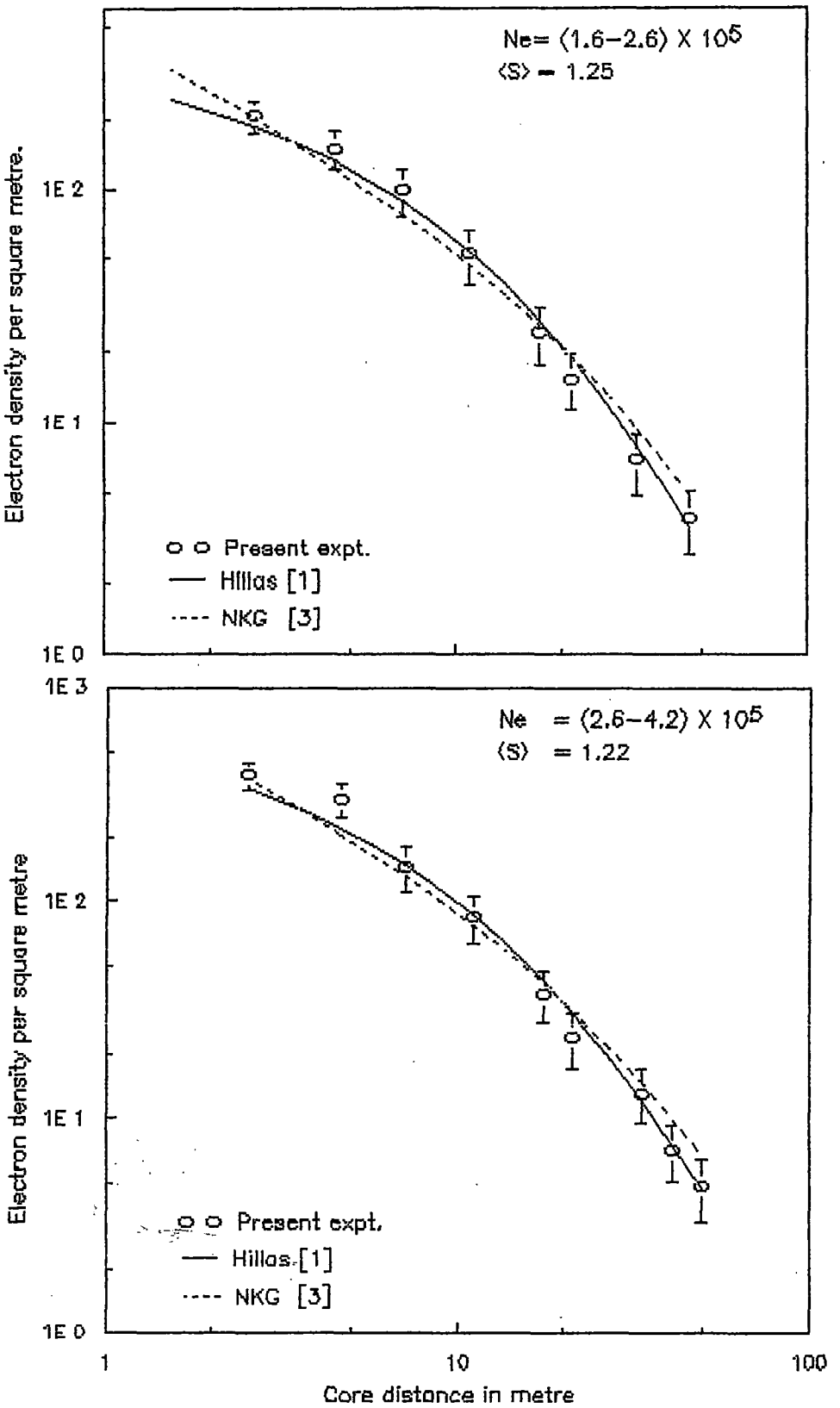

Fig. 4.4(c) THE LATERAL DISTRIBUTION OF ELECTRONS IN EAS WITH SIZES IN TWO DIFFERENT RANGES.

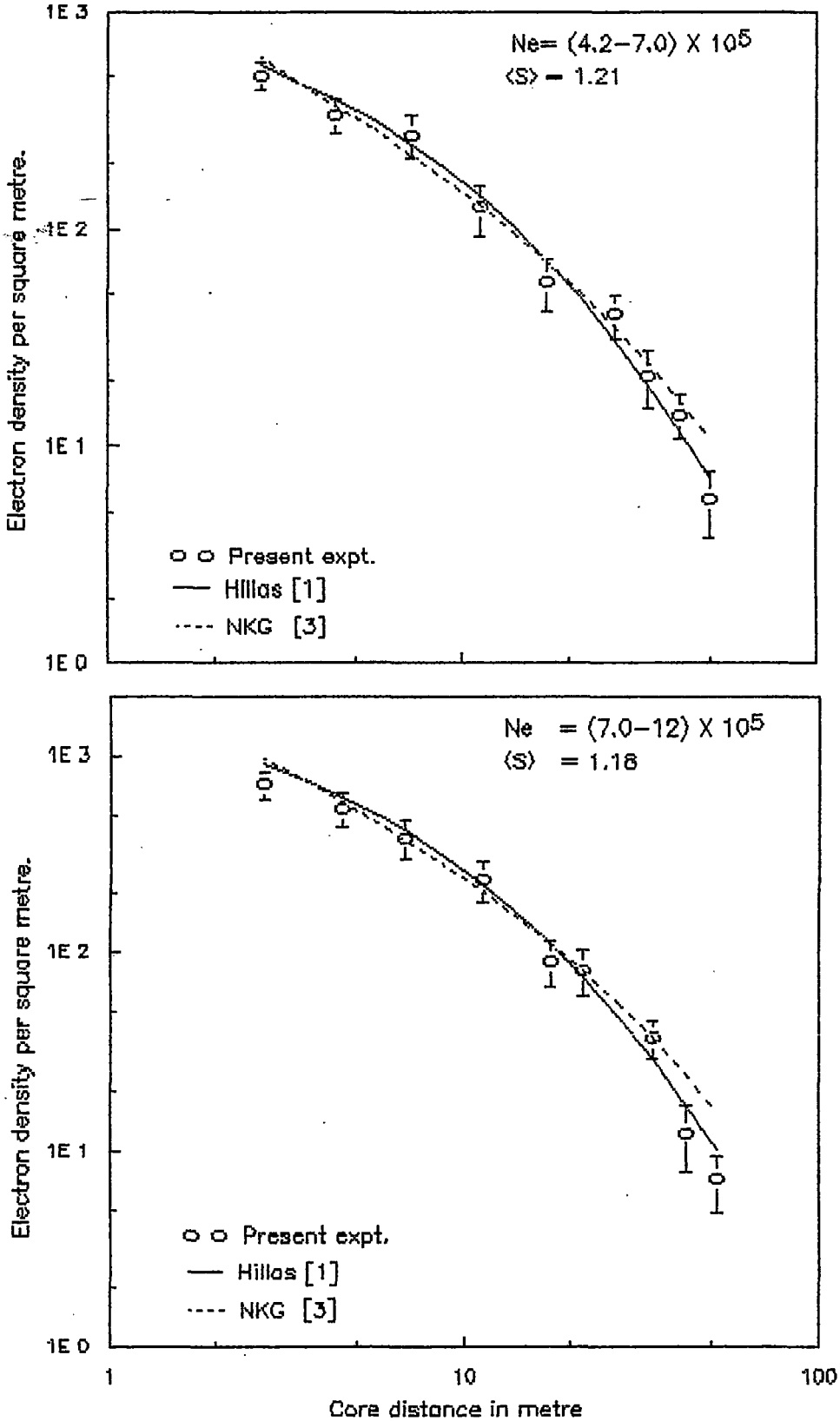

Fig. 4.4(d) THE LATERAL DISTRIBUTION OF ELECTRONS IN EAS WITH SIZES IN TWO DIFFERENT RANGES.

4.3 THE MEASUREMENTS OF MUON DENSITIES AND THEIR DISTRIBUTIONS IN EAS

The muons, associated with the air showers recorded by the array, were detected and their energies were measured by the two magnetic spectrographs each having two limbs or regions of constant magnetic field. The density $\rho_\mu(\geq E_\mu, Ne, r)$ of the muons having energy $\geq E_\mu$ at a distance 'r' from the core of the air shower of size Ne was calculated with a purely statistical consideration. If N(Ne, r) be the total number of recorded showers having average size Ne and their core at a distance of 'r' from the muon detector and n_μ ($\geq E_\mu$,Ne, r) be the number of muons with energy $\geq E_\mu$ detected within those showers by the magnetic spectrographs with effective area A_μ, then the density of muons at that distance 'r' from the core of the shower of average size Ne is given by ,

$$\rho_\mu(\geq E_\mu, Ne, r) = \frac{n_\mu (\geq E\mu, Ne, r)}{N(Ne,r) \times A_\mu} \quad \ldots \quad \ldots \quad \ldots \quad (4.1)$$

Dividing the radial distance (0-50m) from the shower core, within which the muons were detected, into 9 different smaller annular regions or bins with an approximate width of $\Delta \log r = 0.1$ the density $\rho_\mu(\geq E_\mu, Ne, r)$ of muons at different radial distances were calculated by the relation 4.1. Then, the variation of $\rho_\mu(\geq E_\mu, Ne, r)$ with radial distance r from the core, the shower size Ne and the threshold energy E_μ were studied. The muon energy thresholds considered were 2.5, 10, 20, 50 and 100 GeV where the lowest energy 2.5 GeV was the minimum cut off energy of muons for the magnetic spectrographs of NBU air shower array.

4.3.1 THE LATERAL DISTRIBUTION OF MUONS IN EAS

The measured muon densities $\rho_\mu(\geq E_\mu, Ne, r)$ at different distances 'r' from the core of the shower representing the lateral distribution of muons are shown in fig. 4.5(a) to (f) & fig 4.6(a) to (d). The errors indicated in the figure are purely statistical. The measured lateral distributions of muons are presented in two different ways. Fig. 4.5(a) to (f) show the lateral distribution of muons for different muon energy thresholds in EAS having sizes within a particular range, whose average value is indicated in the figure. Similarly, fig. 4.6(a) to (d) show the lateral distribution of

muons in EAS of different sizes for one particular muon energy threshold.

In the present experiment, the measured densities of muons were fitted to a function of the core distance 'r' of the form,

$$\rho_\mu(\geq E_\mu, Ne, r) \sim r^{-\beta(E\mu,Ne)} \exp\left[-\frac{r}{r_o(Ne)}\right] \quad \ldots \quad \ldots \quad (4.2)$$

The parameter r_o was taken as constant for individual group of shower size. The best-fitted curves are shown as smooth lines in the figures showing lateral distributions of muons and the values of exponent '$\beta(E_\mu,Ne)$' obtained for the best fits are presented in Table- 2(a).

Table 2(a): The values of $\beta(E\mu,Ne)$ and $r_o(Ne)$ for different shower sizes and threshold energies of muons

Shower size (Ne)	r_o	$\geq E_\mu$ **(GeV)**	β
2.2×10^4	79	2.5	0.28 ± 0.02
		10	0.45 ± 0.02
		20	0.66 ± 0.03
		50	0.95 ± 0.06
		100	1.35 ± 0.10
3.5×10^4	78	2.5	0.35 ± 0.02
		10	0.51 ± 0.02
		20	0.76 ± 0.04
		50	0.96 ± 0.08
		100	1.35 ± 0.12
5.3×10^4	76	2.5	0.35 ± 0.03
		10	0.49 ± 0.03
		20	0.52 ± 0.05
		50	0.76 ± 0.07
		100	1.34 ± 0.12
8.1×10^4	75	2.5	0.30 ± 0.03
		10	0.51 ± 0.03
		20	0.61 ± 0.05
		50	0.84 ± 0.05
		100	1.31 ± 0.11

Contd.....

Shower size (Ne)	r_0	$\geq E_\mu$ (GeV)	β
1.3×10^5	73	2.5	0.30 ± 0.02
		10	0.52 ± 0.03
		20	0.69 ± 0.06
		50	1.18 ± 0.07
		100	1.68 ± 0.12
2.1×10^5	71	2.5	0.36 ± 0.02
		10	0.50 ± 0.04
		20	0.74 ± 0.04
		50	0.98 ± 0.07
		100	1.48 ± 0.10
3.4×10^5	70	2.5	0.31 ± 0.02
		10	0.54 ± 0.03
		20	0.73 ± 0.04
		50	1.03 ± 0.08
		100	1.41 ± 0.11
5.5×10^5	68	2.5	0.34 ± 0.03
		10	0.58 ± 0.04
		20	0.73 ± 0.06
		50	1.13 ± 0.07
		100	1.45 ± 0.10
9.6×10^5	66	2.5	0.34 ± 0.02
		10	0.53 ± 0.03
		20	0.71 ± 0.05
		50	1.09 ± 0.08
		100	1.43 ± 0.12

It is seen from the table that the exponent $\beta(E_\mu, Ne)$ changes very slowly with shower size (Ne) but increases significantly with the threshold energy of muons ($\geq E_\mu$). This feature is also exhibited in the figures showing lateral distribution of muons. The distributions in EAS with sizes in a fixed range, fig.4.5 (a) to (f), are seen to become steeper with the increase of threshold energy but the shapes of distributions for a fixed muon energy threshold, fig. 4.6 (a) to (d), are seen to be almost similar in EAS of different sizes.

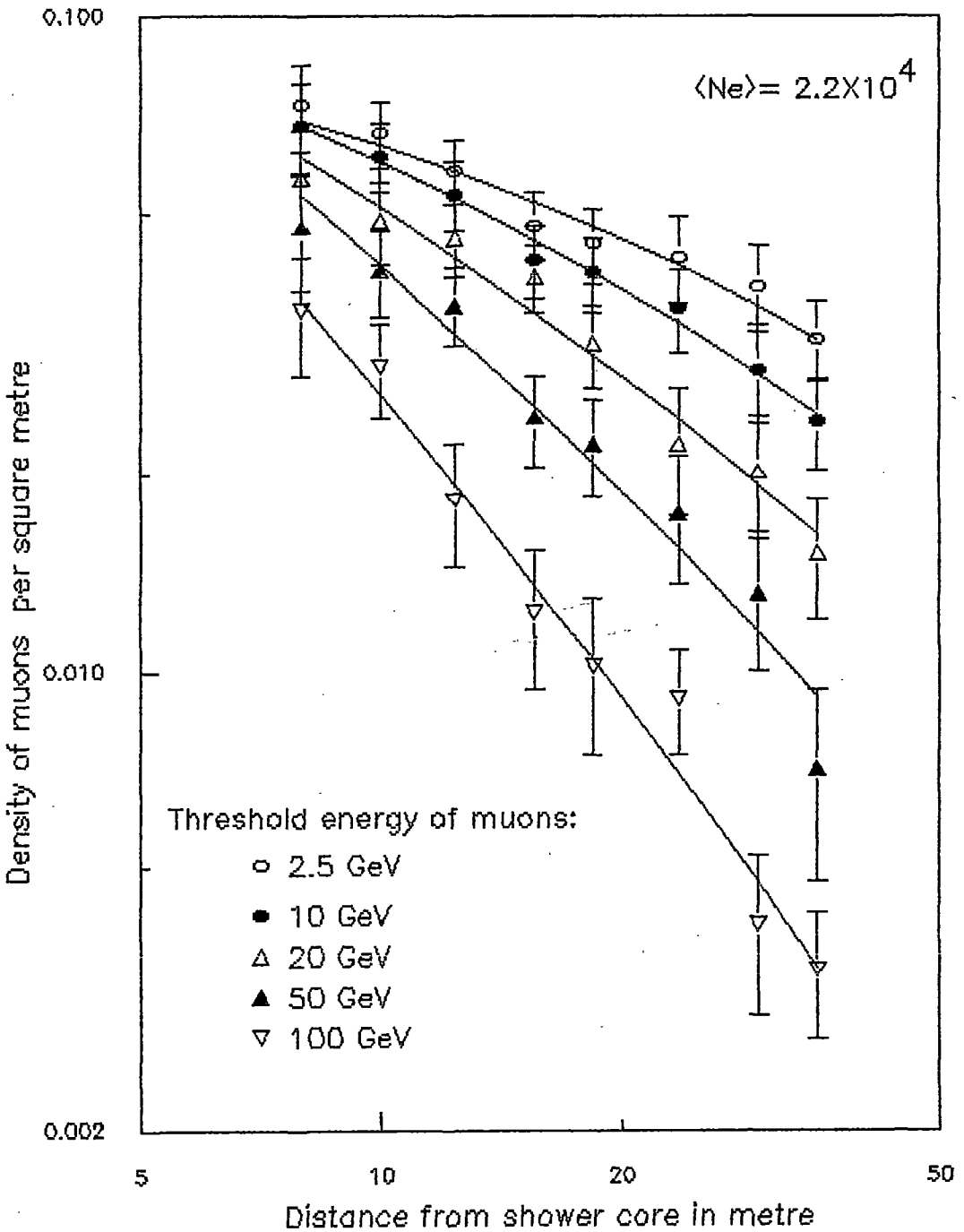

Fig. 4.5(a) LATERAL DISTRIBUTION OF MUONS IN EAS OF SIZES IN THE RANGE (1.5 – 2.5) X 10^4 PARTICLES.

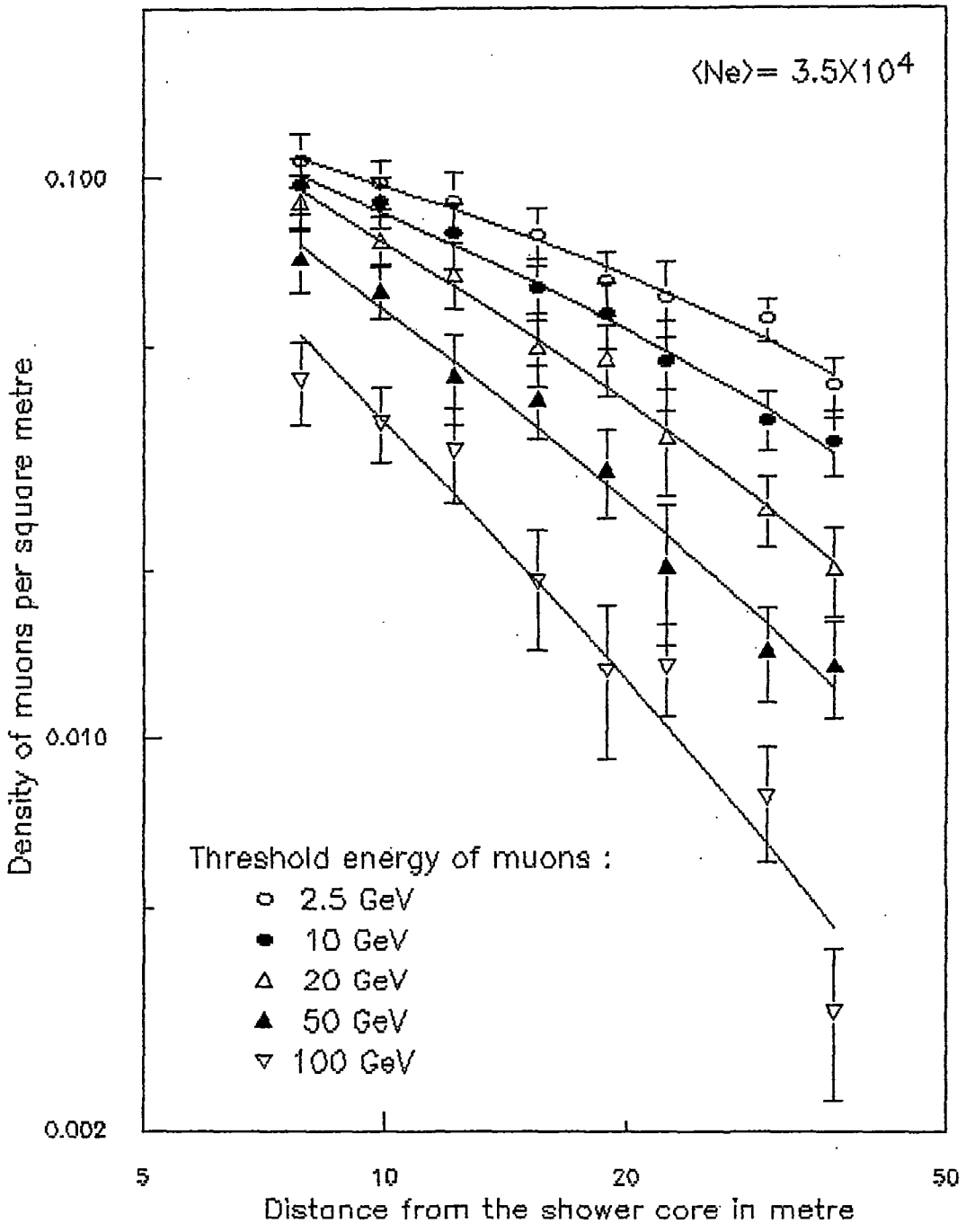

Fig. 4.5(b) LATERAL DISTRIBUTION OF MUONS IN EAS OF SIZE IN THE RANGE (2.5 – 4.0) X 10^4 PARTICLES.

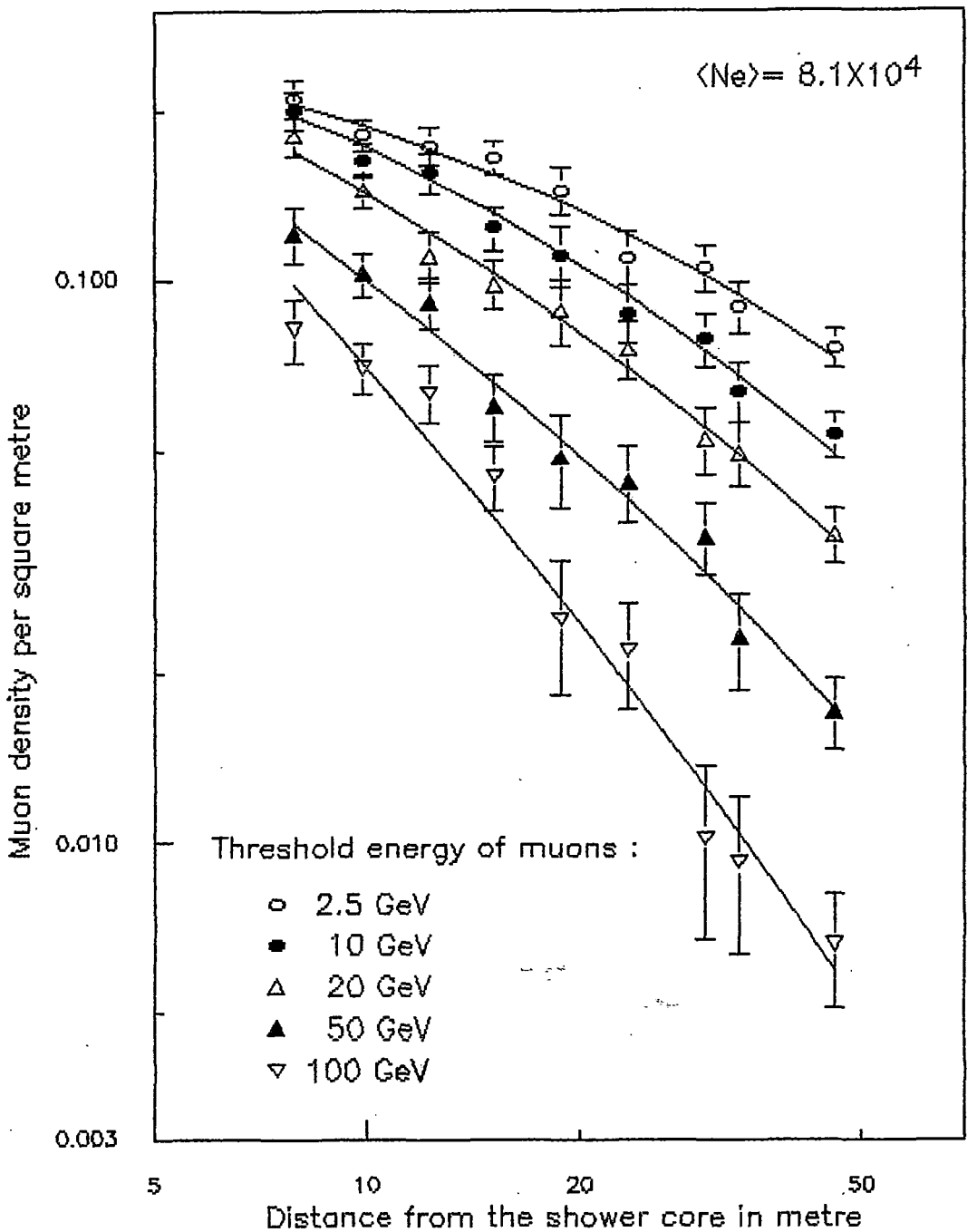

Fig. 4.5(c) LATERAL DISTRIBUTION OF MUONS IN EAS OF SIZES IN THE RANGE (6.5 – 10) X 10^4 PARTICLES

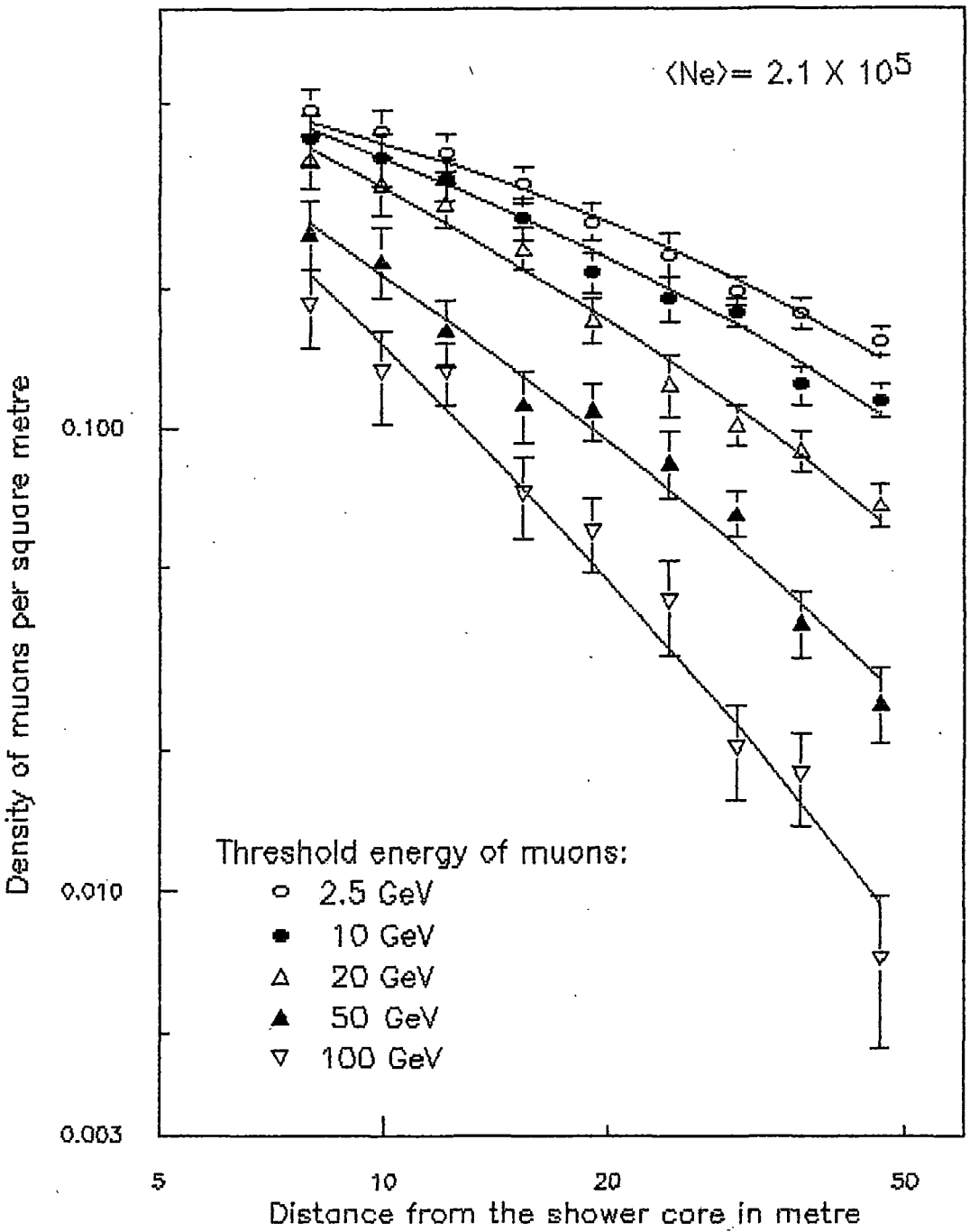

Fig. 4.5(d) LATERAL DISTRIBUTION OF MUONS IN EAS OF SIZES IN THE RANGE (1.6 – 2.6) X 10^5 PARTICLES.

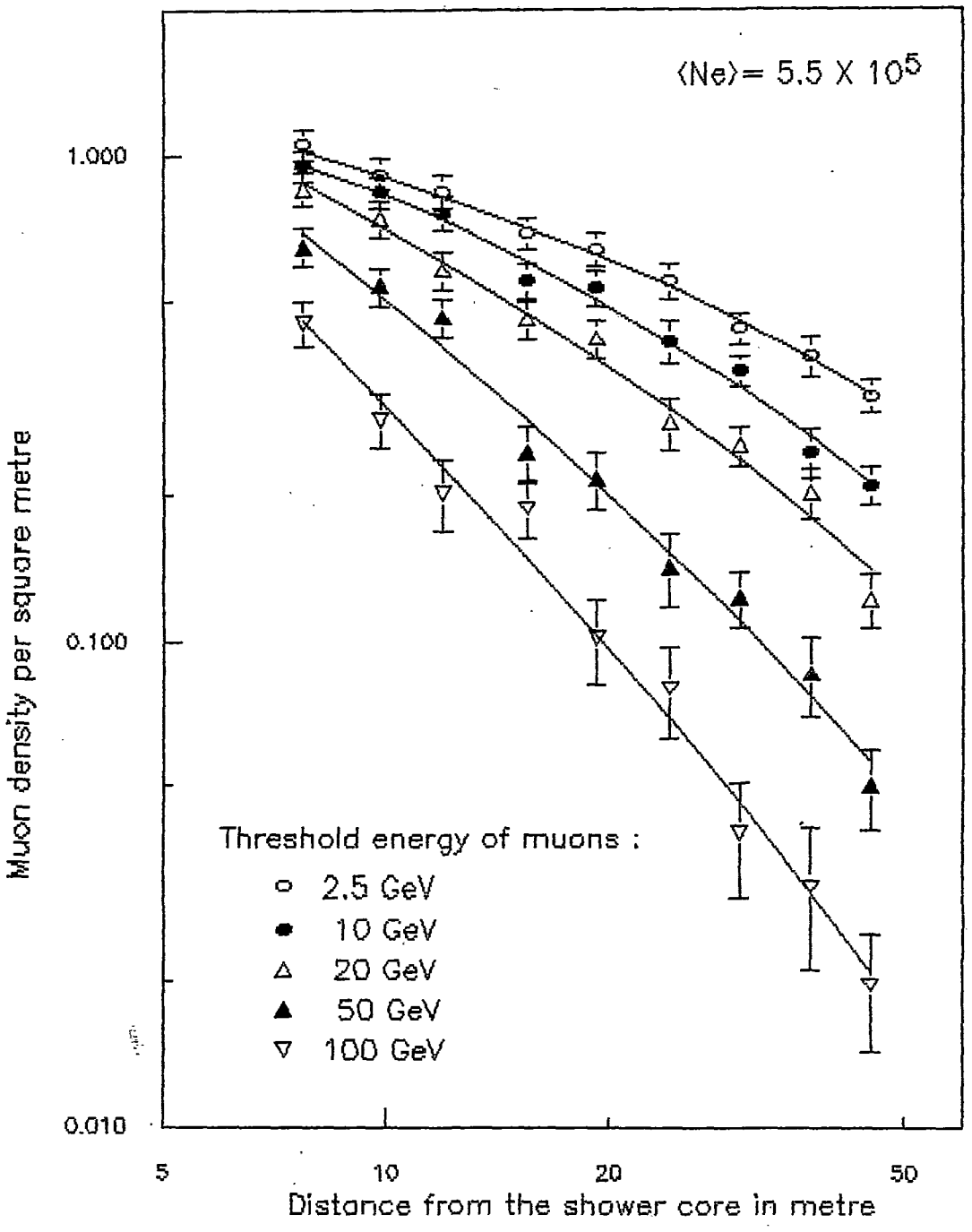

Fig. 4.5(e) LATERAL DISTRIBUTION OF MUONS IN EAS OF SIZES IN THE RANGE (4.2 – 7.0) X 10^5 PARTICLES.

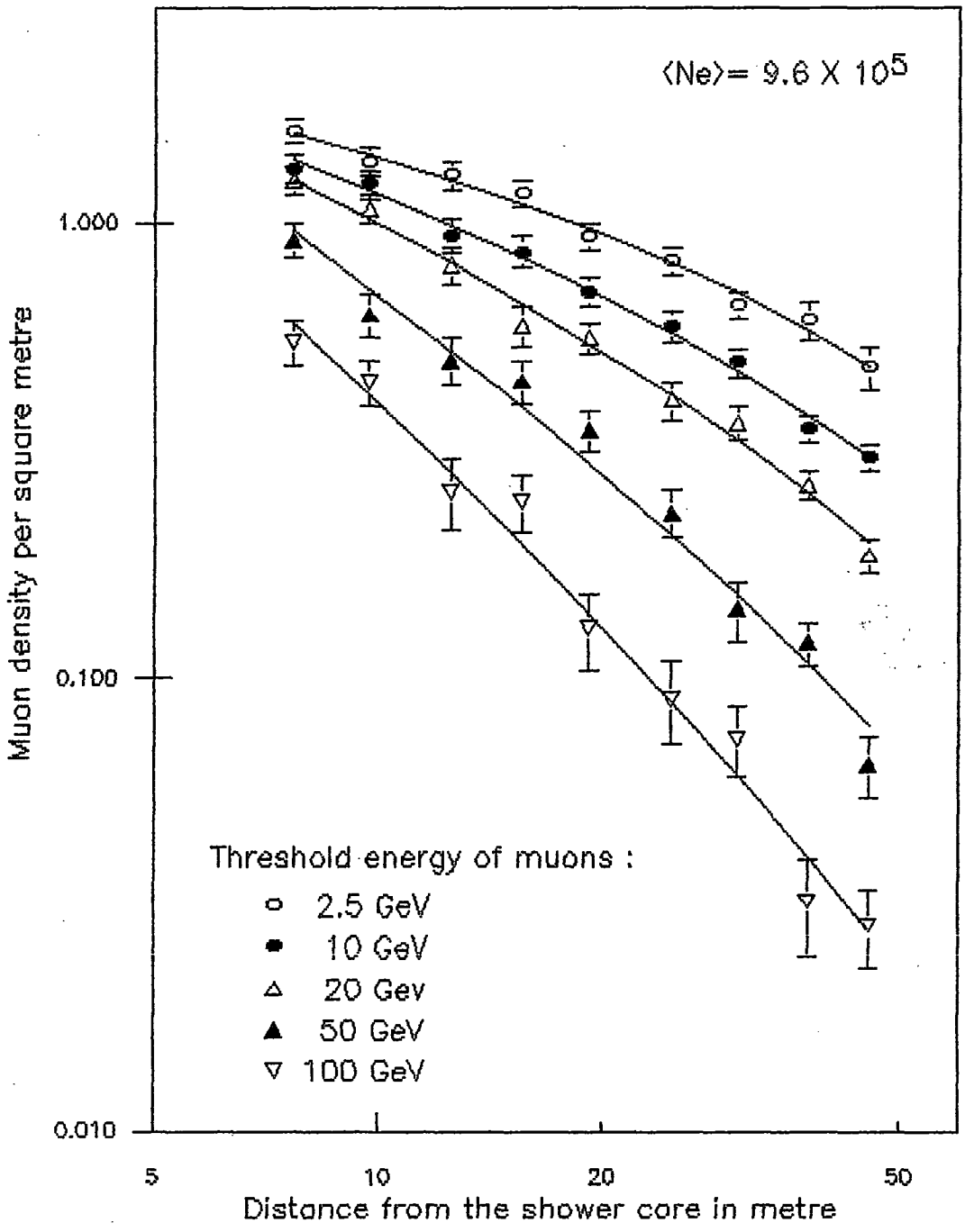

Fig. 4.5(f) LATERAL DISTRIBUTION OF MUONS IN EAS OF SIZES IN THE RANGE (7.0 – 12) X 10^5 PARTICLES.

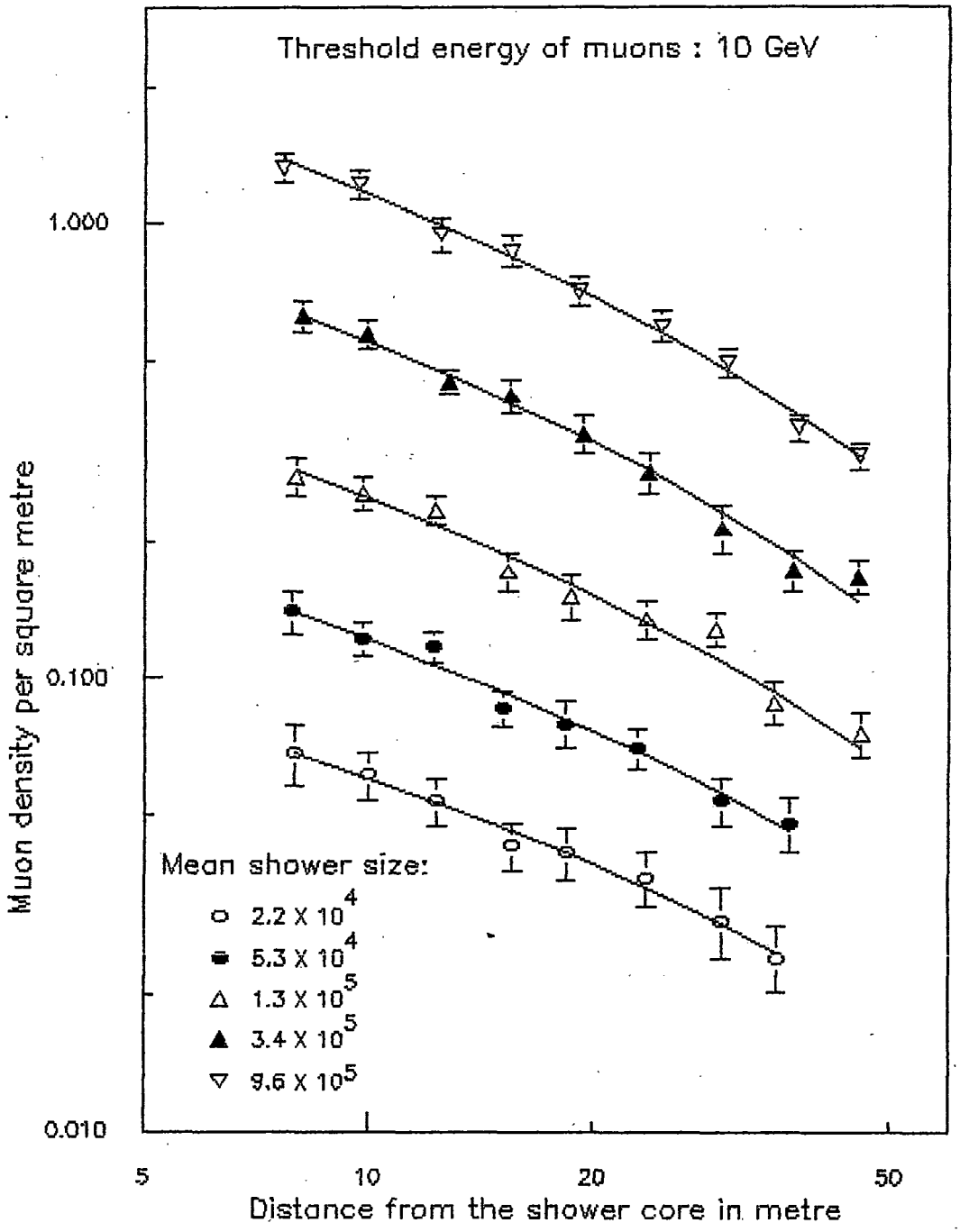

Fig. 4.6(a) LATERAL DISTRIBUTION OF MUONS IN EAS OF DIFFERENT SIZES.

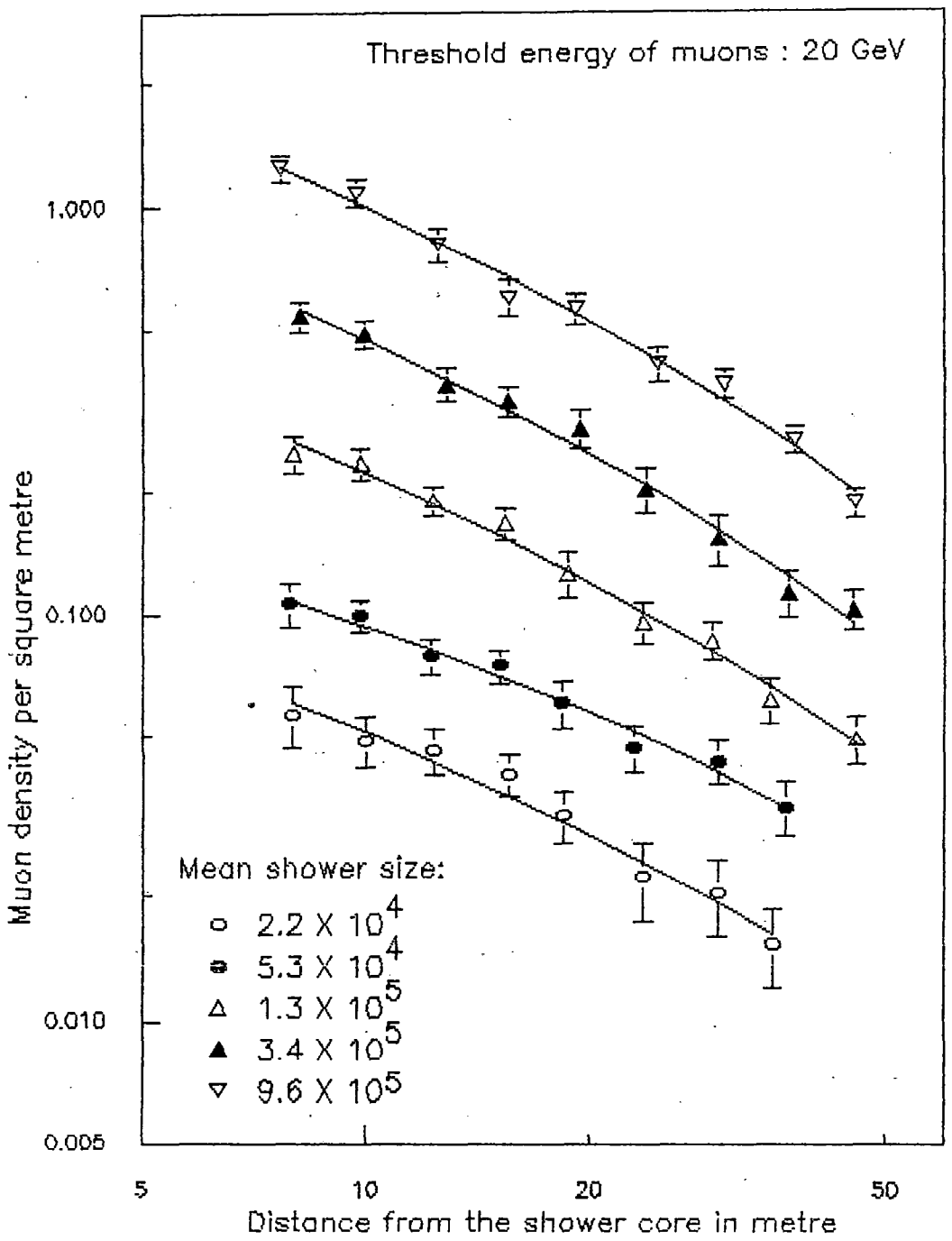

Fig. 4.6(b) LATERAL DISTRIBUTION OF MUONS IN EAS OF DIFFERENT SIZES.

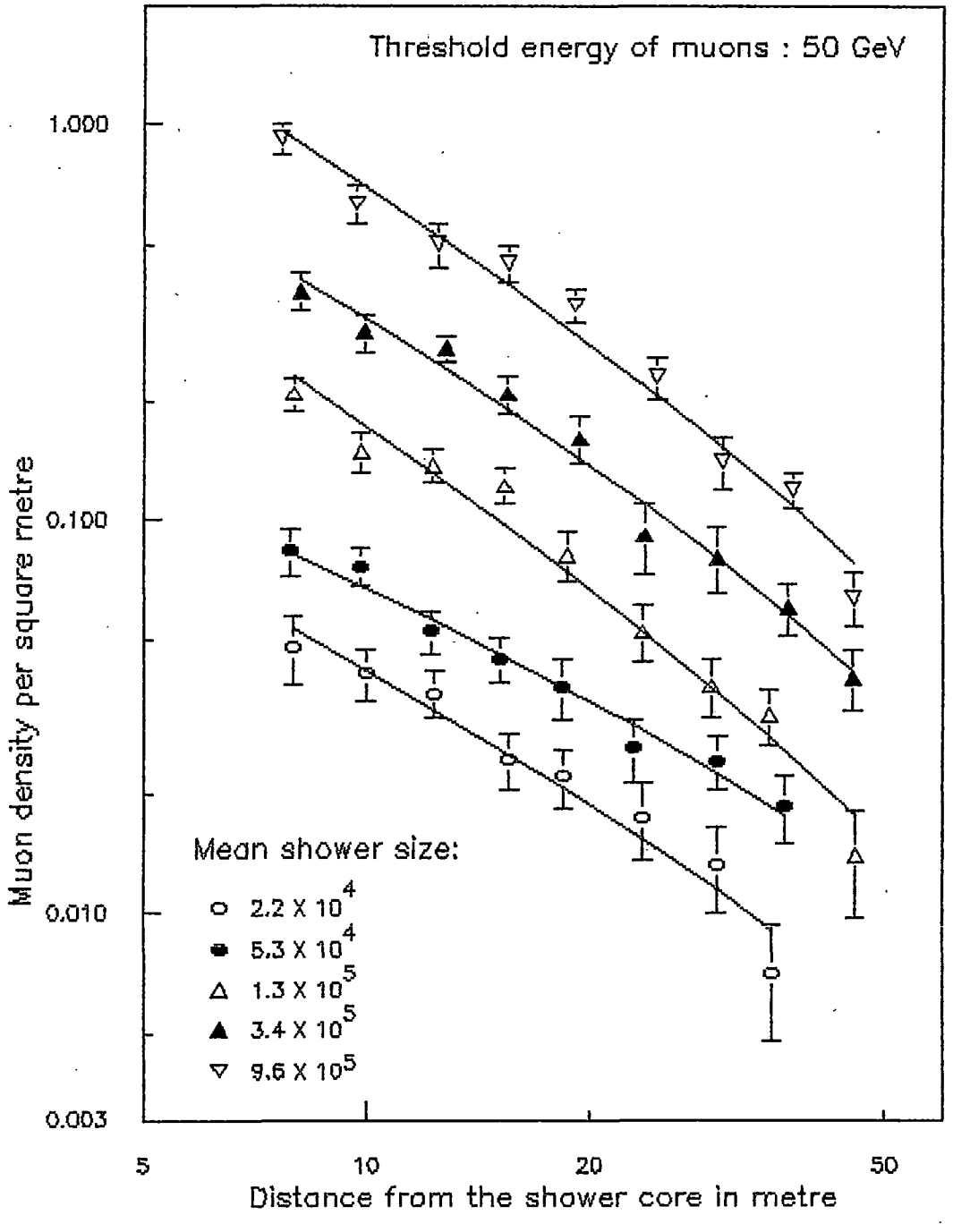

Fig. 4.6(c) LATERAL DISTRIBUTION OF MUONS IN EAS OF DIFFERENT SIZES.

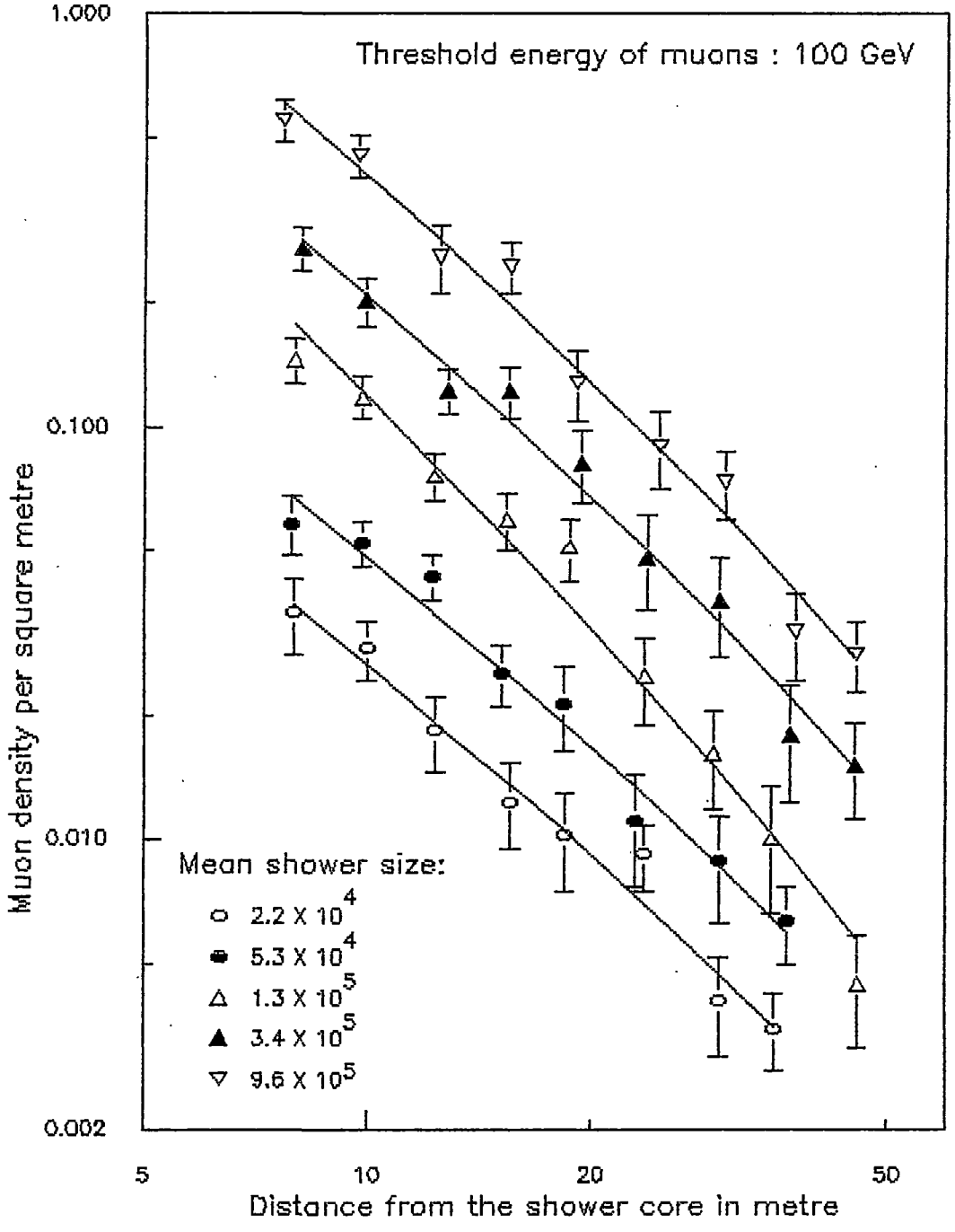

Fig. 4.6(d) LATERAL DISTRIBUTION OF MUONS IN EAS OF DIFFERENT SIZES.

However, if wider ranges of shower size are considered then the average value of 'β' is seen to increase slightly with the increase of shower size. The values of exponent 'β' calculated for two wider ranges of size (Ne) – 2 X 10^4 to 10^5 and 10^5 to 10^6 are shown in Table- 2(b). It is also noticeable from the table that the increment in the values of 'β' enhances with the increase of muon energy thresholds. At the lowest energy threshold $E_\mu \geq$ 2.5 GeV the increment is only by ~3% which rises to almost 11% at $E_\mu \geq$ 100GeV

Table 2(b): The values of exponent $\beta(E_\mu, Ne)$ for wider ranges of shower size

$\geq E_\mu$ (GeV)	Ne= 2X10^4 – 10^5	Ne= 10^5 - 10^6
2.5	0.32±0.03	0.33±0.03
10	0.49±0.03	0.53±0.04
20	0.64±0.04	0.72±0.05
50	0.88±0.06	1.08±0.07
100	1.34±0.11	1.49±0.11

4.3.2 Variation of Muon Density with Size of the EAS

To study the dependence of muon density on size of the shower the average values of densities measured at three different ranges of distances from the shower core were plotted against the shower size. The fig. 4.7 (a) to 4.7 (e) show variation of densities of muons having energies above a particular threshold energy with shower size at different radial distance ranges from the shower core. Similarly, fig. 4.8(a) to 4.8(c) represent the same variations for different muon energy thresholds measured in a fixed range of radial distances from the shower core. The experimental measurements were fitted to a relation of the power form written as

$$\rho_\mu(\geq E_\mu, r) \sim Ne^{\alpha(E_\mu, r)} \quad \cdots \quad \cdots \quad \cdots \quad (4.3)$$

The smooth lines in the figures represent the best fitted lines and the values of power exponent $\alpha(E_\mu, r)$ for different threshold energies of muons and distance ranges are shown in Table- 3.

Table 3: Values of exponent $\alpha(E_\mu,r)$ for different threshold energy of muons and radial distance ranges from the shower core

$\geq E_\mu$ (GeV)	r =5-10 m	r =10-20 m	r =20-40 m
2.5	0.82±0.03	0.82±0.04	0.76±0.03
10	0.82±0.02	0.82±0.03	0.77±0.05
20	0.82±0.03	0.78±0.05	0.78±0.05
50	0.81±0.06	0.76±0.09	0.71±0.07
100	0.80±0.06	0.81±0.06	0.73±0.09

The table shows that the value of the exponent $\alpha(E_\mu, r)$ is a slowly decreasing function of the radial distance from the core but for a particular radial distance range it remains almost constant within the energy range of 2.5-100 GeV. The average vlaues of 'α' are found to be 0.81±0.04, 0.79±0.06 and 0.75±0.06 for three radial distance ranges (5-10)m, (10-20)m and (20-40)m respectively.

4.3.3 The Integral Energy Spectra of Muons in EAS

The integral energy spectra of muons in EAS measured in the present experiment are shown in fig. 4.9 & 4.10. The fig. 4.9 (a) to (c) show the spectra in EAS of different sizes measured at a particular range of distances from the shower core. And, the fig. 4.10(a) & (b) show the spectra in the EAS of a fixed size measured at different ranges of radial distances from the core.

It can be observed from the figure 4.9(a) to (c) that the shapes of the energy spectra do not change much for air showers of different sizes indicating weak dependence of the spectra on the size of the shower. However, in EAS of fixed size the spectra are seen to become steeper with the increase of distance from the shower core.

4.4 The Measurements of Total Number of Muons in EAS

Considering the circular symmetry of air showers, the total number of muons in a particular air shower event can be estimated from the observed radial distribution of muons. If $\rho_\mu(\geq E_\mu, Ne, r)$ be the density of muons , as defined earlier, having energy

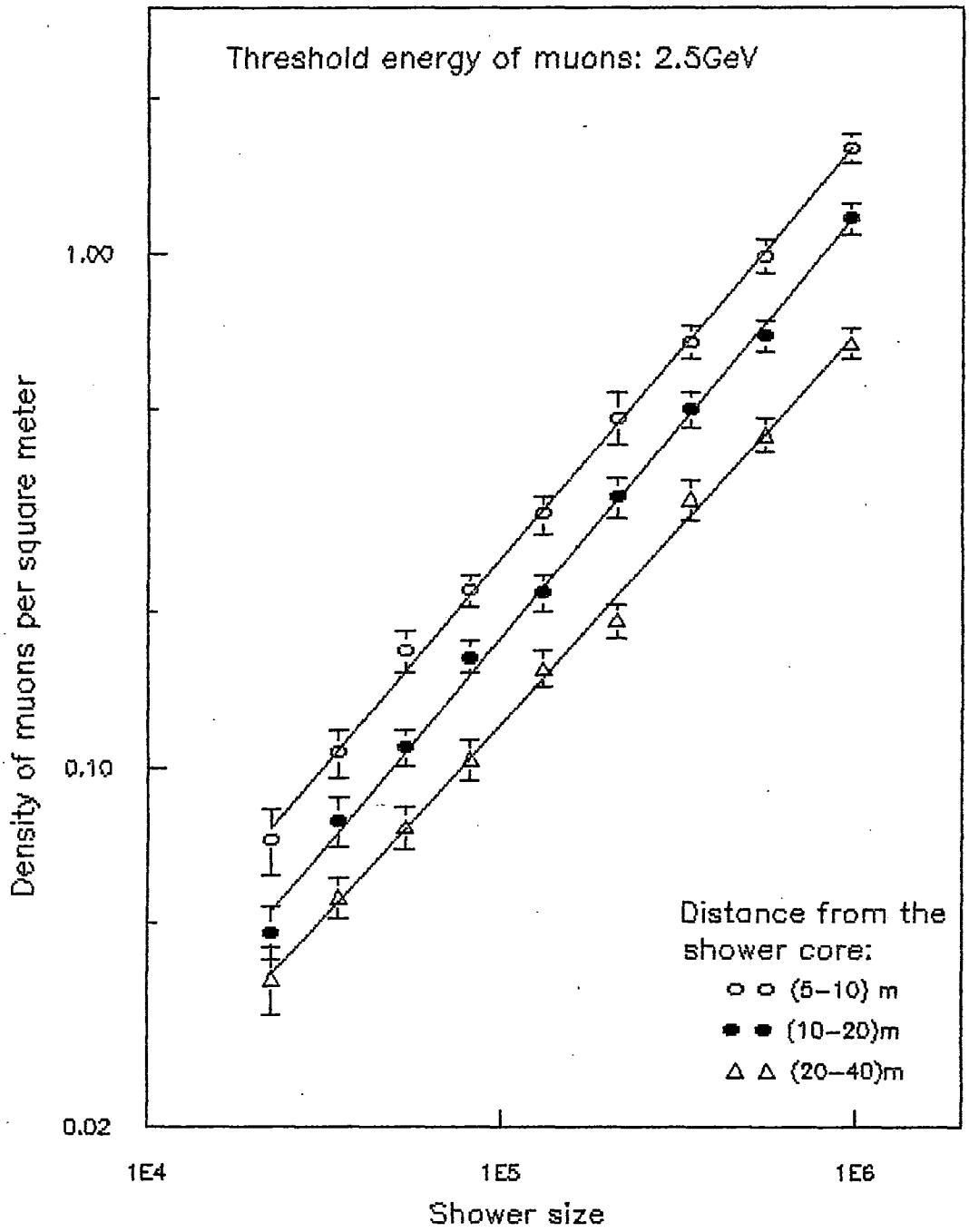

Fig. 4.7(a) VARIATION OF MUON DENSITY WITH SHOWER SIZE AT DIFFERENT RADIAL DISTANCES FROM SHOWER CORE.

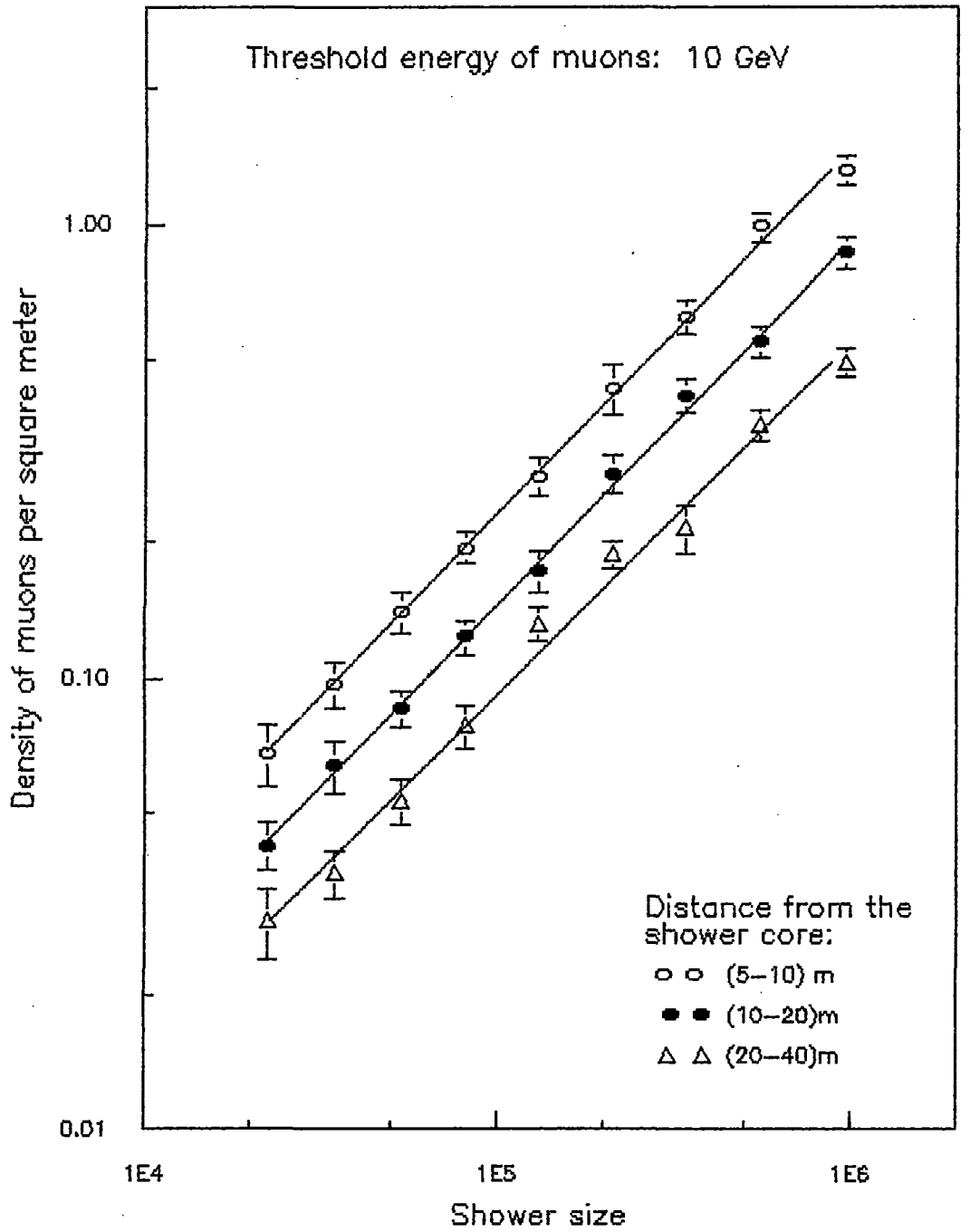

Fig. 4.7(b) VARIATION OF MUON DENSITY WITH SHOWER SIZE AT DIFFERENT RADIAL DISTANCES FROM SHOWER CORE.

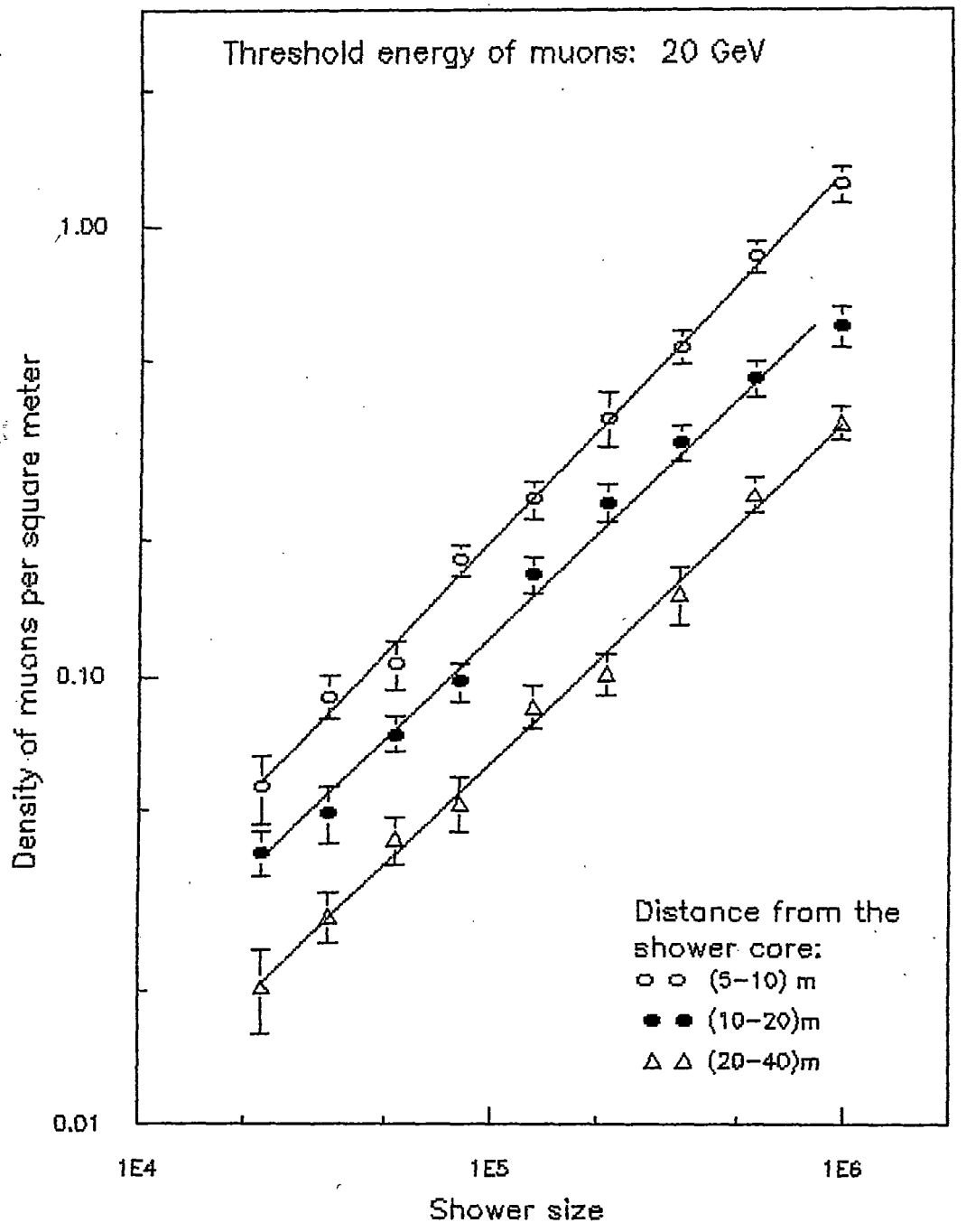

Fig. 4.7(c) VARIATION OF MUON DENSITY WITH SHOWER SIZE AT DIFFERENT RADIAL DISTANCES FROM SHOWER CORE

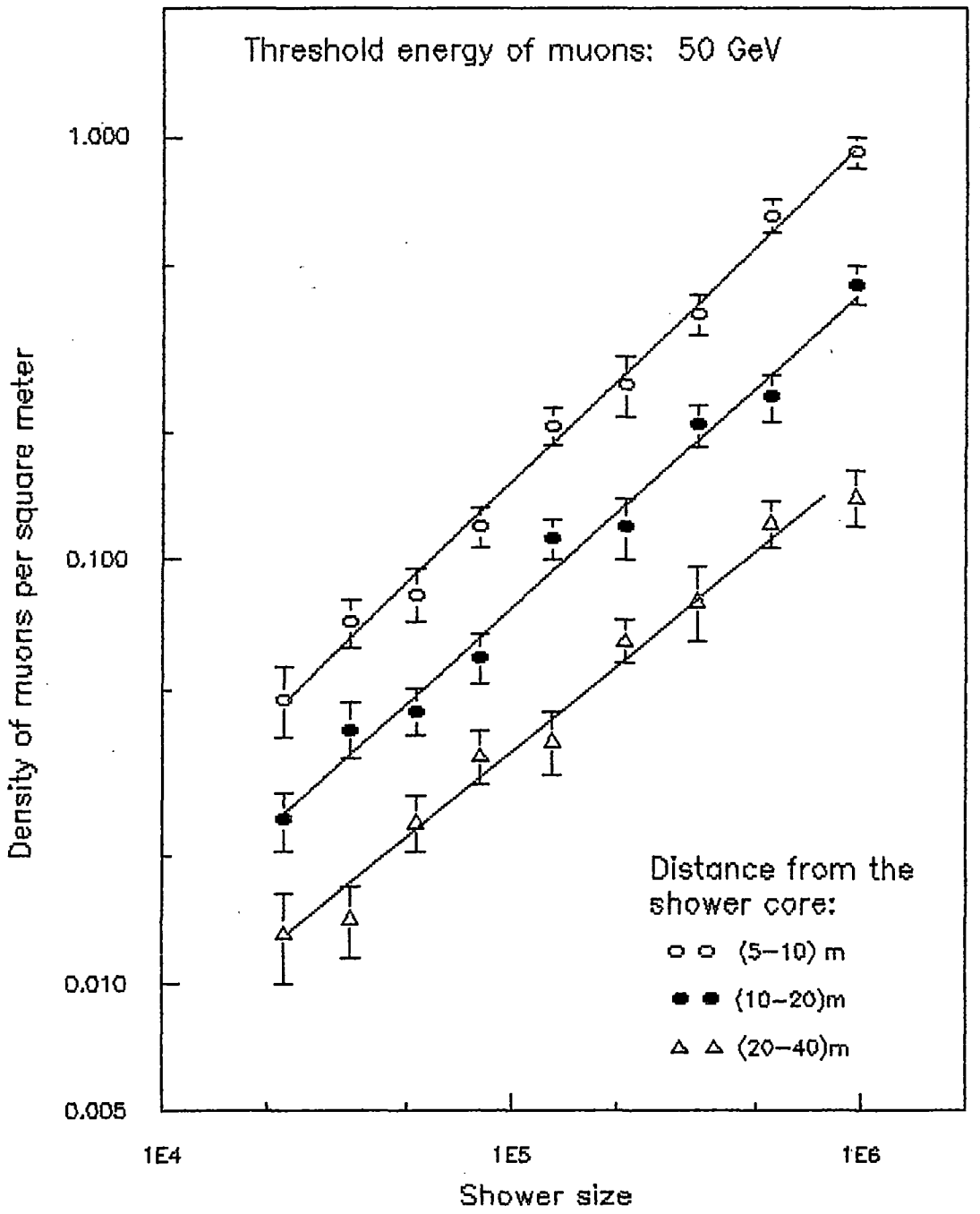

Fig. 4.7(d) VARIATION OF MUON DENSITY WITH SHOWER SIZE AT DIFFERENT RADIAL DISTANCES FROM SHOWER CORE

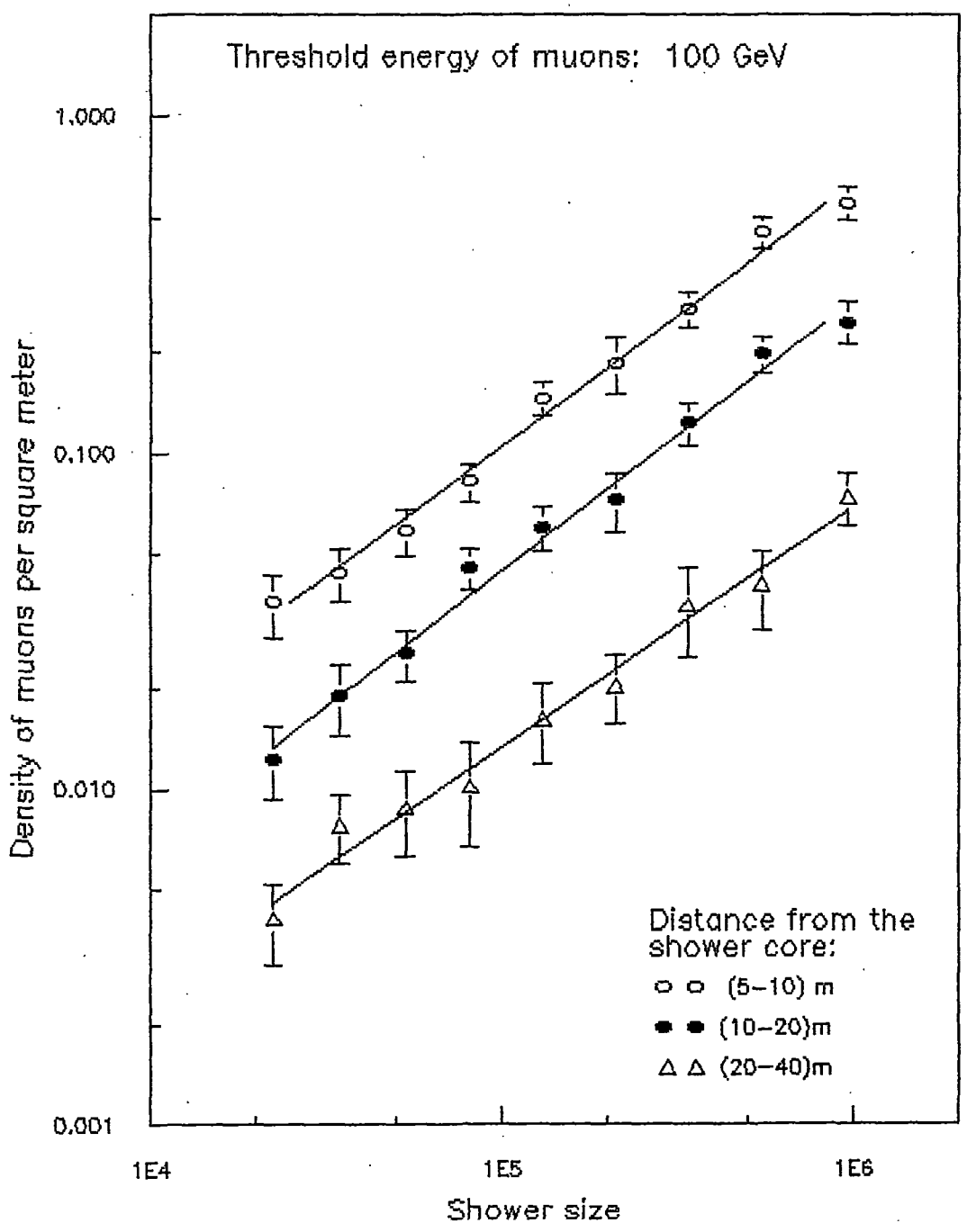

Fig. 4.7(e) VARIATION OF MUON DENSITY WITH SHOWER SIZE. AT DIFFERENT RADIAL DISTANCES FROM SHOWER CORE

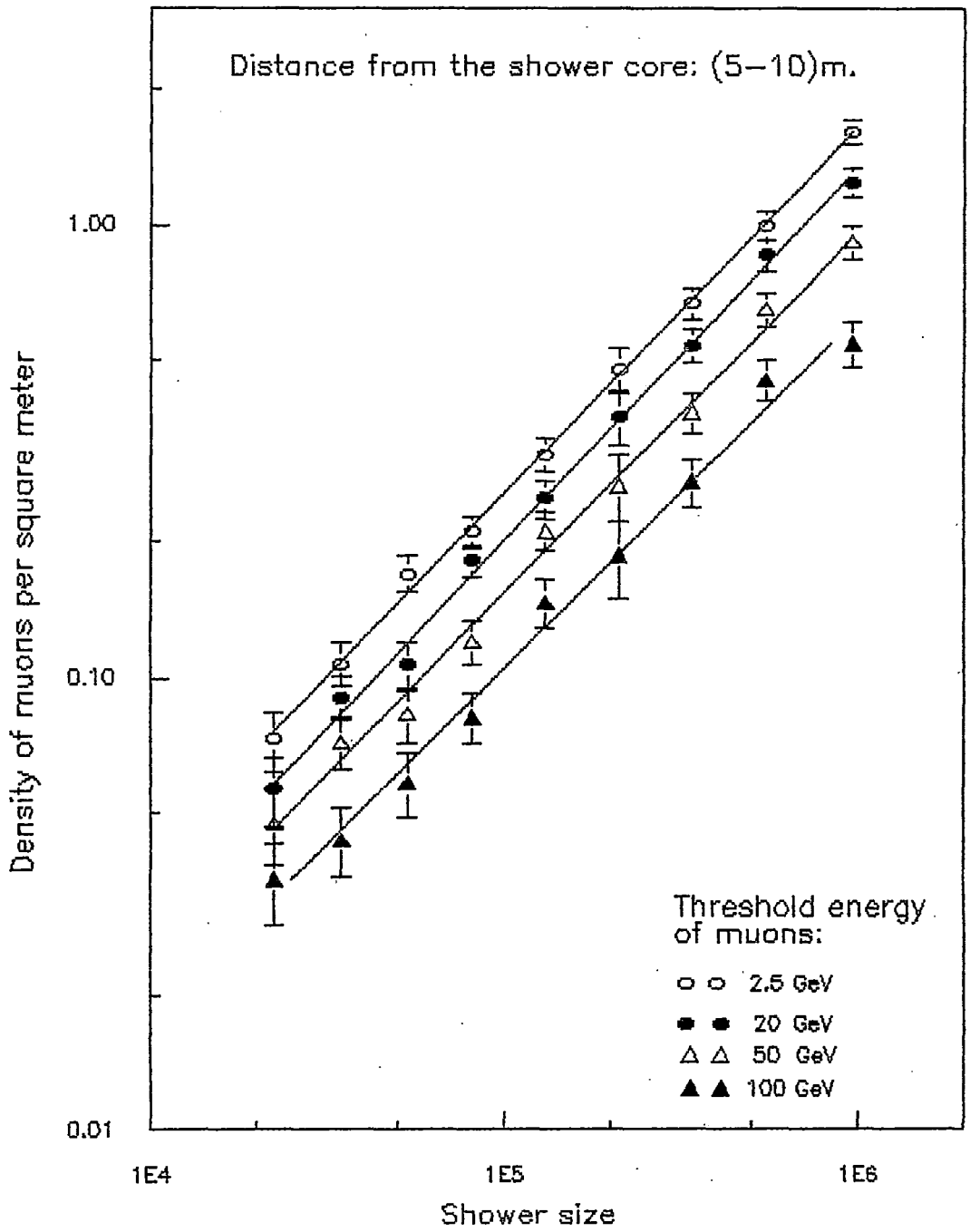

Fig. 4.8(a) VARIATION OF MUON DENSITY WITH SHOWER SIZE AT FIXED RANGE OF RADIAL DIATANCES FROM THE SHOWER CORE

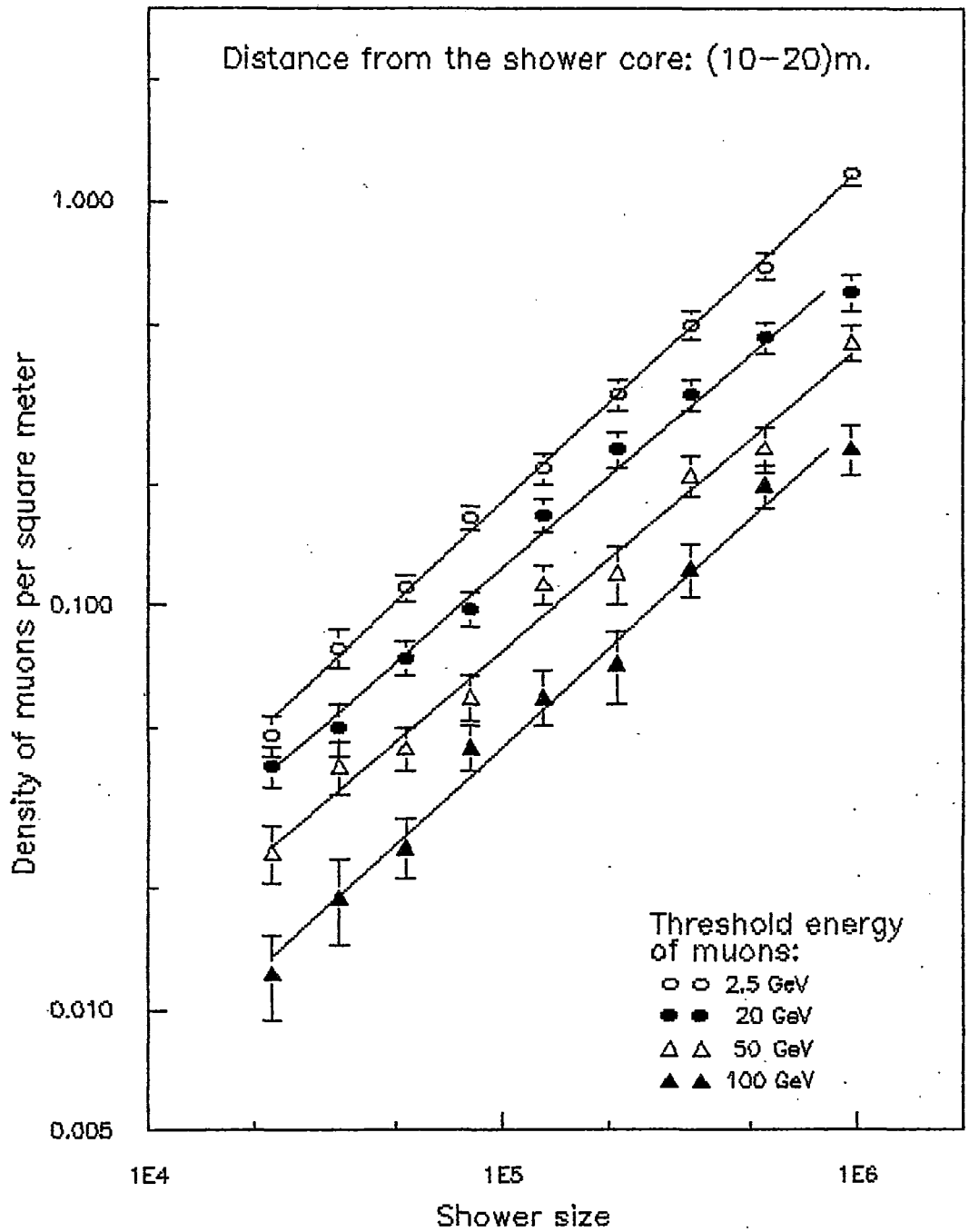

Fig. 4.8(b) VARIATION OF MUON DENSITY WITH SHOWER SIZE AT FIXED RANGE OF RADIAL DISTANCE FROM THE SHOWER CORE

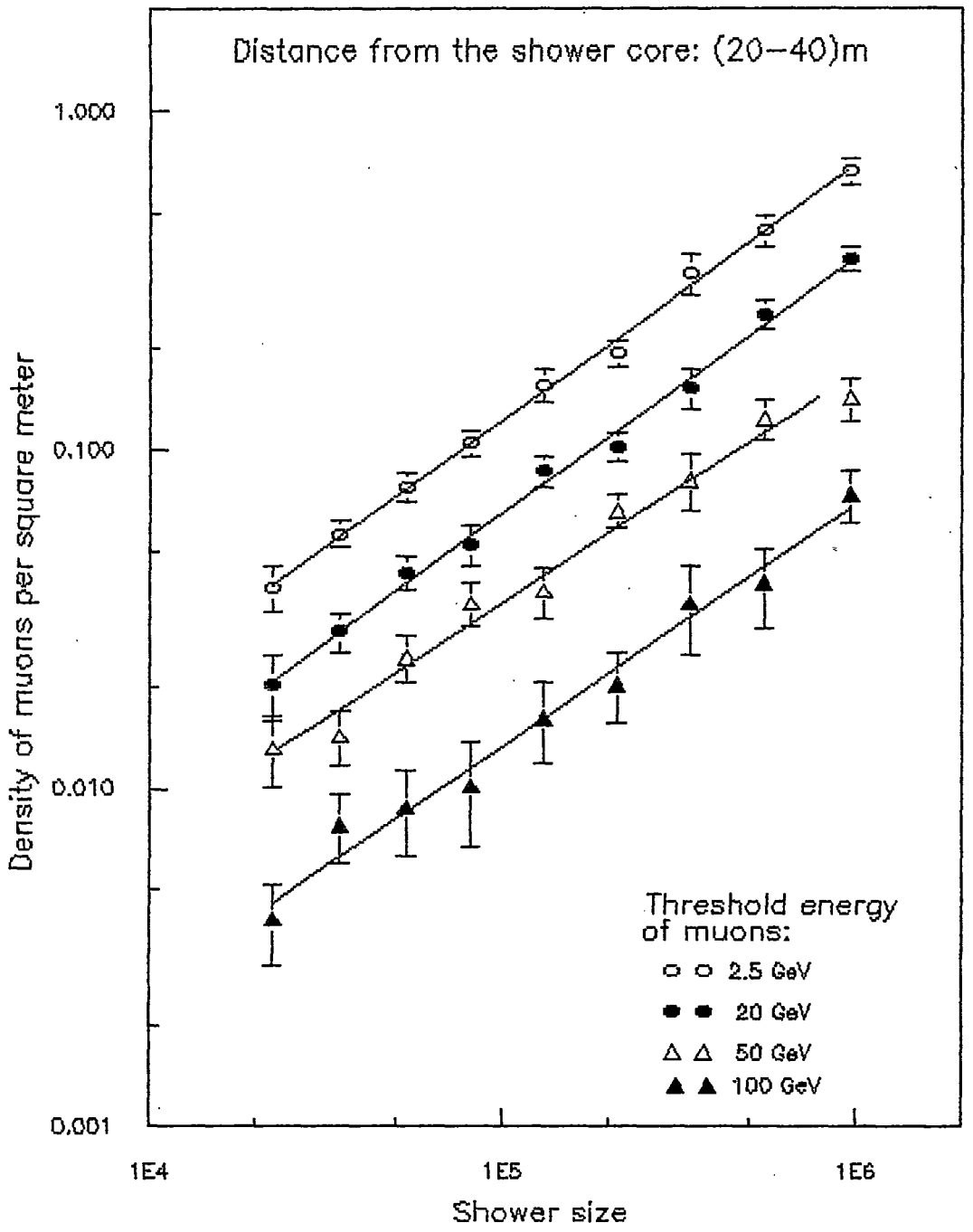

Fig. 4.8(c) VARIATION OF MUON DENSITY WITH SHOWER SIZE AT FIXED RANGE OF RADIAL DISTANCES FROM THE SHOWER CORE

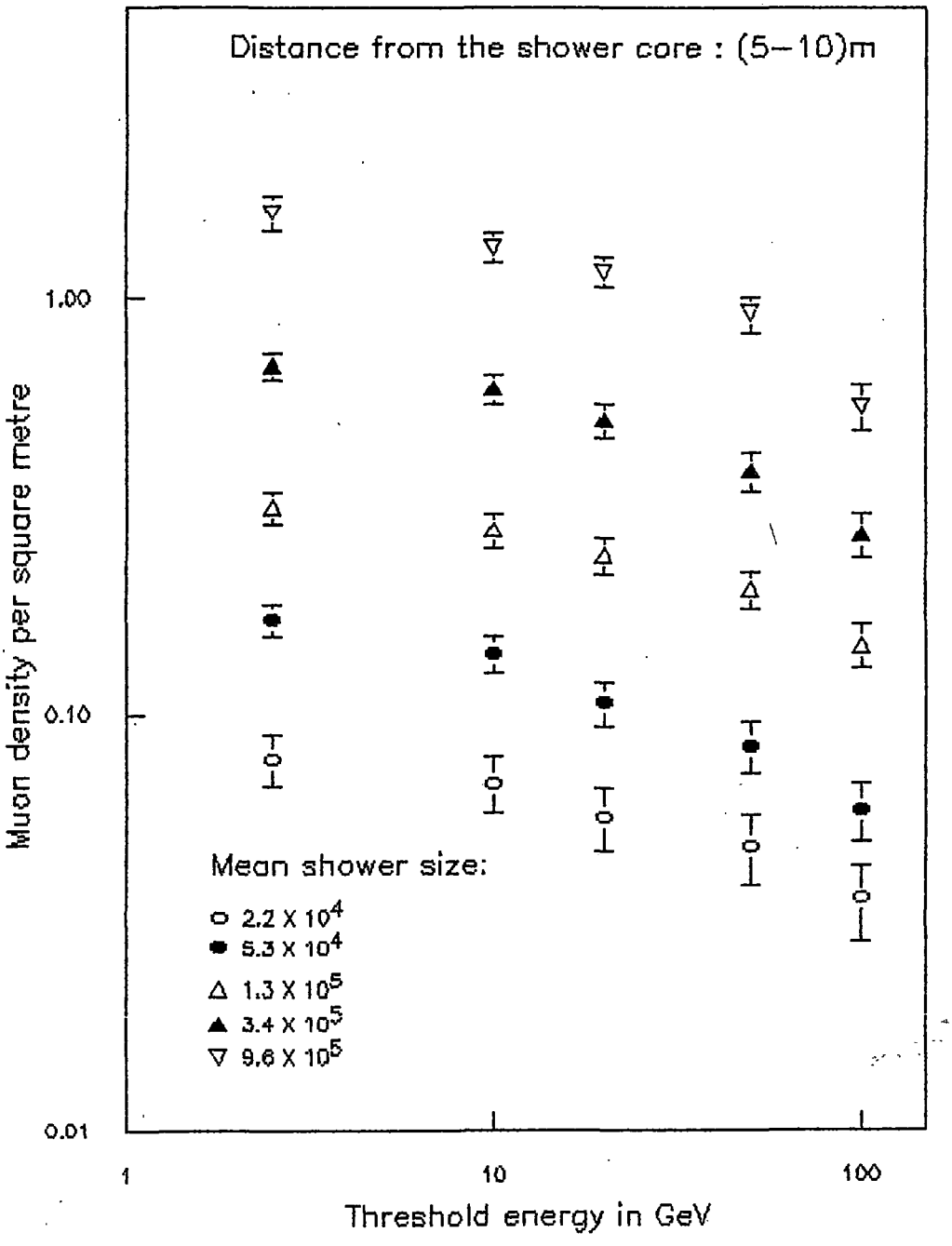

Fig.4.9(a) THE ENERGY SPECTRUM OF MUONS AT A FIXED RANGE OF RADIAL DISTANCES FROM THE CORE OF EAS WITH DIFFERENT SIZES

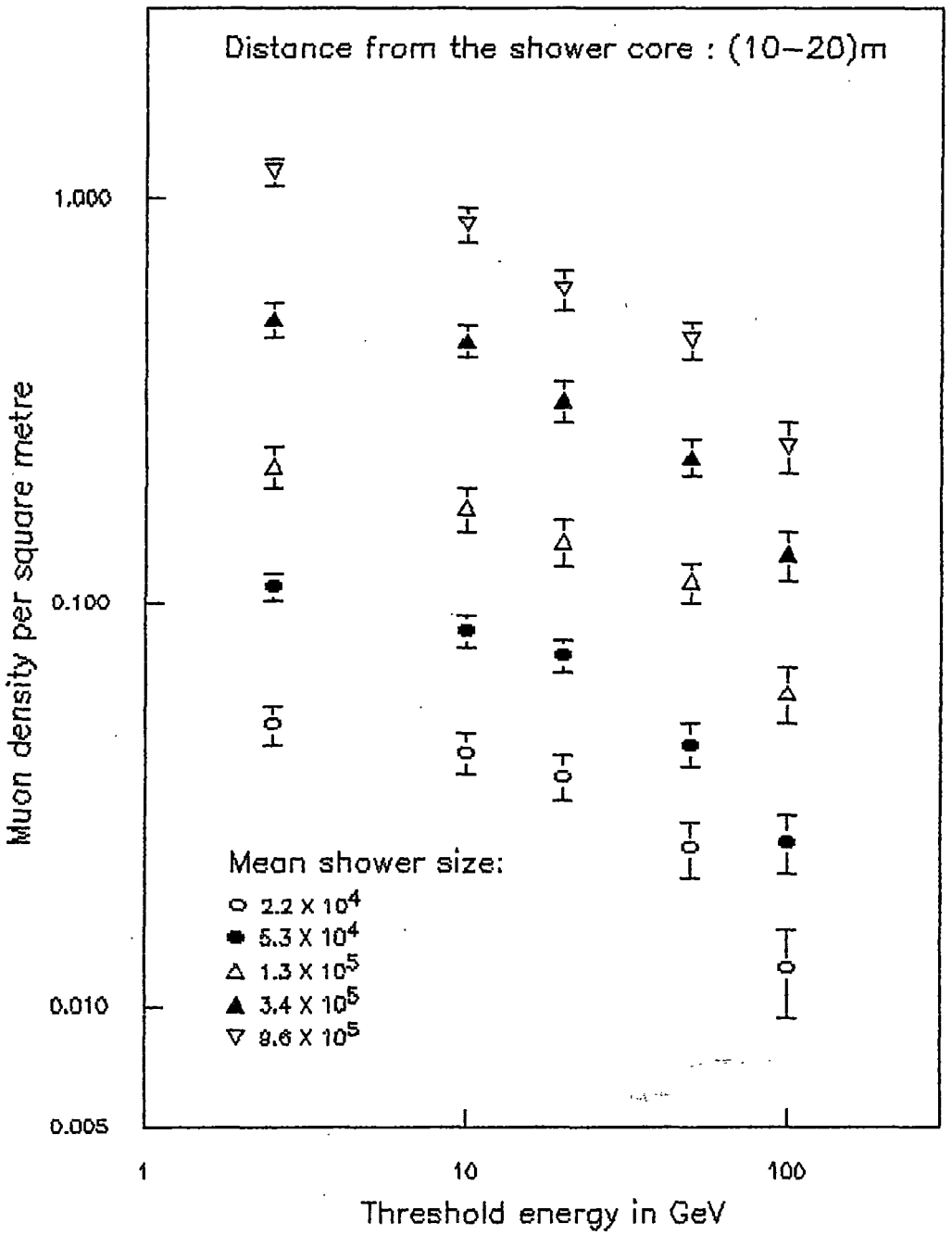

Fig.4.9(b) THE ENERGY SPECTRUM OF MUONS AT A FIXED RANGE OF RADIAL DISTANCES FROM THE CORE OF EAS WITH DIFFERENT SIZES

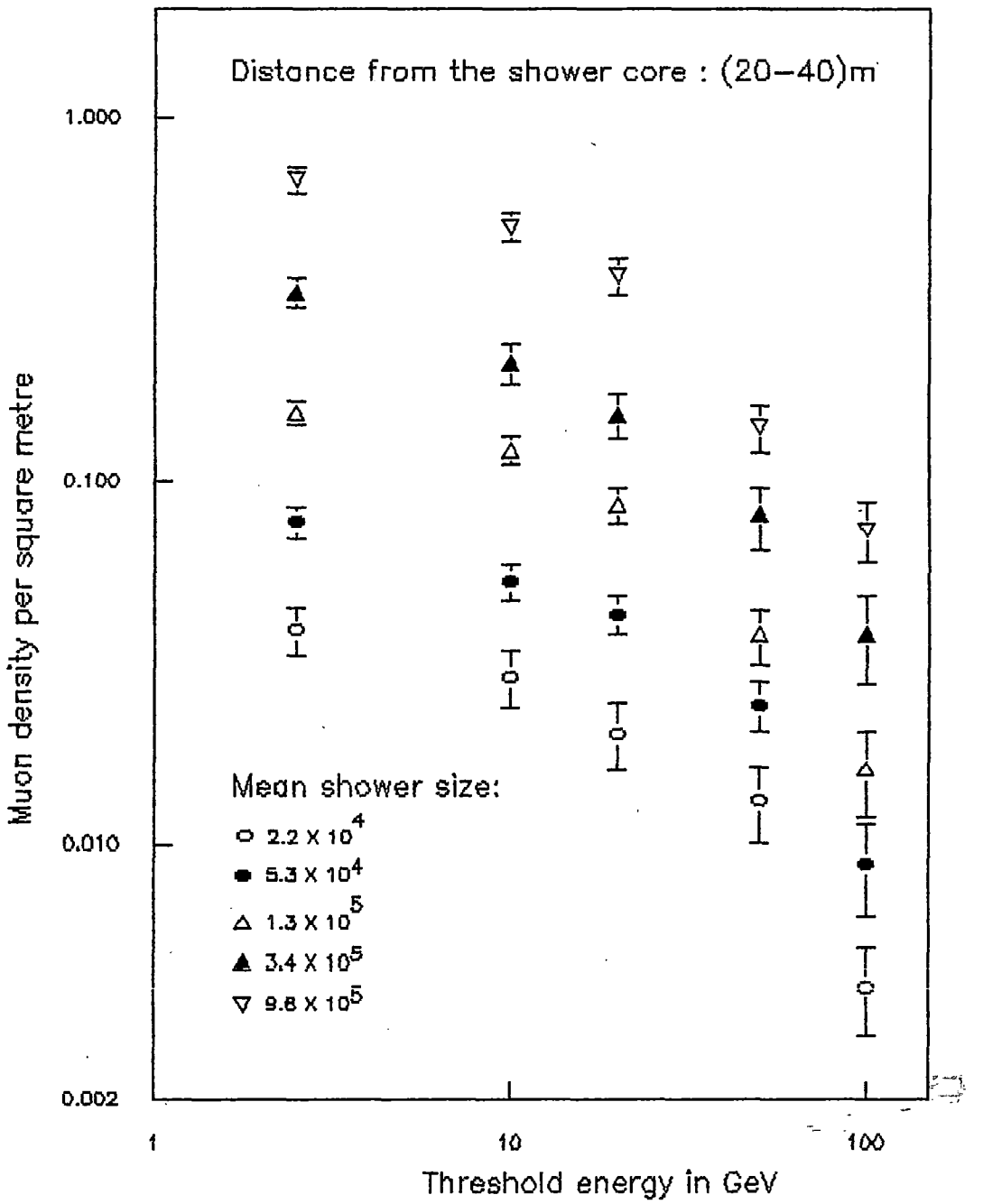

Fig. 4.9(c) THE ENERGY SPECTRUM OF MUONS AT A FIXED RANGE OF RADIAL DISTANCES FROM THE CORE OF EAS WITH DIFFERENT SIZES

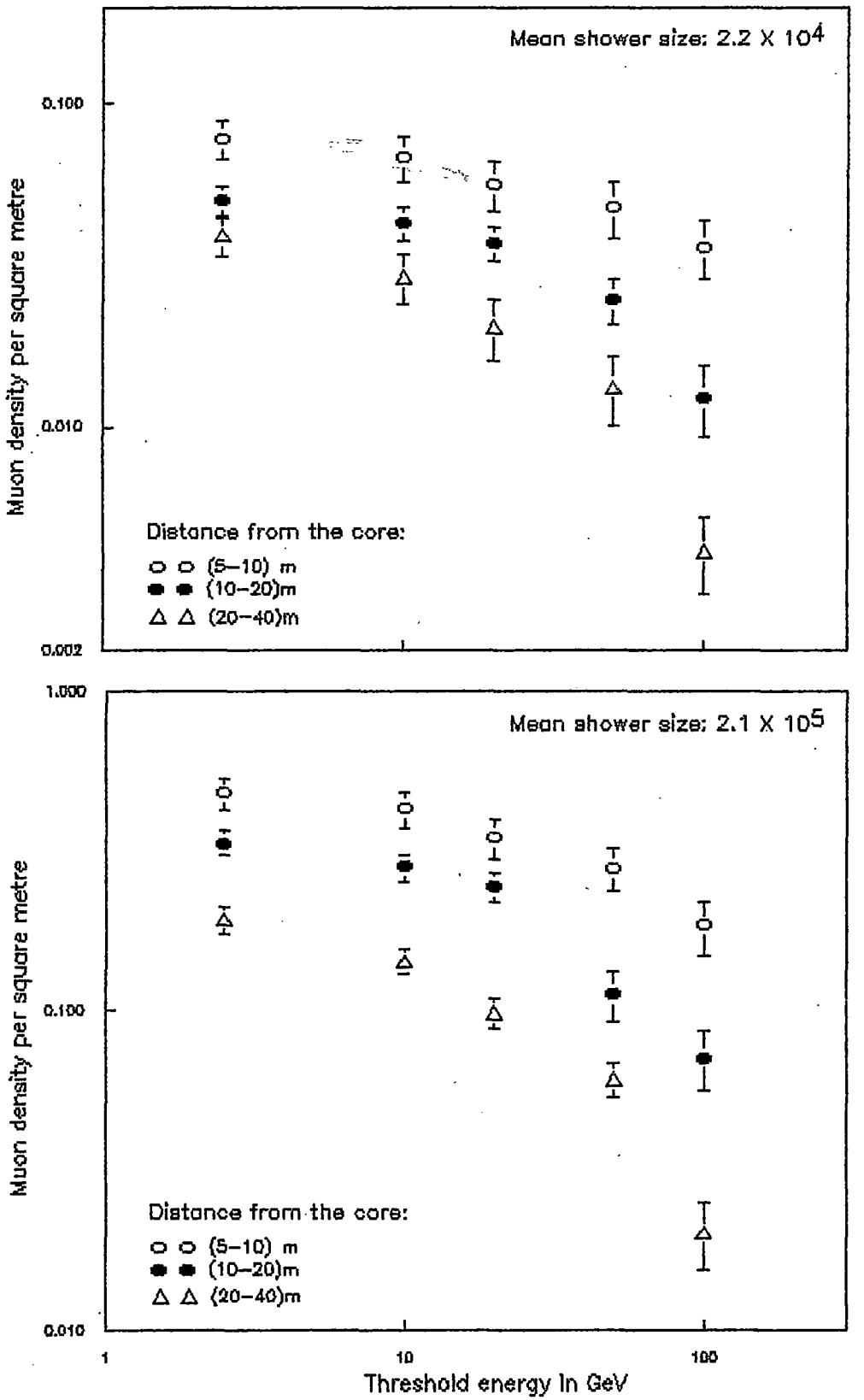

Fig. 4.10(a) THE ENERGY SPECTRUM OF MUONS AT DIEFERENT RADIAL DISTANCES FROM THE CORE OF EAS WITH TWO DIFFERENT SIZES

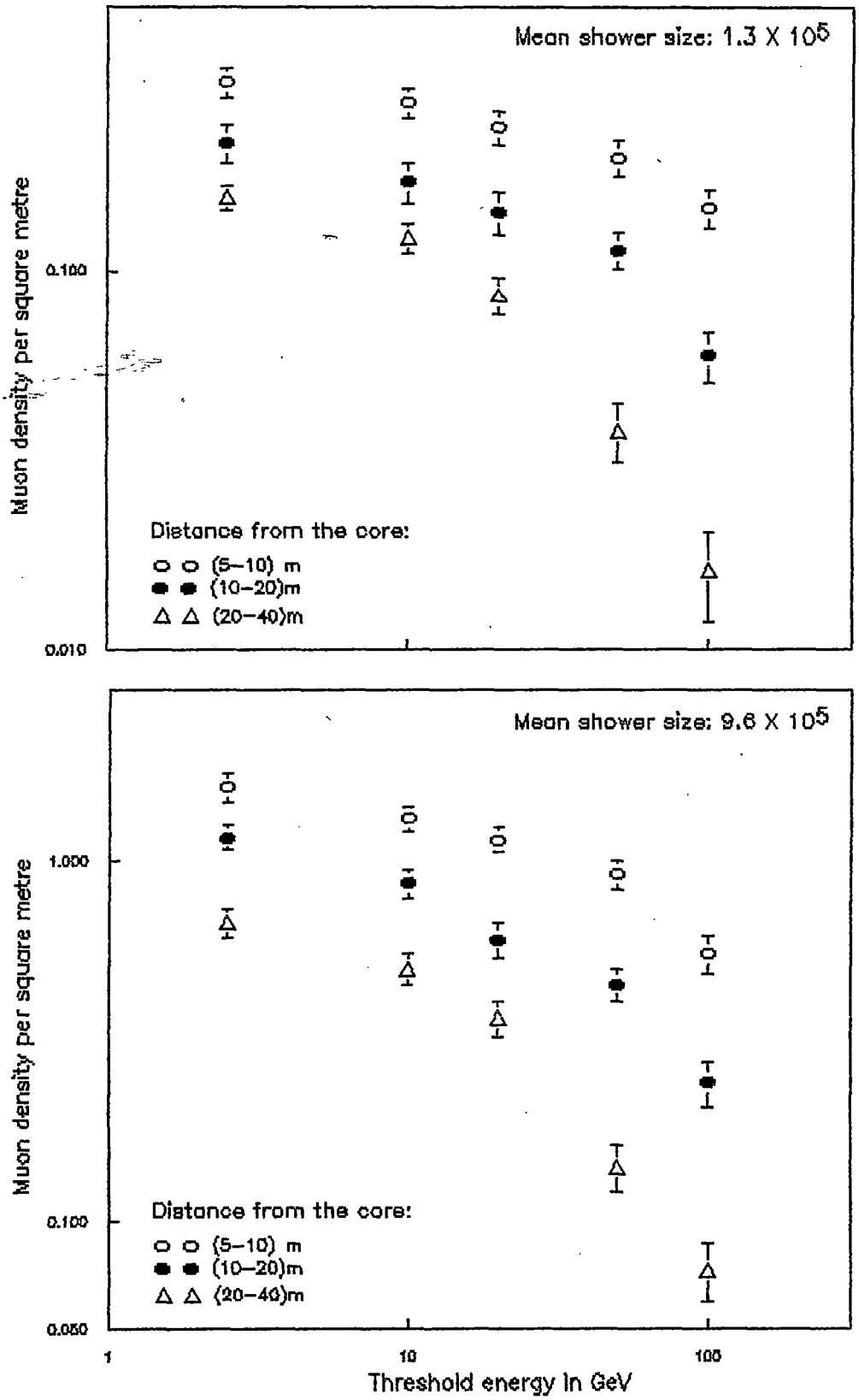

Fig. 4.10(b) THE ENERGY SPECTRUM OF MUONS AT DIFFERENT RADIAL DISTANCES FROM THE CORE OF EAS WITH TWO DIFFERENT SIZES

$\geq E_\mu$ at a distance of 'r' from the core of an air shower of size Ne, then the total number of muons $N_\mu(\geq E_\mu)$ having energy $\geq E_\mu$ in that air shower of size Ne is given by,

$$N_\mu(\geq E_\mu) = \int_0^\infty \rho_\mu (\geq E_\mu, Ne, r) \cdot 2\pi r \, dr \quad \ldots \quad \ldots \quad (4.4)$$

In the present experiment, as mentioned earlier, the radial or the lateral distributions of muons were approximated by the equation (4.2) which represents the muon density $\rho_\mu(\geq E_\mu, Ne, r)$ at a distance r from the shower core and the values of the constants β and r_o, obtained by fitting the experimental data are given in Table- 2(a). Utilizing equation (4.2) for $\rho_\mu(\geq E_\mu, Ne, r)$ with the values of β and r_o from the table, the total number of muons $N_\mu(\geq E_\mu)$ for muon energy thresholds of 2.5 to 100 GeV in the showers of different sizes were calculated by the equation (4.4). And, with these calculated values of total number of muons in the air showers their variation with the shower size and the threshold energies were studied.

4.4.1 Variation of Total Number of Muons with Size of the EAS

To study the variation of total number of muons $N_\mu(\geq E_\mu)$ with the shower size Ne, the experimentally obtained values of $N_\mu(\geq E_\mu)$ were plotted against the shower size and the plots showing the variation of $N_\mu(\geq E_\mu)$ with Ne for muon energy thresholds ($\geq E_\mu$) of 2.5, 10, 20, 50 and 100 GeV are shown in fig. (4.11).

The experimental measurements were fitted to an equation of the form,

$$N_\mu(\geq E_\mu) \sim Ne^{\gamma(E_\mu)} \quad \ldots \quad \ldots \quad \ldots \quad (4.5)$$

The lines in the fig. (4.11) represent the best fit lines and the values of the exponent $\gamma(E_\mu)$ obtained by the fitting are shown in Table- 4.

Table 4: Values of the exponent $\gamma(E_\mu)$ for different muon energy thresholds ($\geq E_\mu$)

$\geq E_\mu$ (GeV)	2.5	10	20	50	100
$\gamma(E\mu)$	0.74±0.03	0.74±0.02	0.73±0.03	0.71±0.04	0.73±0.04

The exponent 'γ', from the table, is seen to remain almost constant with an average value of 0.73±0.03 within the range of the energy 2.5 to 100 GeV of muons

investigated in the present experiment.

The experimentally measured ratio [$N_\mu(\geq E_\mu)$ / Ne] of number of muons having energy above a particular threshold with the shower size representing the percentage of those muons observed in the air showers of different sizes are shown in Table- 5.

Table 5: The percentage of muons for different muon energy thresholds in the EAS of different sizes

Average shower size (Ne)	$\geq E_\mu$ (GeV)				
	2.5	**10**	**20**	**50**	**100**
2.2×10^4	7.82	4.10	2.26	0.94	0.37
3.5×10^4	6.19	3.41	1.80	0.78	0.33
5.3×10^4	5.55	3.17	2.08	0.92	0.28
8.1×10^4	4.72	2.50	1.59	0.78	0.33
1.3×10^5	4.25	2.58	1.50	0.55	0.22
2.1×10^5	3.40	2.02	1.23	0.49	0.20
3.4×10^5	3.85	1.83	1.10	0.47	0.20
5.5×10^5	3.14	1.69	0.98	0.42	0.17
9.6×10^5	2.69	1.60	0.79	0.31	0.12

The above table shows that the percentage of the muons having energy above particular threshold energy decreases with both the shower size and the energy thresholds.

4.4.2 The Integral Energy Spectra of Muons

The experimentally measured variation of number of muons with the threshold energy representing the integral energy spectra of muons in air showers of different sizes are shown in fig. 4.12(a). It was observed from the figure that the spectrum for the whole range of the energy 2.5 to 100 GeV could not be approximated by a functional form of power type. So, the measured spectra within a smaller range of

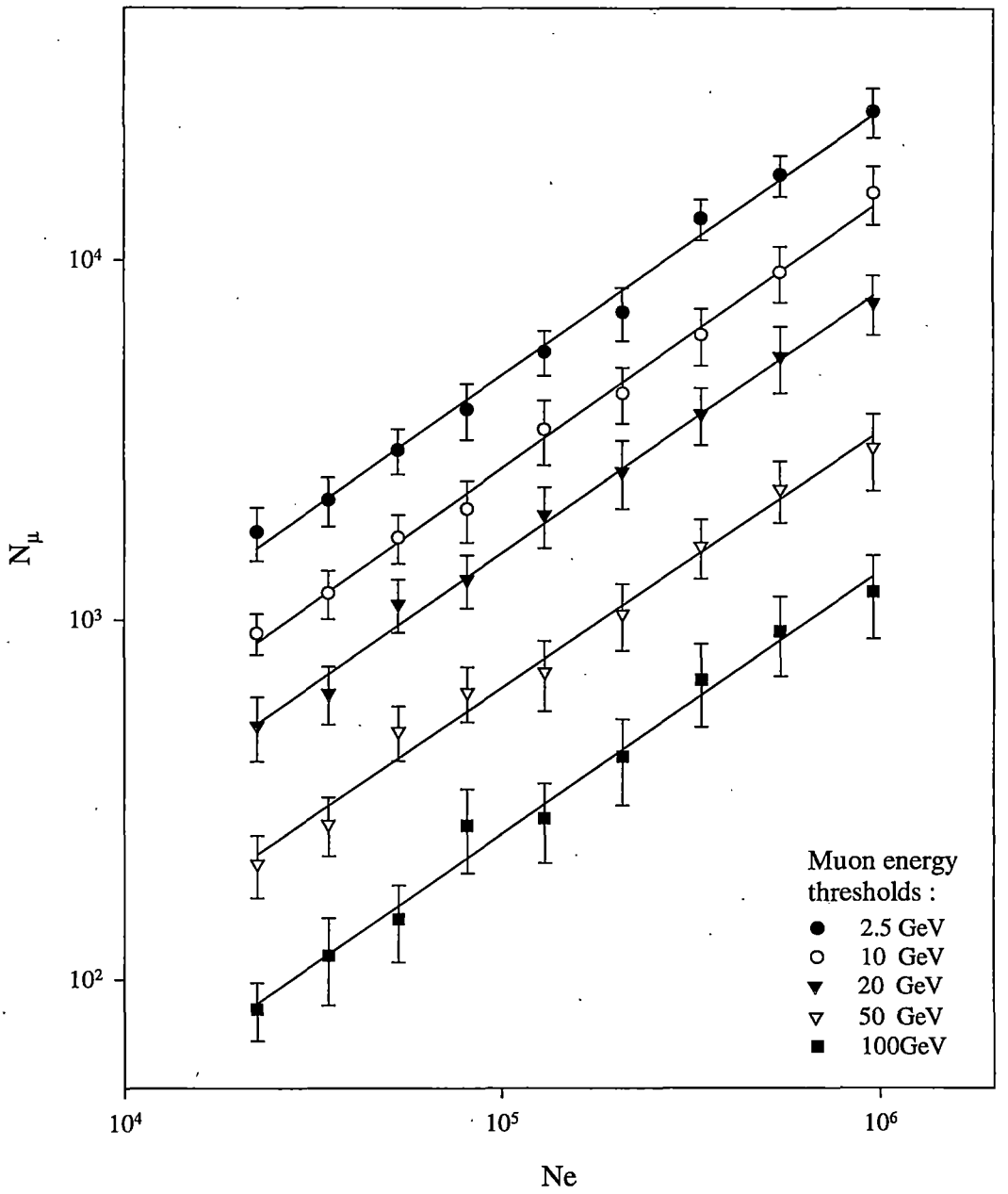

Fig. 4.11 THE VARIATION OF NUMBER OF MUONS(N_μ) WITH SHOWER SIZE (Ne) FOR DIFFERENT MUON ENERGY THRESHOLDS.

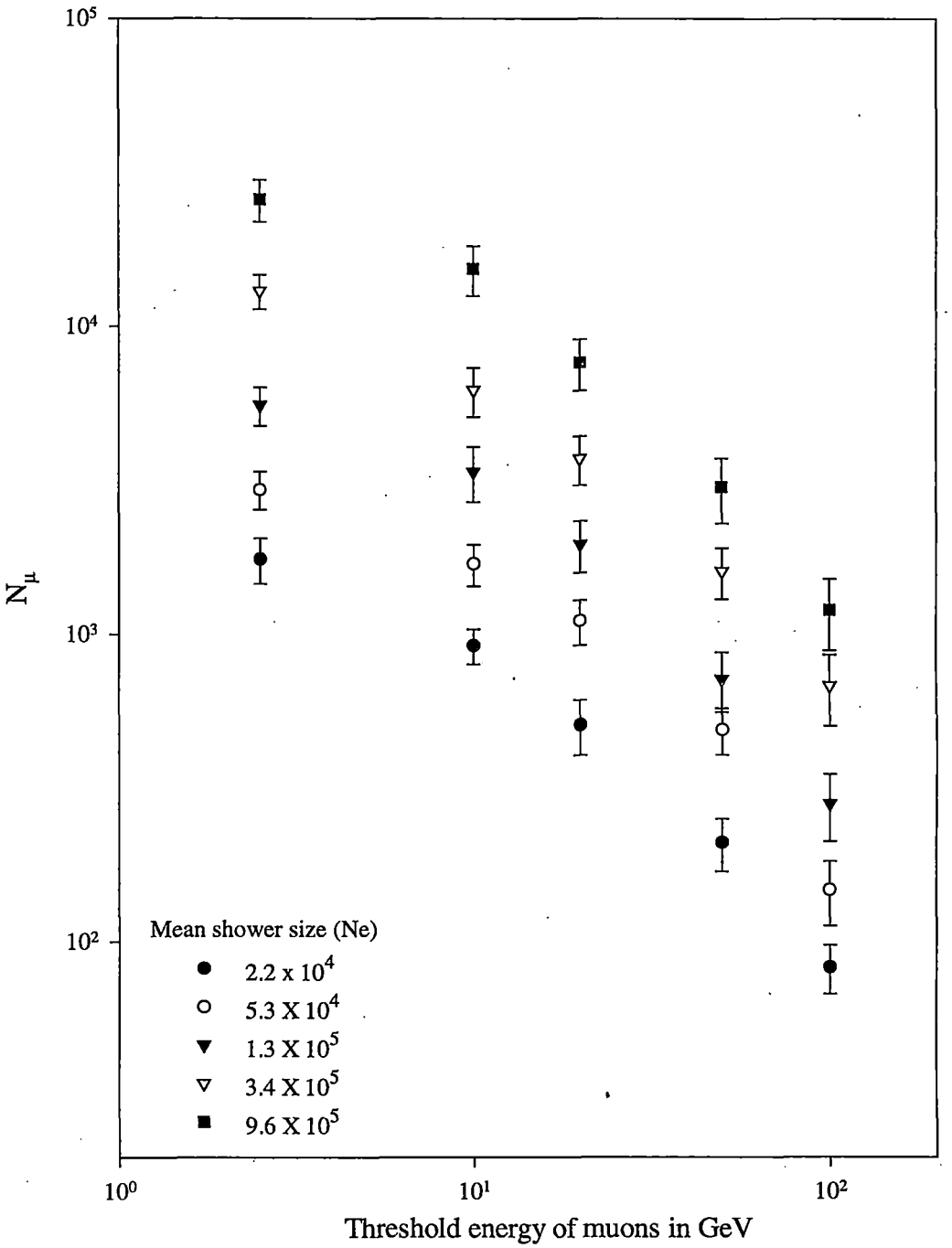

Fig. 4.12(a) THE ENERGY SPECTRUM OF MUONS IN EAS OF DIFFERENT SIZES.

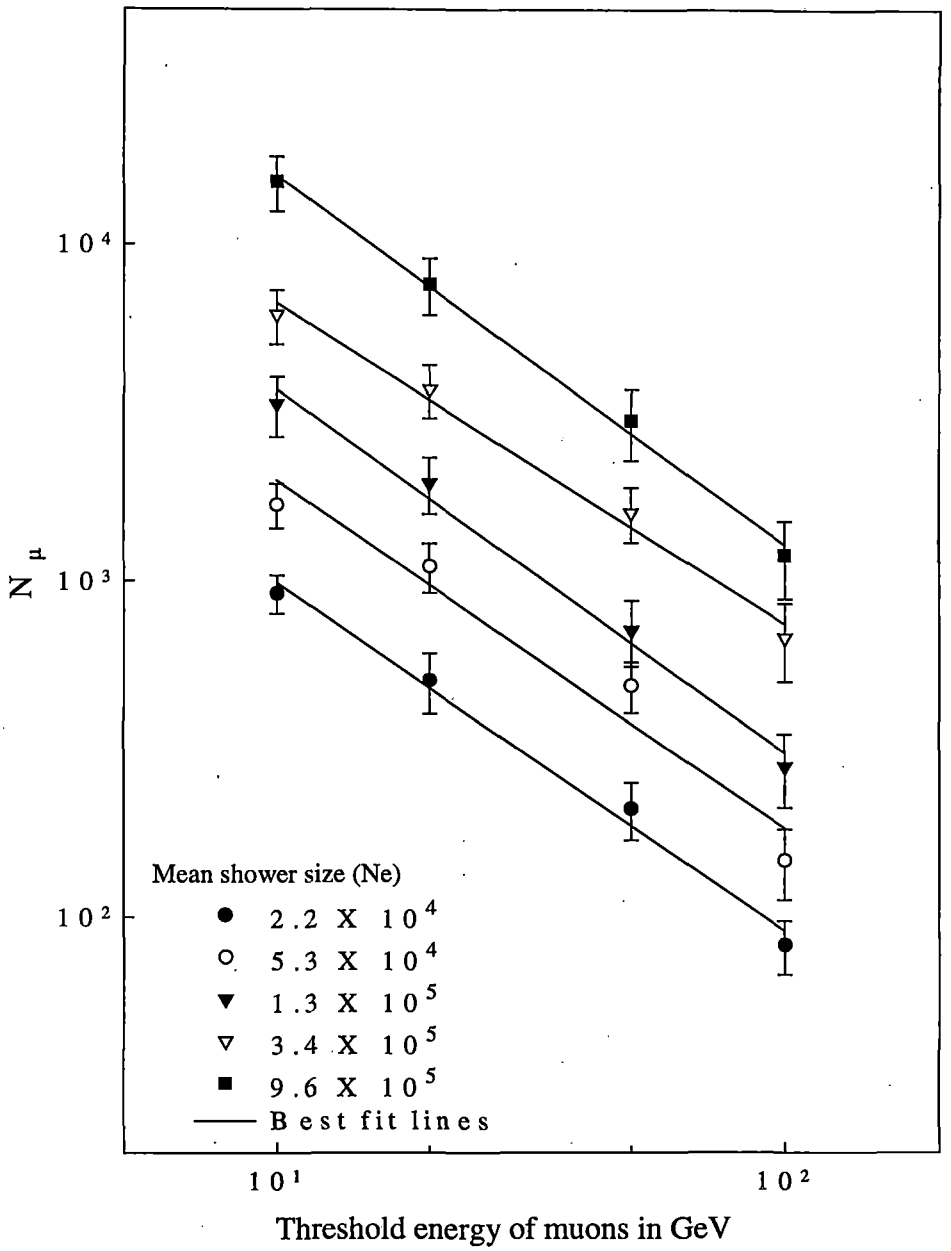

Fig. 4.12 (b) THE ENERGY SPECTRUM OF MUONS IN EAS OF DIFFERENT SIZES WITH THE BEST FIT LINES

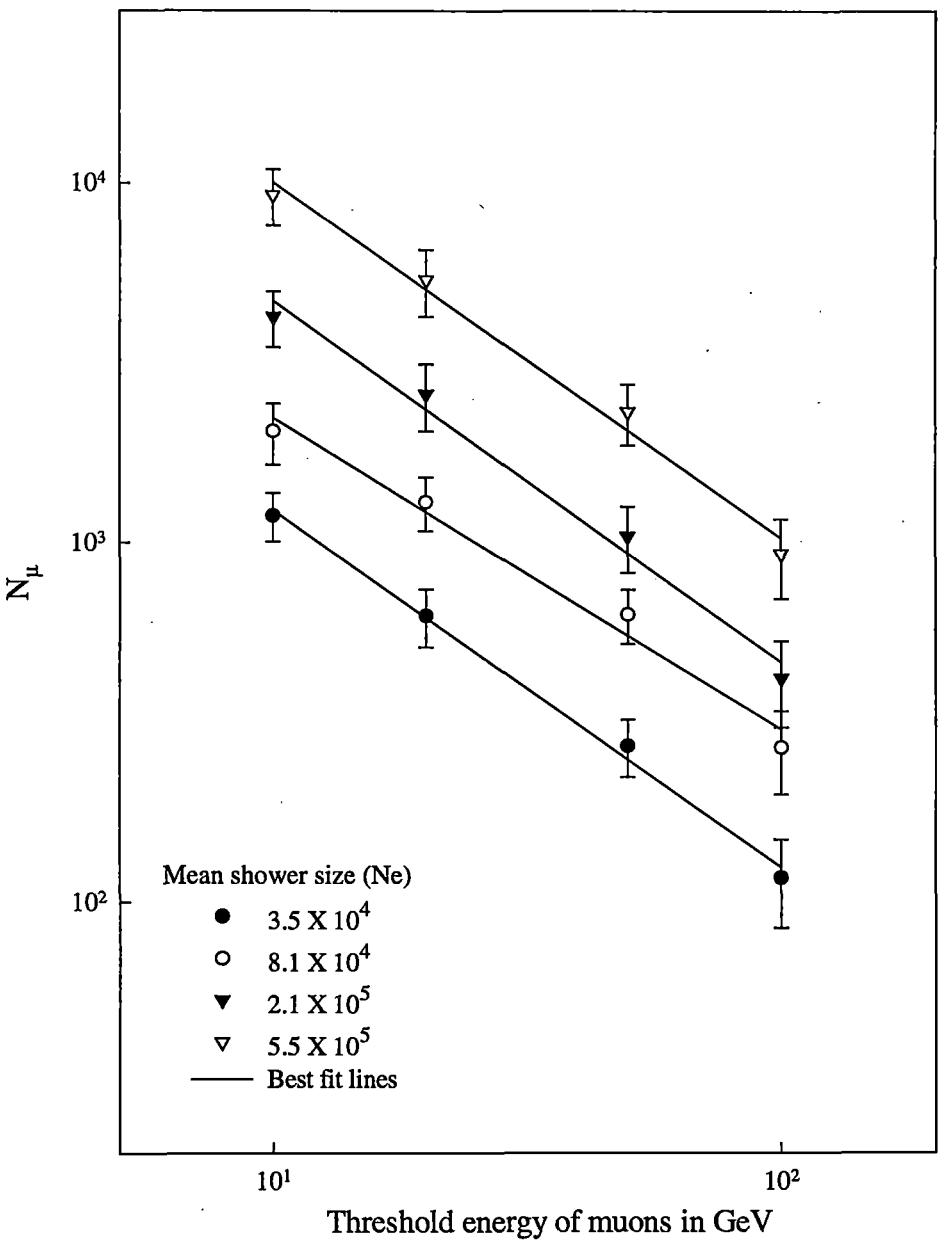

Fig. 4.12(c) THE ENERGY SPECTRUM OF MUONS IN EAS OF DIFFERENT SIZES WITH THE BEST FIT LINES.

energy (10-100) GeV were fitted to the functional form of power type written as,

$$N_\mu \sim E_\mu^{-\delta\,(Ne)} \quad \ldots \quad \ldots \quad \ldots \quad (4.6)$$

The fig.4.12 (b) & (c) show the experimentally measured spectra along with the best fit lines represented by smooth lines. The values of exponent δ(Ne) obtained by fitting the measured N_μ for energy thresholds of (10-100) GeV is presented in Table-6.

Table 6: The exponent δ(Ne) for different shower sizes

Average shower size (Ne)	δ (Ne)	Average shower size (Ne)	δ (Ne)
2.2×10^4	1.03±0.05	2.1×10^5	1.01±0.08
3.5×10^4	0.99±0.04	3.4×10^5	0.95±0.05
5.3×10^4	1.03±0.08	5.5×10^5	0.99±0.06
8.1×10^4	0.87±0.06	9.6×10^5	1.10±0.04
1.3×10^5	1.08±0.07		

From the table, it can be seen that apart from statistical fluctuations the values of exponent δ of the equation representing energy spectra of muons in the energy region of 10GeV to 100GeV remain almost constant. And, in the range of shower sizes studied the average value of δ is observed to be equal to 1.01±0.06.

4.5 Comparison of the Measurements of Present Experiment with those of other Experiments

A number of experiments have been performed in the past and recent years to study the muon component of the Cosmic Ray EAS at different places such as Haverah Park in Australia, Kiel in Germany, Durham in U.K., Moscow State University (MSU) in Russia and TIFR in India. These experiments, whose results have been reported by different authors [4-8], have studied various features regarding the distribution of muons having different energies (E_μ) and associated with EAS of different sizes. A brief review of the results of various recent experiments performed both at sea level and mountain altitudes is presented in Section 2.2 of Chapter II. Among the experiments performed at same level of observation as that of the present experiment, the regions of shower sizes (Ne) and the energy of muons (E_μ) investigated in the MSU experiment ($Ne \sim 10^5$-10^7 and E_μ- 10 to 500 GeV) overlap with that of the present experiment ($Ne \sim 10^4$-10^6 and E_μ - 2.5 to 100 GeV). A

comparative study of some representative measurements of present experiment and those reported by the investigators of MSU experiments is presented here.

In the MSU experiments, the measurements of EAS muon component were obtained with magnetic muon spectrometer and large hodoscopic detector of muon flux situated underground at the depths of 40 m.w.e. The muon flux detector located at this depth measures the flux of muons with an energy threshold of 10 GeV. The magnetic spectrometer, working as a part of MSU EAS array, measures the energy of the muons associated with the shower. The results of the experimental measurements are reported [9-13] in the form of lateral distributions, the energy spectra and the measurements of total number of muons having different energies and associated in the air showers of different sizes.

4.5.1 THE MEASUREMENTS OF MUON DENSITIES IN EAS

The densities of muons at different distances from the core of air showers measured and reported by different investigators of MSU experiments [9-11, 13] are shown in fig. 4.13 (a) to (c) along with the corresponding measurements obtained in the present experiment. The fig. 4.13(a) & (b) show the muon densities for energy thresholds of 10 GeV and 100 GeV measured in EAS of sizes, respectively, 2.10^5 and 10^6. And, the fig. 4.13(c) shows the densities measured for energy threshold of 50 GeV in EAS of two different sizes. These figures representing the lateral distribution of muons show that the measurements of present experiment are in fairly good agreement with those of MSU experiments.

Khristiansen et al. [9] have reported of fitting the muon densities for energy threshold of 10GeV measured in air showers of sizes ranging from 2 X 10^5 to 10^6 to a function of form $\rho_\mu \sim r^{-\beta} \exp(-r/80)$, and the value of exponent β obtained by fitting was equal to 0.52 ± 0.02. As described in previous section 4.3.1 of this chapter, the corresponding measurements of the present experiment fitted to the same type of function gives the value of β as 0.53 ± 0.04 in the shower size range 10^5 to 10^6 which is in close agreement with that obtained in the above MSU experiment.

Bazutov et al. [12], presenting the results of another MSU experiment, have reported of approximating the variation of muon density ρ_μ with shower size (Ne) by a functional relationship of power type written as $\rho_\mu \sim Ne^{\alpha}$. And, the average values

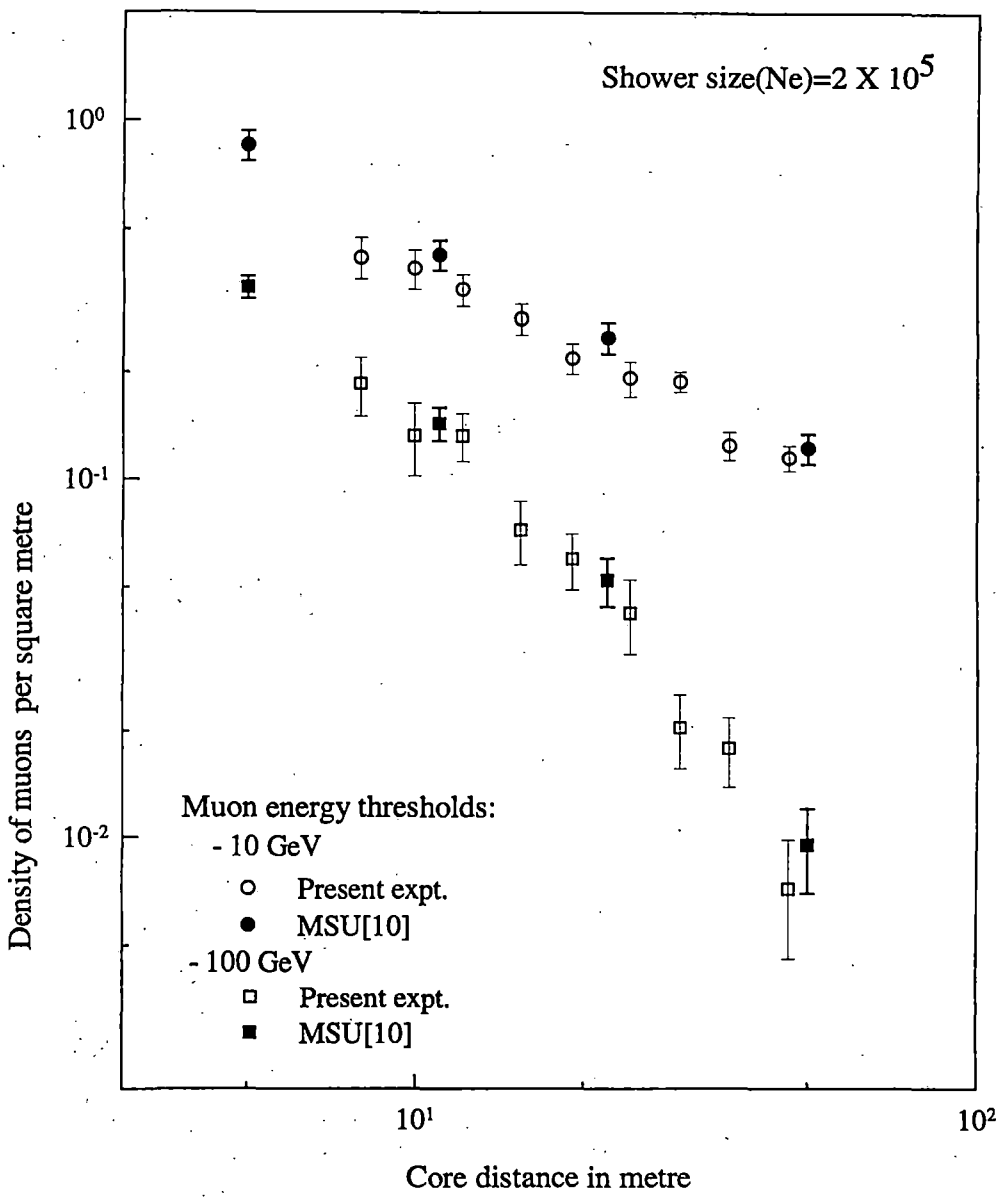

Fig.4.13(a) COMPARISON OF LATERAL DISTRIBUTION OF MUONS IN EAS OF AVERAGE SIZE 2 X 10^5 MEASURED IN THE PRESENT AND MSU EXPERIMENTS [10] FOR MUON ENERGY THRESHOLDS OF 10 & 100 GeV.

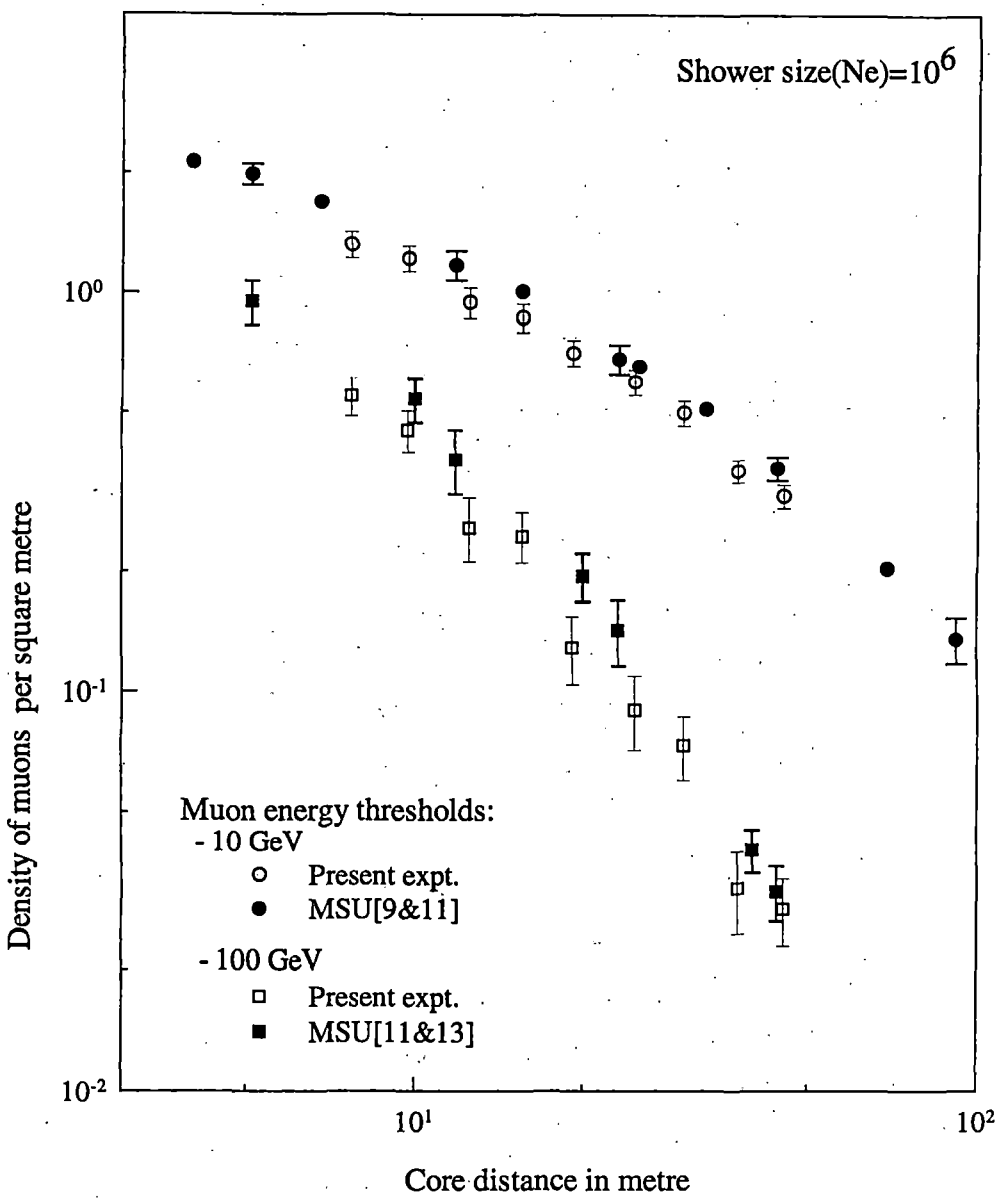

Fig. 4.13(b) COMPARISON OF LATERAL DISTRIBUTION OF MUONS IN EAS OF AVERAGE SIZE 10^6 MEASURED IN THE PRESENT AND MSU EXPERIMENTS [9,11 & 13] FOR MUON ENERGY THRESHOLDS OF 10 & 100 GeV.

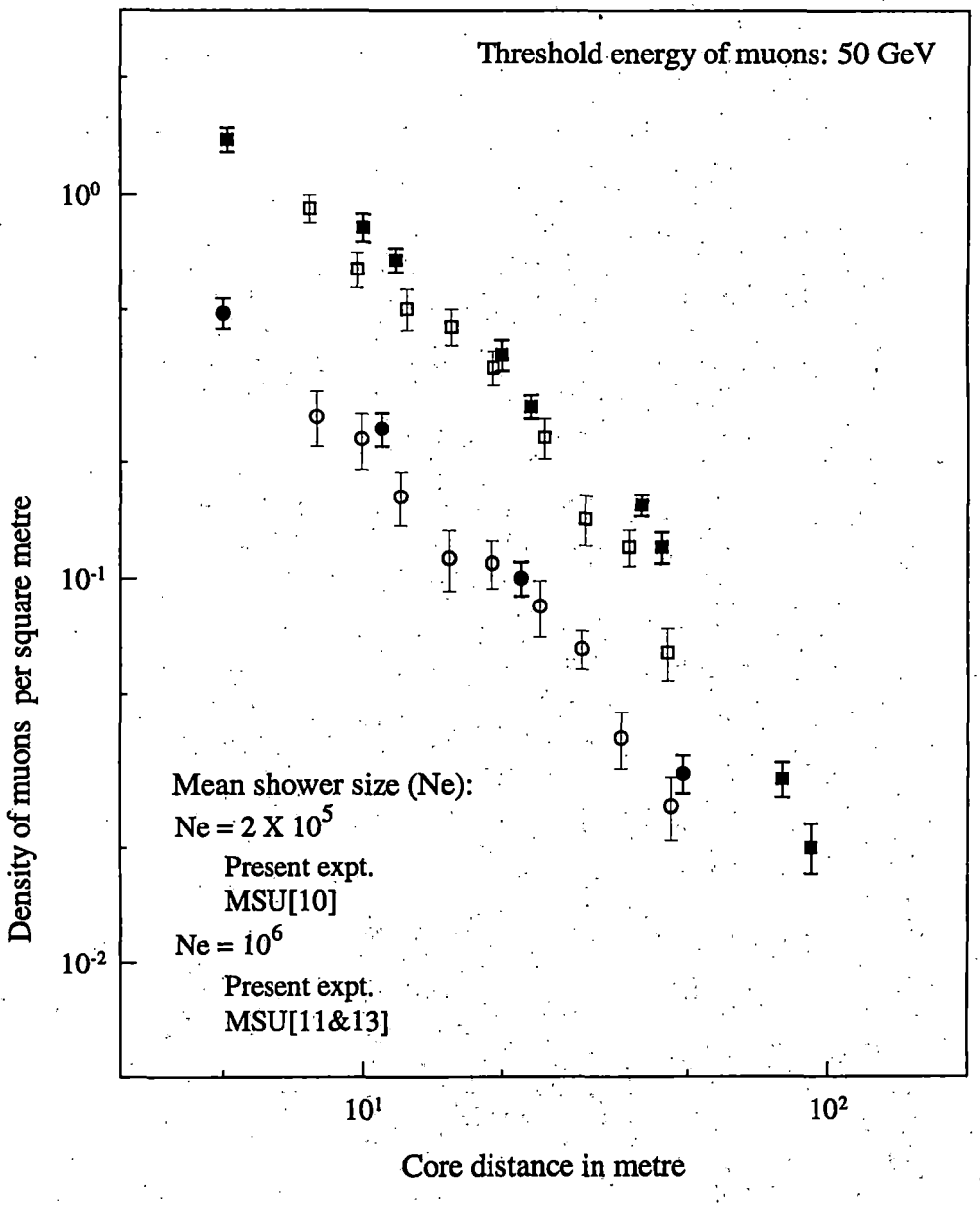

Fig. 4.13(c) COMPARISON OF LATERAL DISTRIBUTION OF MUONS IN EAS OF TWO DIFFERENT SIZES MEASURED IN THE PRESENT AND MSU EXPERIMENTS [10, 11 & 13] FOR MUON ENERGY THRESHOLD OF 50 GeV.

of 'α' obtained by fitting the measured densities of muons were observed to be 0.78±0.04 and 0.77±0.05, respectively, for the muon energy thresholds of 50 and 100 GeV in the shower size range of 6.10^4 to 3.10^6. Using the same approximation for the measurements of the present experiment, as pointed out in the previous section 4.3.2 of this chapter, the exponent 'α' was observed to vary with the radial distance 'r' from the shower core. The values of 'α' obtained in the present experiment along with those reported by Bazutov et al. [12] are shown below in Table-7.

Table-7: Values of exponent α obtained in the MSU and present experiment

$\geq E_\mu$ (GeV)	MSU [12]	Present experiment		
		5-10 m	10-20 m	20-40
50	0.78±0.04	0.81±0.06	0.76±0.09	0.71±0.07
100	0.77±0.05	0.80±0.06	0.81±0.06	0.73±0.09

4.5.2 THE MEASUREMENTS OF TOTAL NUMBER OF MUONS IN EAS

The total number of muons (N_μ) with different energies in air showers of different sizes and their variation with the size (Ne) of the showers have been most important features of muon component of EAS studied in different experiments. And, they have been investigated in both MSU and the present experiments. In Table-8 the number of muons in showers of three different sizes as measured in the present experiment are shown with those measured and reported by the different investigators of MSU experiments.

Table 8: The total number of muons with different threshold energies in the showers of fixed size measured in MSU and present experiments

$\geq E_\mu$ (GeV)	Ne = 10^5		Ne = 2 X 10^5	
	Bazutov et al.[12]	Present expt.	Grishina et al.[10]	Present expt.
10	3.4 X 10^3	3.3 X 10^3	5.5 X 10^3	4.2 X 10^3
20	1.9 X 10^3	2.0 X 10^3		
50	5.2 X 10^2	7.1 X 10^2	9.4 X 10^2	1.0 X 10^3
100	1.7 X 10^2	2.8 X 10^2	3.7 X 10^3	4.1 X 10^3

Contd.....

$\geq E_\mu$ (GeV)	$Ne = 10^6$		
	Bazutov et al.[12]	**Vaskevich et al.[13]**	**Present expt.**
10	1.8×10^4	1.9×10^4	1.6×10^4
20	8.1×10^3		7.9×10^3
50	2.9×10^3	3.1×10^3	3.1×10^3
100	1.1×10^3	1.2×10^3	1.2×10^3

The above comparison shows that the two sets of measurements are fairly close to each other. The overall percentages of differences are low, within a range of 3 to 15%. However, for few observations the differences are comparatively high, being almost 25 to 30 %.

To compare the observed variations of N_μ with Ne, the number of muons for three different energy thresholds of 10, 50 & 100 GeV in EAS of different sizes as measured in the present and MSU experiments are shown in figure 4.14.

Approximating the above variation by a function of the form $N_\mu \sim Ne^\gamma$ and fitting the number of muons with threshold energy of 10 GeV measured in showers of sizes between 10^5 to 5.10^7, Khristiansen et al. [9] had reported of obtaining the value of exponent γ as 0.78±0.01. Bazutov et al.[12], using similar approximation, have reported of observing the same value of γ as 0.78 for the muons with threshold energies of 10 to 500 GeV in the showers of sizes ranging from 6.10^4 to 3.10^6. Similarly, Vaskevich et al. [13], fitting the number of muons with threshold energies of 50 & 100 GeV measured within a circular region of radius 32m around the axis of air showers with sizes from 5.10^4 to 3.10^6, have reported of obtaining the value of γ as 0.76±0.03. As pointed out earlier in the section 4.4.1 of this chapter, the total number of muons measured in the present experiment when fitted to the same type of equation gives the values of γ between 0.71±0.04 to 0.74±0.02 with an average of 0.73±0.03. The results of these experiments are summarized in Table-9.

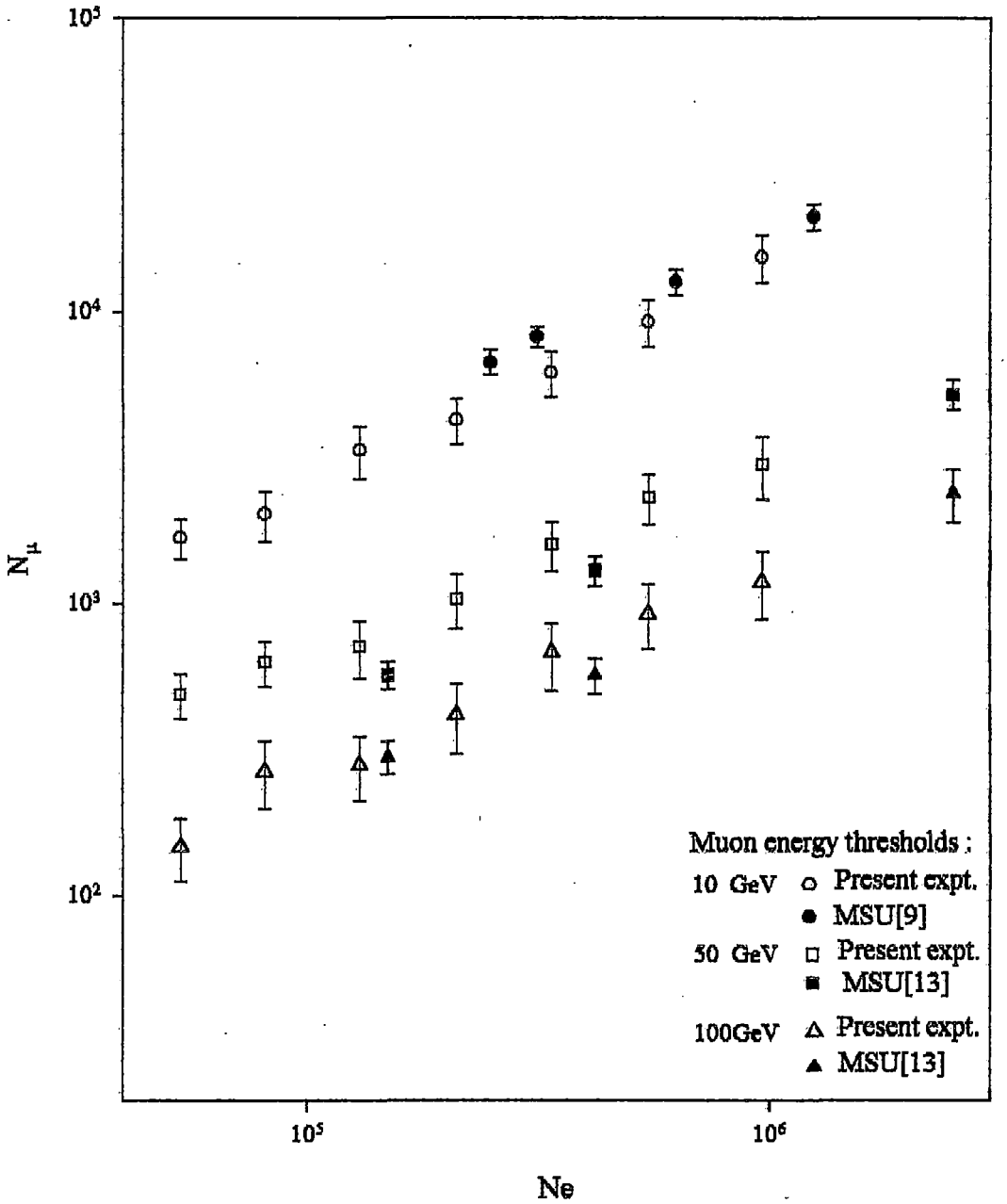

Fig. 4.14 THE VARIATION OF NUMBER OF MUONS(N_μ) WITH SHOWER SIZE (Ne) FOR DIFFERENT MUON ENERGY THRESHOLDS AS MEASURED IN THE PRESENT AND MSU EXPERIMENTS[9 & 13].

Table 9: The values of exponent γ obtained in MSU and present experiments

Expt.	Reference	Ne	$\geq E_\mu$ (GeV)	γ
MSU	Khristiansen et al.[9]	10^5-5.10^7	10	0.78±0.01
MSU	Bazutov et al. [12]	6.10^4-3.10^6	(10-500)	0.78
MSU	Vaskevich et al.[13]	5.10^4-3.10^6	50	0.76±0.03
			100	0.76±0.03
Present expt		2.10^4-10^6	(2.5-100)	0.73±0.03

Atreshkvich et al.[11], presenting the measurements of another MSU experiment have reported the measured ratios of number of muons $N_\mu(\geq E_\mu)$ to the shower size Ne representing the percentage of muons having energy above a particular threshold energy E_μ in EAS of size $Ne=10^6$. These values of percentages of muons measured and reported by them are shown in Table-10 along with those measured in the present experiment.

Table 10: The percentages of muons in EAS of size $Ne=10^6$ measured in MSU and present experiments

Experiment	$\geq E_\mu$ (G eV)				
	10	20	50	100	200
MSU [11]	2.2	---	0.33	0.13	0.047
Present	1.6	0.79	0.31	0.12	---

The table shows that the two measurements are in good agreement at higher threshold energies but differs slightly at lower energies.

Vaskevich et al. [13], measuring the integral energy spectra of muons in showers of size 10^6, have pointed out that the measured energy spectra cannot be represented by a power type of function written as $N_\mu \sim E_\mu^{-\delta}$ with the same exponent throughout the energy range of 10-500 GeV. So, taking smaller ranges of energies and fitting their measurements to the above function they have reported of obtaining the values of exponent δ as 1.19±0.03 and 1.58±0.05 respectively for the energy ranges (10 to 100) GeV and (100 to 500) GeV. In the present experiment too, it was observed

that the measured energy spectra of muons for the whole range of energy 2.5 to 100 GeV could not be represented by a function of power form. But, as pointed out earlier in section 4.4.2, the spectrum in the smaller range of 10 to 100 GeV can be approximated by such a function. And, as mentioned in Table-6, the value of exponent δ obtained by fitting the number of muons measured in the showers of size 10^6 is equal to 1.10 ± 0.04, which is seen to be close to that obtained by Vaskevich et al.[13] in the MSU experiment.

4.6 Comparision of the Measurements of Present Experiment with Some Theoretical Results Calculated with Different Models of High Energy Particle Interaction

The phenomenon of EAS, as such, is a great source of information about the characteristics of particle interactions at high energies, which are much beyond the energy region of accelerators. However, many interactions intervene between the initial collision of Primary Cosmic Ray (PCR) particle with the nuclei of atmospheric target and the observed air shower of particles at some level of observation, which is usually at great depths of atmosphere. Hence, to interpret the results of EAS observations a detailed reconstruction of shower formation is necessary. For this reconstruction, assuming a particular model which describes the characteristics of particle interactions at high energy, air shower events are theoretically simulated with different composition of PCR and a number of observable features of the EAS are calculated. These calculated results could then be compared with those measured in experiments for testing the validity of the assumed models.

An introduction of theoretical models and the techniques of simulation of EAS in general are presented in section 1.3 and 1.4 of Chapter I of this thesis. And, a brief summary of important characteristics of different high-energy particle interaction models, which were used by different authors for the simulation of EAS events, is presented in section 2.3 of Chapter II. Here, in this section, a comparative study of some theoretical results describing the different characteristic features of muon component of EAS, as calculated and reported by different authors using various theoretical models, with some of the representative measurements of the present experiment is presented.

4.6.1 Results obtained with the Scaling Model

Many investigators have used the scaling model of high-energy hadron

interaction proposed by Feynman [14] to calculate the different features of EAS. In fig. 4.15 the lateral distribution of muons in the air showers of an average size of 2.10^5 calculated by Grishina et al.[10] using the above model with proton and iron as the primaries are shown along with those measured in the present experiment. Similarly, in fig. 4.16 the calculated variations [15] of total number of muons N_μ for the energy threshold of 10 GeV with shower size Ne are shown along with the measurements of the present experiment.

These figures (4.15 & 4.16) show that the measurements of the present experiment do not agree with the calculated results obtained with scaling model assuming mono-nuclear compositions of the PCR. However, it is noticeable from the above comparisons that the calculations performed with heavier primaries (A=56) show some improvement in comparison to that calculated with pure proton primaries but still the discrepancies are seen to be significant.

4.6.2 Results obtained with some Scale Breaking Models

As described earlier in section 2.3.1 of Chapter II, the earlier indications of failure of the scaling model to predict the EAS characteristics as measured in different experiments, which is also observed in the present experiment, have led to the proposals of a number of so-called scale breaking models. The calculated results obtained by using some of these models are compared, in fig. 4.17 & 4.18, with the measurements of the present experiment

In fig. 4.17 the variation of number of muons having energy $E_\mu \geq 10$ GeV with the shower size Ne calculated by Mikocki et al. [16] and Cheung & MacKeown [17] for two different mononuclear (proton and iron) compositions of PCR are shown along with that measured in the present experiment. The calculated result of scaling model as reported by Gaisser et al. [15] is also shown in the figure for comparison.

The basic features of the models for particle interaction at high energy used by the above authors for the simulation of the air showers are summarized in section 2.3.2 of Chapter II. The model used by Cheung and MacKeown [17] for their calculation incorporates violation of scaling to the degree suggested by Wdowczyk and Wolfendale [18] for the spectrum of secondary particles resulting from the interactions of leading nucleons at energies more than 2.10^{13} eV but for all other interactions scaling in radial variable (X_R) is retained. Whereas, the model W00 utilized by Mikocki et al. [16] in their simulation of air showers has features that show

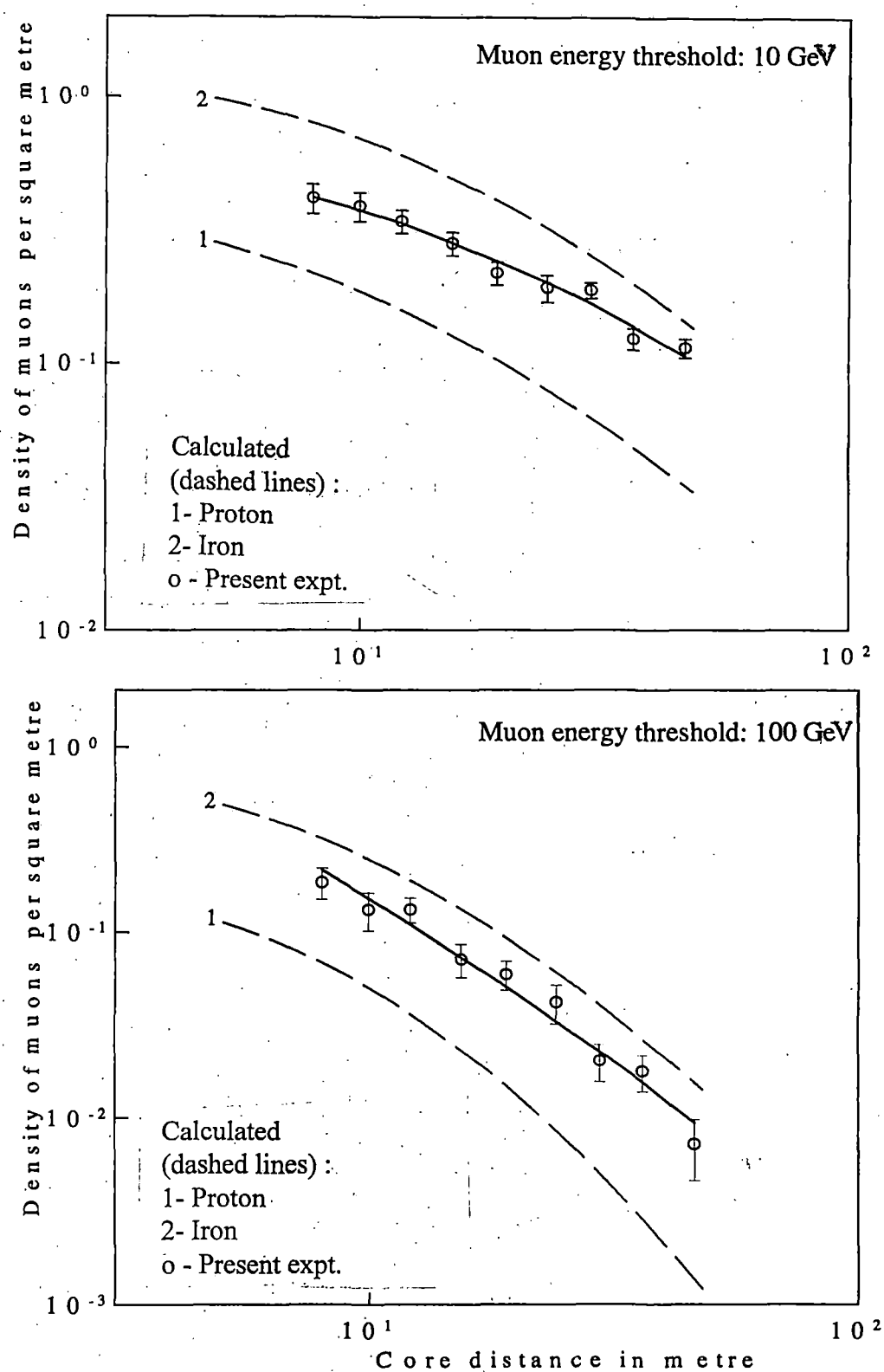

Fig. 4.15 COMPARISON OF LATERAL DISTRIBUTION OF MUONS IN EAS OF AVERAGE SIZE 2 X 10^5 MEASURED IN THE PRESENT EXPERIMENT WITH THOSE CALCULATED BY GRISHINA et al.[10] WITH SCALING MODEL FOR TWO DIFFERENT PRIMARIES. THE EXPERIMENTAL MEASUREMENTS ARE SHOWN WITH THE BEST FITTED LINES (SOLID)

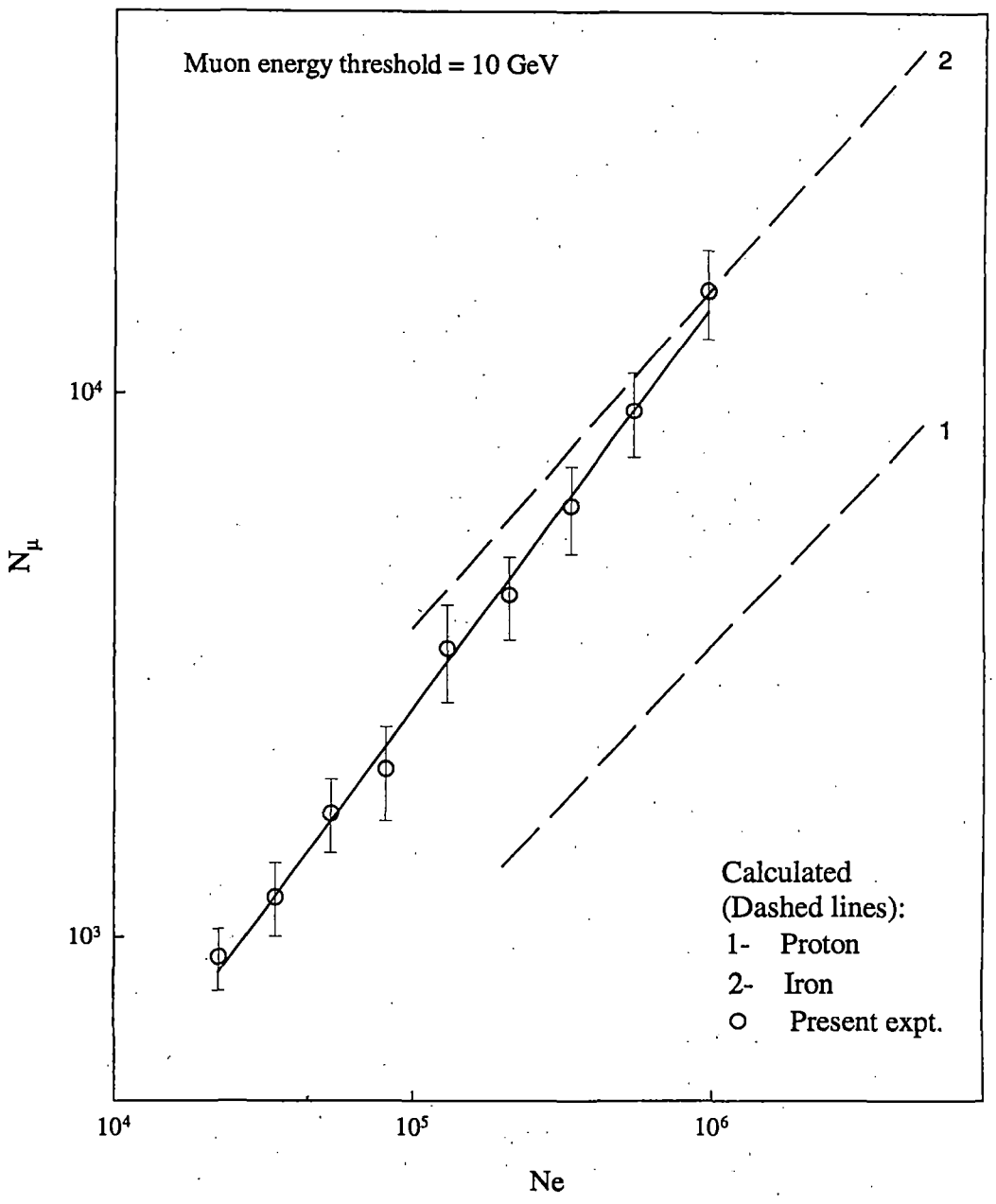

Fig. 4.16 COMPARISON OF THE VARIATION OF NUMBER OF MUONS(N_μ) WITH SHOWER SIZE (Ne) MEASURED IN PRESENT EXPERIMENT WITH THAT CALCULATED BY GAISSER et al.[15] WITH SCALING MODEL FOR TWO DIFFERENT PRIMARIES. THE MEASUREMENTS OF THE PRESENT EXPERIMENT ARE SHOWN WITH BEST FITTED LINE (SOLID).

scaling behavior below the energy of 1TeV, which at higher energies is violated mildly in the fragmentation region but strongly in the central region.

The fig. 4.17 shows that the measurements of the present experiment are comparatively closer to the results calculated with the models violating scaling at higher energies and assuming proton as the primary than to those calculated with scaling model.

Similarly, in fig. 4.18 the measurements of present experiment are compared with the calculated results of Wdowczyk & Wolfendale [18], Kalmykov et al. [19,20] and Capdevielle [21] obtained by using other scale breaking models of particle interaction and the normal mixed composition of the primary cosmic rays.

Wdowczyk & Wolfendale [18, 22-24], analyzing the data on inclusive spectra of secondary pions produced in hadron-hadron collisions at different energies E_o (laboratory system) measured in FNAL (E_0~10^{10}eV), ISR (E_0~10^{12}eV) and CERN Sp$\bar{p}$ S (E_0~2.10^{14} eV) experiments, had pointed out indications of scaling violation at the energy region investigated by these experiments. And, they had further proposed to introduce a scale-breaking factor $(s/s_0)^{\alpha}$ in the energy spectrum of the secondary particles as,

$$\frac{1}{\sigma_t}\frac{d\sigma}{dp_l\,dp_t} = \frac{K(s,s_0)}{E}\left(\frac{s}{s_0}\right)^{\alpha} f\left[\frac{p_l}{p_{max}}\left(\frac{s}{s_0}\right)^{\alpha}, p_t\right]$$

where, σ_t is the total cross-section for p-$\bar{p}$ collision in which a secondary pion has momentum components p_l (longitudinal) , p_t (transverse) and energy E. The parameter 'α' represents the degree of scaling violation between energies $\sqrt{s}$ and $\sqrt{s_0}$ in center of mass system. The inelasticity factor $K(s,s_0)$ is the ratio of inelasticities of charged pions at energies $\sqrt{s}$ and $\sqrt{s_0}$. The values of the parameter 'α' and $K(s,s_0)$ estimated by them in the energy range of E_0 ~2.10^{14} eV were, respectively, between 0.18 to 0.20 and 0.6.

Using this distribution of the secondaries, the same authors have calculated different observable features of EAS [18,23-24] and their calculated results representing the variation of N_μ ($E_\mu \geq 10$GeV) with Ne by considering a normal mixed composition of PCR, as reported in [18], is shown as dotted lines in the fig. 4.18. In

this calculation the values of parameters α & $K(s,s_0)$ of the above equation, considered to change with primary energies E_0, were taken as α = 0.173, 0.21,0.248 & 0.285 respectively at $E_0 = 10^{14}$, 10^{15}, 10^{16} & 10^{17} eV , $K(s,s_0) = K_{\pi}\pm(s) / K_{\pi}\pm(s_0) = (s/s_0)^{-0.061}$ and $K_{\pi}o = (s/s_0)^{-0.042}$.

The calculated results reported by Kalmykov et al.[19] and Capdevielle[21], which are also shown in the fig. 4.18, were obtained by using the Quark Gluon String (QGS) model and the Dual Parton (DP) model respectively. In these models, the particle interactions at high energies are described with the quark-gluon (parton) picture of the hadron structure. The multiple hadron productions at these interactions are considered as the result of creation and breaking of quark-gluon strings, which are created by gluon exchange and stretches between the two colliding hadrons. The interaction cross-section and the inclusive spectra of secondary particles are calculated in terms of functions describing the distribution of quarks in the colliding hadrons and fragmentation of quarks & diquarks into secondary hadrons.

Combining this QGS model of hadron interactions at high energies with the theory of Super Critical Pomeron, which is a pomeron for which the value of Regge Pole trajectory at zero momentum transfer $\alpha_p(0) = 1+\Delta$ ($\Delta > 0$), Kalmykov et al. [19-20,25-26] have calculated different characteristic features of muon and hadron components of EAS with different values of the parameter Δ . The results of their calculation [19] showing the variation of N_{μ} ($E_{\mu} \geq 10$ GeV) with shower size Ne is shown as long dashed lines in the fig. 4.18. In this calculation the composition of the PCR was considered to be normal mixed composition with 40% proton and 15% each of other elements with mass number A= 4,15,29 & 56 and the value of parameter Δ was taken as 0.07.

Among the different calculated results describing the variation of N_{μ} with Ne obtained by assuming normal mixed composition of the PCR shown in fig. 4.18, the calculation of Kalmykov et al. is seen to be comparatively in closer resemblance with the measurements of present experiment. The slope 0.74±0.02 of the best fitted line (represented as solid line in the figure) obtained by fitting the measurements of the present experiment to the function of the form $N_{\mu} \sim Ne^{\alpha}$ was also observed to be nearer to that of the line representing the calculations of Kalmykov et al., which was

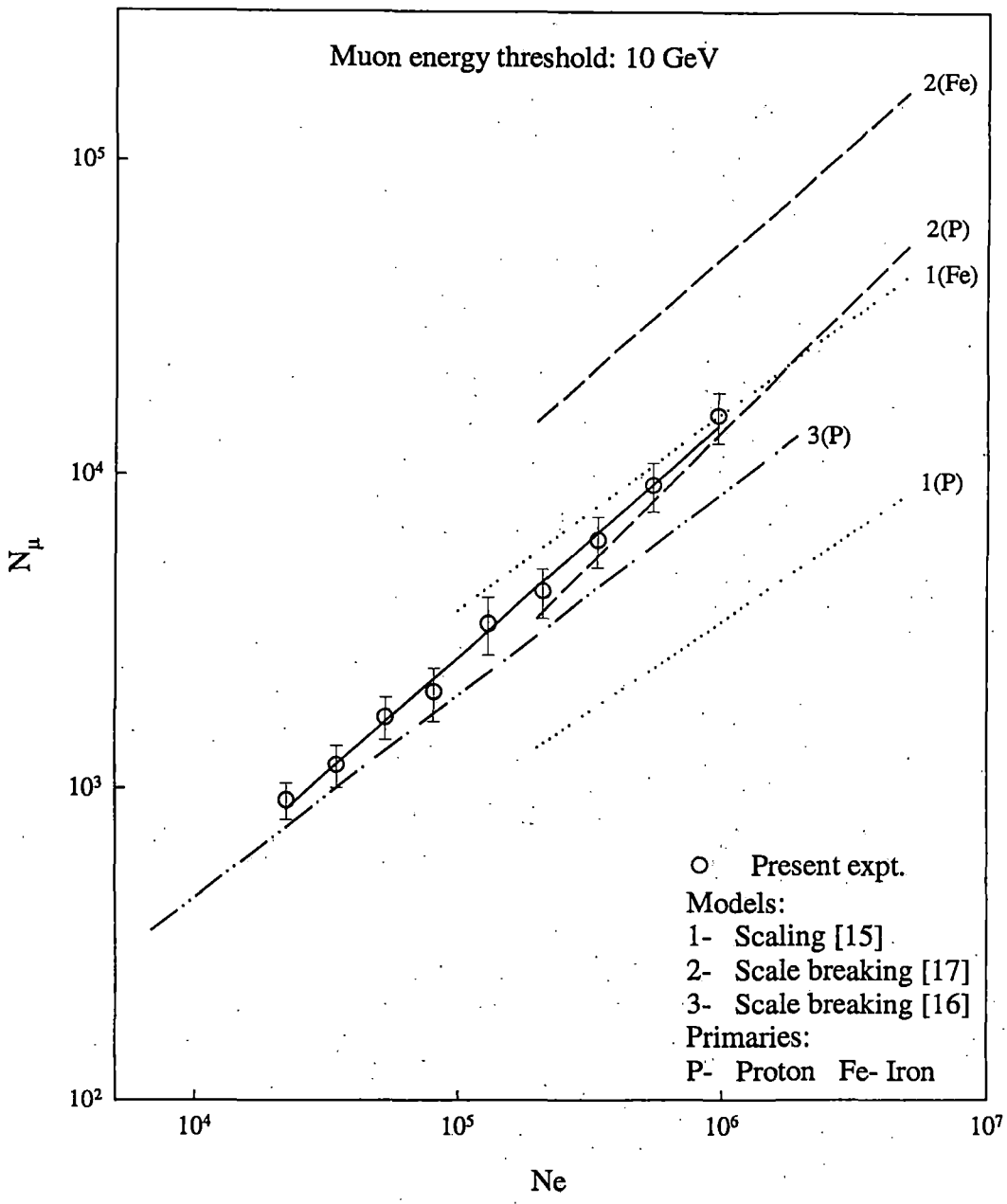

Fig. 4.17 COMPARISON OF THE VARIATION OF NUMBER OF MUONS (N_μ) WITH SHOWER SIZE (Ne) MEASURED IN PRESENT EXPERIMENT WITH THOSE CALCULATED WITH SCALING (GAISSER et al.[15]) AND SCALE BREAKING (CHEUNG & MACKEOWN[17] AND MIKOCKI et al.[16]) MODELS ASSUMING DIFFERENT PRIMARY COMPOSITIONS. MEASUREMENTS OF PRESENT EXPERIMENT ARE SHOWN WITH BEST FITTED LINE (SOLID).

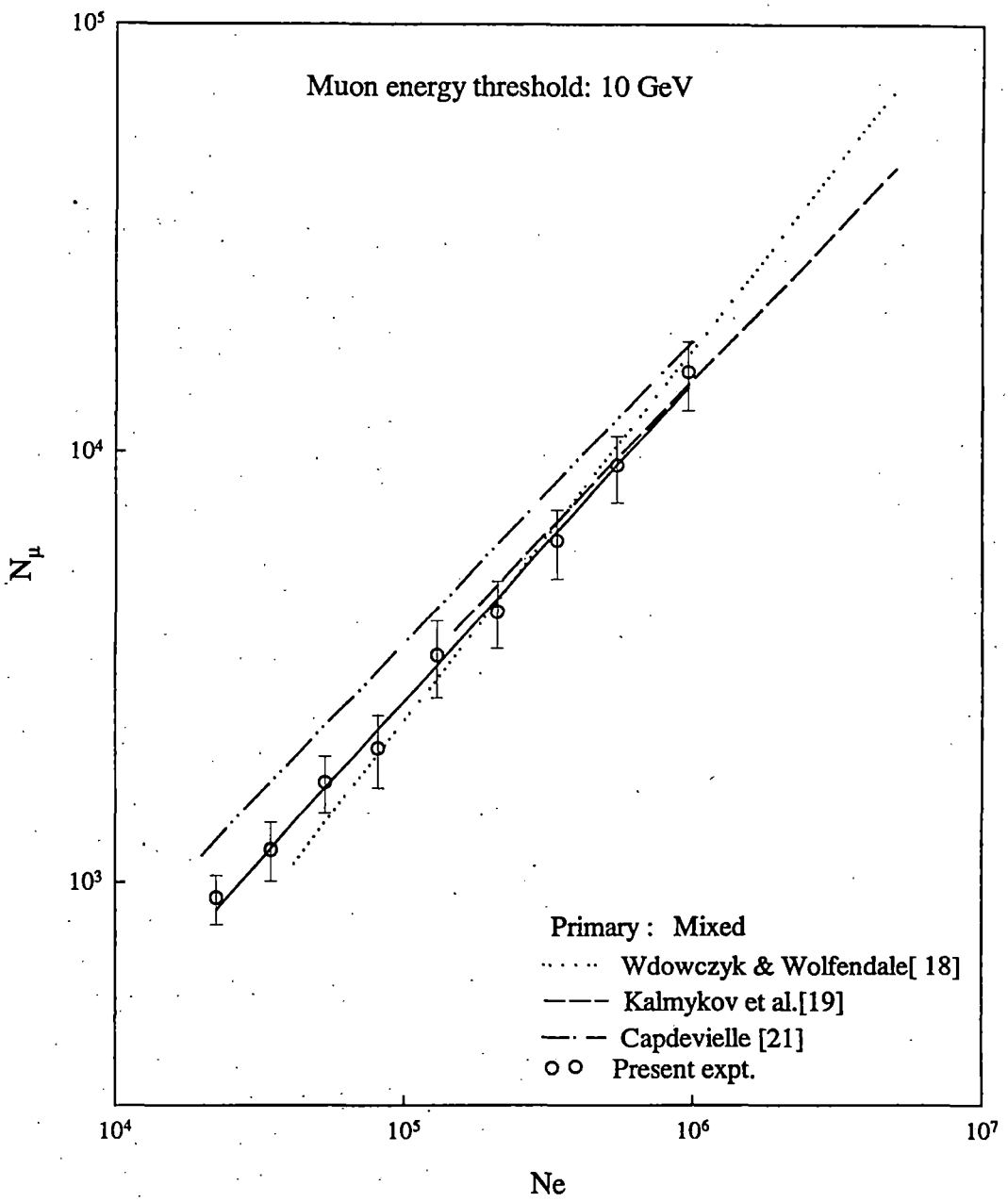

Fig. 4.18 COMPARISON OF THE VARIATION OF NUMBER OF MUONS (N_μ) WITH SHOWER SIZE (Ne) MEASURED IN PRESENT EXPERIMENT WITH THOSE CALCULATED WITH SOME SCALE BREAKING MODELS ASSUMING NORMAL MIXED COMPOSITION OF PRIMARIES. MEASUREMENTS OF PRESENT EXPERIMENT ARE SHOWN WITH BEST FITTED LINE (SOLID).

reported by the authors [20] to be equal to 0.73. Whereas, the slopes of the lines representing the calculated results of Wdowczyk & Wolfendale and Capdevielle, estimated from their reported results were, respectively, 0.81 and 0.70.

4.6.3 Results obtained with the Quark Gluon String (QGS) Model

It was pointed out earlier in section 2.3.3 of Chapter II of this thesis, that many investigators have used the QGS model of hadron interactions at high energies for the simulation of EAS events to study their various features at different levels of observation. Several authors such as Vaskevich et al. [27], Sleptsova et al. [28] and Atrashkevich et al.[29] have reported results of their calculations describing the distribution of muons in EAS at sea level obtained by using this model. Some of the calculated results reported by these authors are compared here with the results of measurements in the present experiment.

Vaskevich et al. [27], utilizing the characteristic properties of hadron-hadron and hadron-nucleus interactions calculated on the basis of QGS model by Kalmykov et al. [19,26], Kaidalov et al. [30] and Shabelskii [31], had performed extensive calculations of different features of muons in EAS. And, they have pointed out that number of muons N_μ ($\geq E_\mu$) in an EAS with fixed shower size Ne to be the most sensitive, amongst the different features of EAS, to the variation in values of the model parameter Δ and inelasticity coefficient K. Allowing the values of Δ and K to vary from 0.07 to 0.12 and 0.5 to 0.6, respectively, the authors have calculated different features describing the distribution of muons with energies $E_\mu \geq$ 50 to 2000 GeV in air showers of sizes 5.10^4 to 3.10^6. Some of their calculated results obtained by assuming normal mixed composition of primary with average mass number $\langle A \rangle = 14.7$ and different values of Δ and K are shown in fig. 4.19 to 4.21 along with the corresponding measurements of the present experiment.

The fig. 4.19(a) & (b) show the lateral distribution of muons with energies $E_\mu \geq$ 50 and 100 GeV in EAS of size $Ne=10^6$ calculated by Vashkevich et al. [27] with Δ=0.07 to 0.12 and K= 0.5 to 0.6 along with the corresponding measurements obtained in the present experiment. It can be observed from these figures that the densities of muons measured in the present experiment are fairly well represented by the calculated distribution. However, with the measurements of the experiment no distinction can be made among the distributions calculated with different values of

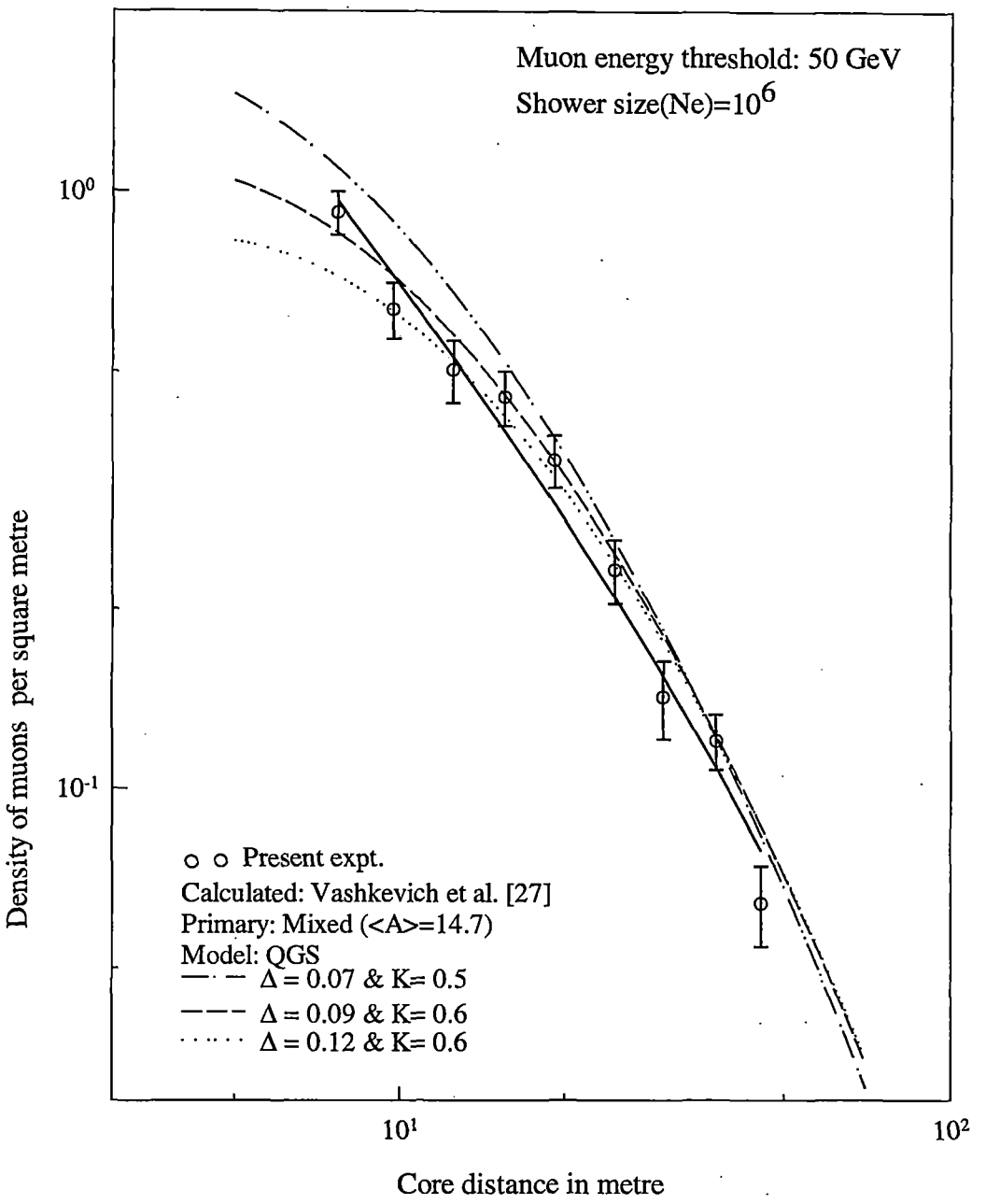

Fig. 4.19(a) COMPARISON OF LATERAL DISTRIBUTION OF MUONS IN EAS OF AVERAGE SIZE 10^6 MEASURED IN PRESENT EXPERIMENT WITH THOSE CALCULATED BY VASHKEVICH et al. [27] USING QGS MODEL WITH DIFFERENT PARAMETERS (Δ & K). THE MEASUREMENTS OF THE PRESENT EXPERIMENT ARE SHOWN WITH BEST FITTED LINE (SOLID).

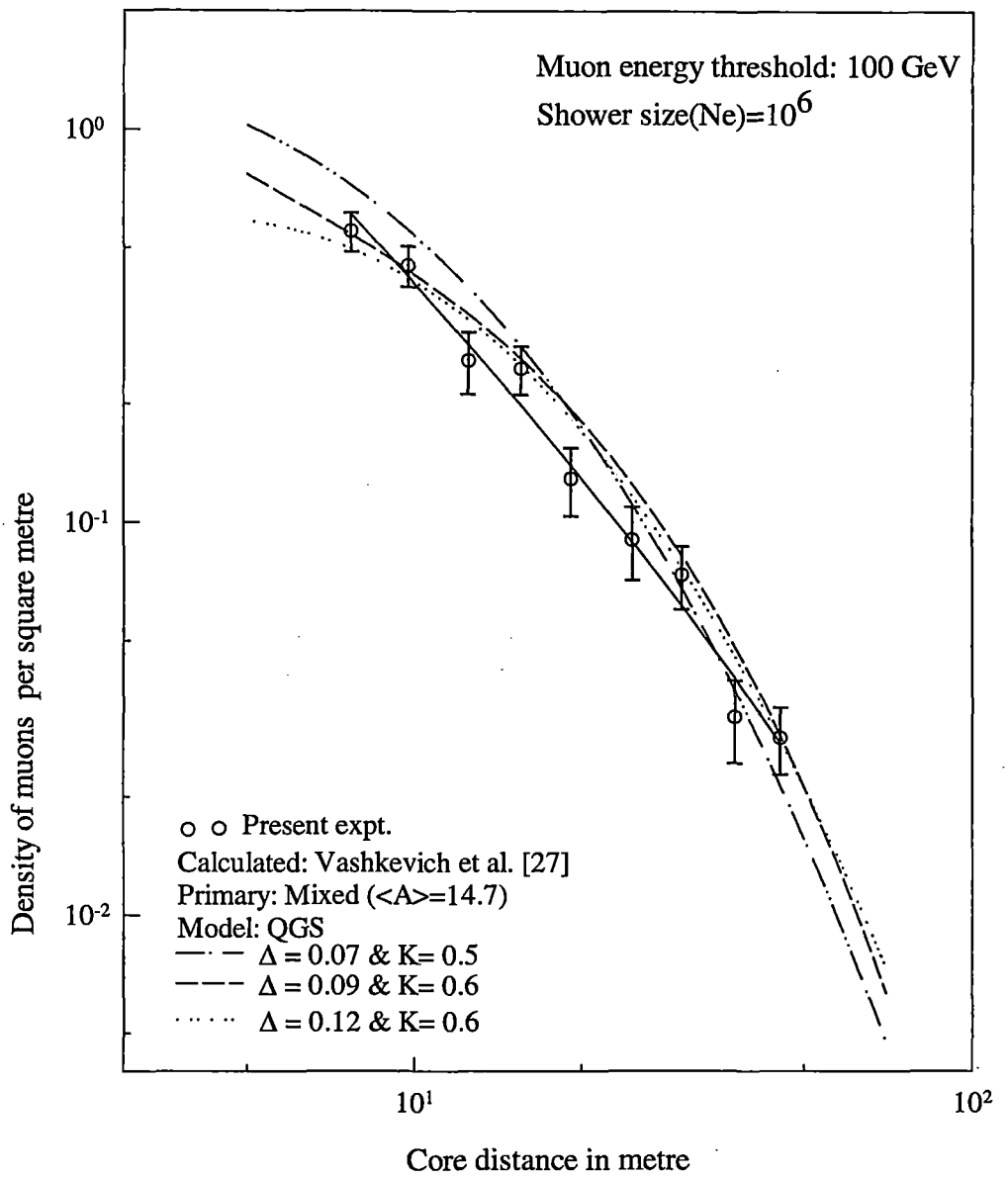

Fig. 4.19(b) COMPARISON OF LATERAL DISTRIBUTION OF MUONS IN EAS OF AVERAGE SIZE 10^6 PARTICLES MEASURED IN THE PRESENT EXPERIMENT WITH THOSE CALCULATED BY VASHKEVICH et al.[27] USING QGS MODEL WITH DIFFERENT PARAMETERS (Δ & K). THE MEASUREMENTS OF PRESENT EXPERIMENT ARE SHOWN WITH BEST FITTED LINE (SOLID).

parameters.

Atrashkevich et al. [29] have pointed out that the lateral distribution of muons calculated with QGS model, if approximated by a function of the form $\rho_\mu \sim r^{-\beta} \exp(-r/r_o)$, show a weak dependence on the size of the shower. They have further reported that the value of 'β', determined from the calculated distribution of muons with threshold energy 10 GeV, changes from 0.61 to 0.70 when shower size Ne is increased from 10^5 to 5.10^7. Similar feature about the lateral distributions of muons was also observed in the present experiment. As mentioned earlier in the section 4.3.1 of this chapter, the distributions measured in the present experiment approximated by the same type of function shows a slow variation of exponent 'β' with shower size Ne. And, for muons with threshold energy of 10 GeV 'β' was observed to change from 0.45 ± 0.02 at $Ne=2.10^4$ to 0.53 ± 0.03 at $Ne = 10^6$.

The integral energy spectrum of muons in the EAS of size $Ne=10^6$ calculated by the vaskevich et al.[27] with the values of model parameters $\Delta=0.09$ & $K=0.6$ considering normal mixed composition of the primary with $\langle A \rangle = 14.7$ is shown in fig. 4.20. The calculated spectrum represented by the dashed line in the figure is seen to be in excellent agreement with the measurements of the present experiment. Representing the calculated spectrum in the energy range (10-100) GeV by the function of the form $N_\mu \sim E_\mu^{-\delta}$, the value of '$\delta$' reported by the authors was 1.14 which is very close to the value 1.10 ± 0.04 obtained by fitting the measurements of present experiment with the function of same form.

In Table-11, the percentages of muons for different energy thresholds in EAS of two different sizes as calculated by Vaskevich et al.[27] and Sleptsova et al. [28] using the same QGS model of particle interactions but with different compositions of primaries, are compared with that measured in the present experiment .

It is seen from the table that the percentages of muons in EAS measured in the present experiment are very close to that calculated by Vaskevich et al.[27] with mixed composition of the primary but on the other hand, those calculated by Sleptsova et al.[28] with only proton as the primary are much less than that measured in the experiment.

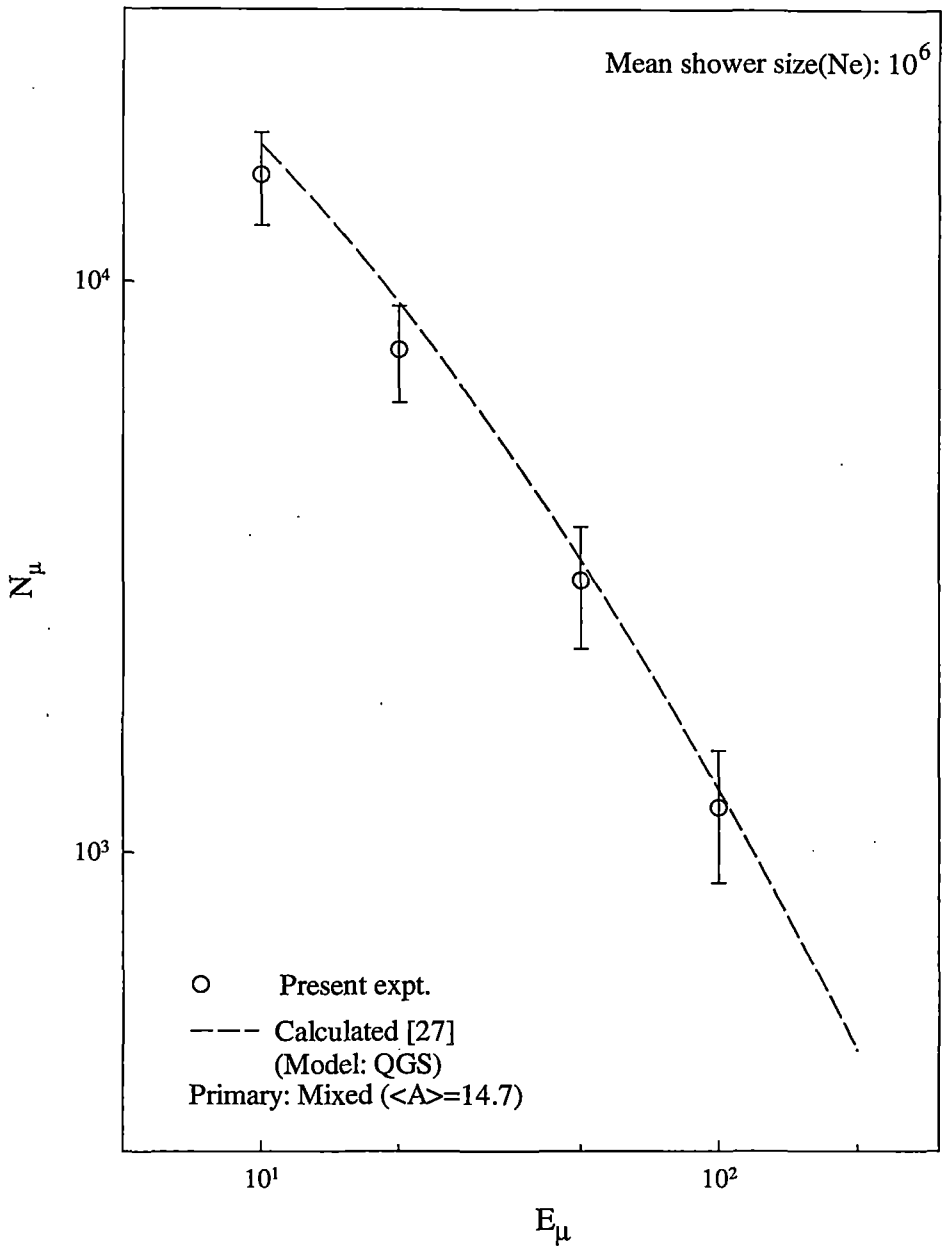

Fig. 4.20 COMPARISON OF THE INTEGRAL ENERGY SPECTRUM OF MUONS IN EAS OF AVERAGE SIZE (Ne) 10^6 MEASURED IN PRESENT EXPERIMENT WITH THAT CALCULATED BY VASHKEVICH et al. [27] USING QGS MODEL (Δ=0.09 & K=0.6) AND NORMAL MIXED COMPOSITION OF PRIMARY.

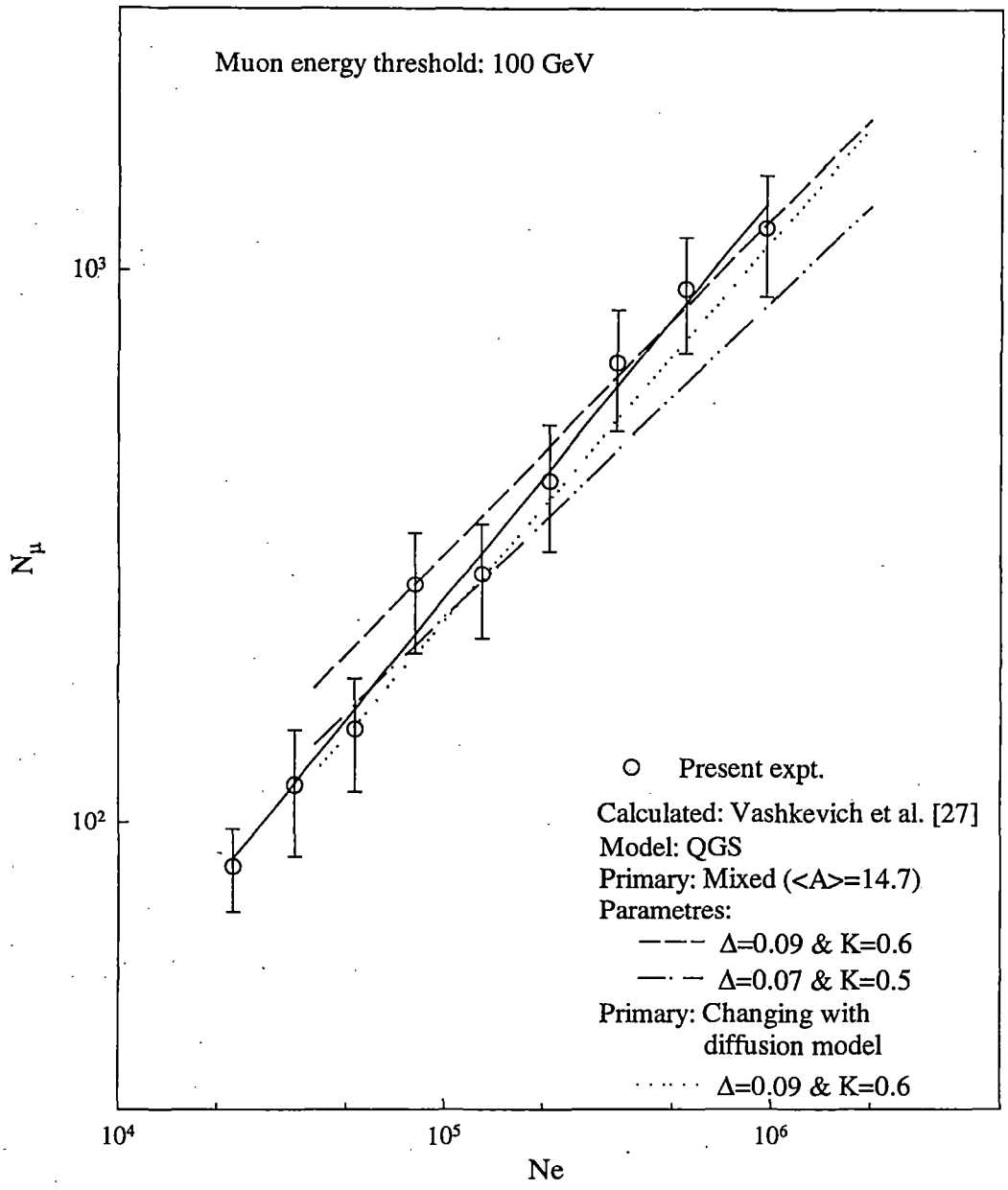

Fig. 4.21 COMPARISON OF THE VARIATION OF NUMBER OF MUONS (N_μ) WITH SHOWER SIZE (Ne) FOR MUON ENERGY THRESHOLD OF 100 GeV MEASURED IN THE PRESENT EXPERIMENT WITH THOSE CALCULATED ON THE BASIS OF QGS MODEL [27] ASSUMING DIFFERENT PRIMARY COMPOSITIONS. THE MEASUREMENTS OF PRESENT EXPERIMENT ARE SHOWN WITH BEST FIT LINE (SOLID).

Table 11: Percentages of muons in EAS calculated with QGS Model assuming different primary compositions and measured in present experiment

$\geq E_\mu$ (GeV)	Ne=10^6		Ne=5.10^5	
	Primary Mixed [27]	Present expt.	Primary Proton [28]	Present expt
10	1.85	1.60	1.21	1.69
20	0.84	0.79	0.56	0.98
50	0.32	0.31	0.16	0.42
100	0.13	0.12		

In fig. 4.21, the calculated results of Vashkevich et al. [27] representing the variation of number of muons having energy $E_\mu \geq 100$ GeV with the size of the shower is shown along with the corresponding measurements of the present experiment. The dashed and dash-dot-dot lines in the figure represent the variations calculated by assuming the same mixed primary with <A>=14.7 but for two different sets of model parameters. It can be observed from the figure that the total number of muons $N_\mu(\geq E_\mu)$ measured in the present experiment are well within the values calculated by the model with the parameters Δ & K, respectively, ranging from 0.07 to 0.09 and 0.5 to 0.6. However, it is seen that the slope of calculated variations are smaller than that of the measured variation represented by the best fit line (indicated by solid line) obtained with the measurements of the experiment. But, it can further be noted that the resemblance between the two improve if the variation calculated with primary composition changing with energy is considered. The dotted line in the figure represents the result of calculation obtained by the same authors with the assumption of a change in the nuclear composition of primary cosmic ray according to the diffusion model [32] in the region of so called 'bend' in the primary energy spectrum at $E_0=3.10^6$ GeV. In their assumption of the primary composition, the fraction of proton was taken to be 0.65 at energy range below the bend (10^6-3.10^6 GeV) which decreases to 0.41 at energy $E_0=10^7$ GeV.

4.7 DISCUSSION AND CONCLUSION

The investigation of two primary components of EAS, the electron and muon components, carried out in the present experiment with NBU air shower array, has provided various information about the characteristic features of structure or the

distributions of these two components in the EAS of size ~10^4 to 10^6. Before summarizing these results, a few points about the performance of the air shower array as a whole, the procedures of data acquisition and their subsequent analysis may well be discussed here, even though it has been described in detail in Chapter III of this thesis.

The NBU air shower array, initially operating with 21 scintillation detectors, covers comparatively a small area. And hence, has the limitation of recording density information only from a small portion of the incident shower of particles, which usually spreads up to large distances. These density information were utilized to determine the different parameters which characterize each of the recorded showers. However, the closely packed arrays such as this one, with small detector spacing (~ 7 meter in the NBU array) will have a definite advantage in its ability to locate the shower core from the measured densities more accurately than the arrays covering wide areas but detectors arranged with larger spacing.

In the present experiment, the shower parameters- shower size (Ne), shower age (s) and coordinates of the shower core (X_0,Y_0) were estimated by using Hillas structure function and the method of χ^2-minimization through an iterative process based on the method of steepest descent. To estimate the uncertainties in the results obtained due to the statistical fluctuations and any systematic error in calibration procedures, which might produce a systematic biasing of the results, a careful analysis of artificially simulated air showers (described in section 3.7.1 of Chapter III) were performed with the same method. From this analysis the average values of uncertainties in the determination of shower size (Ne), shower age (s) and the shower core (X_0,Y_0) were calculated as, respectively, ±0.15Ne, ±0.09 and ±1.1m.

Here, it may be pointed out that the observed decrease of average age 's' of air showers with their size (Ne) in the present experiment is consistent with the earlier observations of other investigators. Hara et al. [33] and Acharya [34], respectively, reporting the results of Akeno (Japan) and TIFR (India) experiments, had observed such decrease in the shower age when the showers were grouped according to their sizes. Similarly, the overall average value of shower age calculated for all the recorded showers in the present experiment is 1.28 which is not very far from the theoretical estimate, 1.33 of Fenyves [35] for the air showers observed at sea level.

It has been pointed out in section 3.7.2 of Chapter III that the detection efficiency of the array was observed to vary with both shower size and the radial distance from the array center. Furthermore, it has also been noted that the detection efficiency of the array falls off rapidly after a certain distance of (30-35) metre from the center of the array and this distance is still smaller, about (20-22) metre for the showers of smaller sizes. This variation of detection efficiency might lead to an underestimation of muon density in the showers, as in the present experiment the density of muons were estimated in purely statistical method from the number of showers detected with and without muons passing through the two magnetic spectrographs. However, since the number of shower events analysed in the experiment was quite large (above 36,000) the error due to this underestimation is expected to be low.

In addition to these overall performances of the array, the performances of other different components of the array may as well be mentioned here. The transition effect arising from the multiplication and absorption of shower particles due to finite thickness of plastic scintillators used in the scintillation counters of the EAS array was taken into account by correcting the observed density in the manner as suggested by Asakimori et al. [2]. The calibration of each of the scintillation counters were verified time to time and the pulse height of each of them was kept nearly same by regulating the operating voltage.

Similarly, in the operation of magnetic spectrographs, the high-voltage pulses applied to the neon flash tubes were maintained according to the requirement for maximum efficiency of the flash tubes. The width and the height of the pulses were chosen in compromise for the minimum occurrence of so called 'spurious flashes' which could have been misleading in the analysis of photographic films while determining the momentum of recorded muons. The stability of the magnetic fields of the solid iron electro-magnets were tested and an optimum value of the excitation current was used, which was also decided in compromise for the minimum heat production in the coil of the magnets. The leakage field outside the magnets, which might cause error in the measurement of deflection of muons was checked and found to be negligible. The alignment of each of the four units of the two magnetic spectrographs, which might cause a large error in momentum measurement was ensured up to an accuracy of 0.2mm and was checked time to time. Moreover, to

estimate the error in deflection measurement due to defect in alignment, error in location of tracks at each neon flash-tubes tray and the multiple Coulomb scattering in the iron, the spectrograph was operated by means of G.M. pulse only without the excitation current and hence no magnetic field. In this condition, the observed deflections of the muons passing through the spectrograph would purely be due to the reasons mentioned above. However, the later two of them cause the deflections positive and negative with equal probability and hence the distribution of deflection in the zero magnetic field condition was seen to follow a sharp Gaussian distribution with mean value zero, indicating the error in alignment of the spectrograph to be small. The momentum corresponding to this most probable error in the deflection, called the maximum detectable momentum (m.d.m.) of the magnetic spectrograph was calculated to be 484(±23) GeV/c. In the present experiment a few number of muons with energies near to this value were detected but due to their small number and hence low statistics the maximum muon energy threshold for the analysis of final results was kept at 100 GeV.

The measurements obtained in the present experiment show a fairly good consistency, when compared with few representative high precision measurements of MSU experiments. As pointed out earlier, apart from the similarities in the level of observation and methods of measurement, a significant portion of the regions of shower size and threshold energy of muons investigated in MSU experiment overlap with that investigated in the present work. And hence, the comparison was possible and justified too.

The different characteristic features of the distribution of muons in EAS of sizes 2.10^4 to 10^6 observed in the present experiment are also seen to be consistent with those reported by other authors as observed in their experiments or in the analysis of their data calculated by theoretical simulation of EAS events. The measurements, in the present experiment, of lateral distribution and energy spectra of muons in the air shower of different sizes have shown that the shape of these both, such distribution and spectra, do not change much with the size of the shower in the region of shower sizes studied. Similar observations were reported by Vashkevich et al. [13] from their experimental investigation of air showers with sizes $\sim 10^5$-10^6 particles, and by Atreskevich et al. [29] from their analysis of results obtained theoretically with QGS model of hadron interactions at high energy in the shower size

range of 10^5 to 10^7.

Similarly, in another observation of the present experiment the variation of muon density (ρ_μ) with the shower size (Ne), when approximated by a function of the form $\rho_\mu \sim Ne^\alpha$ then the value of exponent 'α' was seen to vary with the radial distance from the shower core. Similar observations were reported earlier by Fomin et al. [36] and Capdevielle et al. [37]. These authors, respectively, using QGS and a sort of semi-empirical model inspired by Dual Parton model of hadron interactions, had noted that their theoretically simulated data, if fitted to a function of the above type, then the value of exponent 'α' decreased with radial distance from the shower core.

However, in the analysis of dependence of the total number of muons N_μ with shower size Ne, expressed as $N_\mu \sim Ne^\gamma$, the variation of exponent 'γ' with muon energy threshold observed in the energy range of 50 to 500 GeV as noted by Vaskevich et al. [13] was not observed in the analysis of the present experiment with muons having threshold energies 2.5 to 100 GeV. Whereas, their observation of integral energy spectra of muons being not representable by a function of power type with same exponent in the whole range of energy investigated (50-500GeV), which in smaller ranges of energy such as 10 to 100 and 100 to 500 GeV can be approximated by this function, is well supported by the results of the present experiment and value of 'δ' for the spectra in the range 10 to 100 GeV determined in these experiments are seen to be quiet close to each other.

The comparison of few representative measurements of the present experiment with the results calculated by using scaling models of particle interactions, as reported by different authors, show large discrepancies, which of course lessen if heavy primary composition is considered but still the discrepancies are seen to be significant. The comparison is observed to improve if the calculations based on models violating scaling are taken. The experimental measurements representing the dependence of N_μ ($E_\mu \geq 10$GeV) with the size of the shower (Ne), when compared with the calculations of some scale breaking models, as presented in fig. 4.17 & 4.18, show closer resemblance with the calculated results obtained by using QGS model and normal mixed composition of the primary cosmic ray. The value of exponent 'γ' in the relation $N_\mu \sim Ne^\gamma$, representing the above dependence, obtained from the

calculated result and the experimental measurement are also observed to be close to each other. But, it may be mentioned here that Kalmykov et al. [20] have reported increase in the value of exponent 'γ' from 0.73 to 0.78 if the primary composition is assumed to change with the energy according to diffusion model. Similar feature of increase in the slope of the variation (N_μ vs. Ne) is shown by Vaskevich et al.[27] for muons with $E_\mu \geq 100$ GeV when primary changing with energy is considered and measurements of present experiment show better resemblance with this calculation in comparison to that calculated with permanent non-changing mixed composition. However, further comparison of the other features of muons in EAS show that the measurements of the present experiment are fairly well represented by the calculated results obtained with permanent normal mixed composition of the primary.

It may also be pointed out here that, in the further effort of improving the calculations based on QGS model Kalmykov et al. [20 & 38] have investigated the effect of charm production and jet generation in the EAS calculations and have pointed out that the variation due to the inclusion of these two processes on the number of particles at cascade maximum is less than 1%. Similarly, in recent years [39 & 40] they have further improved the traditional QGS model by including new features of high energy interactions shown by the experimental evidences. Observing the fluctuations in EAS generated by primary nuclei exceeding the predictions of superposition model used previously for calculations of nucleus-nucleus interactions, the configuration of these interactions has been simulated directly according to Glauber approach. Diffractive dissociation of nucleons is included in the model. Fragmentation of the spectator part of the projectile nucleus is taken care by Percolation-evaporation model [41]. In the hadron-nucleus interactions the fluctuations associated with number of interacting nucleons of target nucleus, number of pomeron strings and the process of string fragmentation are taken into account. Similarly, taking note of the indications from modern collider data about the increasing influence of the so called semi-hard processes on high energy hadron interactions this mechanism is included in the base model of QGS. However, the authors have pointed out that the calculated results with this new improved model do not change the average characteristics of EAS but they appreciably enhances the fluctuations in comparison with those calculated with the previous version of the model. The inclusion of semi-hard processes have been observed to produce some

changes in the prediction of EAS characteristics but these change are seen to be significant only at primary energies $E_o > 10^{17}$eV.

The calculations of inclusive spectra of secondaries with QGS model show violation of scaling both in the central and fragmentation region. Furthermore, as pointed out by Shabelskii [31], this violation gets stronger in the case of hadron-nucleus collisions. Here, it may be pointed out that even though the data obtained by the investigators of UA5 collaboration experiment [42] at CERN SPS $p\bar{p}$ collider and CDF collaboration experiment [43] at FNAL Tevatron have shown firm indications of scaling violation in the central region but the observations in the fragmentation region was not clear in these experiments as it was restricted by the conditions of the experiment itself. However, the investigators of UA7 collaboration experiment [44], measuring the inclusive differential cross-section of photons in the fragmentation region at $\sqrt{s}$ =630 GeV (rapidity region studied being $5 < y < 7$), have reported that scaling holds in this region at $\langle p_t \rangle$ = 150 MeV/c. They have pointed out that in comparison with the data from SPS and ISR experiments at, respectively, $\sqrt{s}$= 6.85 and 52.7 GeV, the production cross section at the fragmentation region does not change with incident energy. And, by studying the rapidity density distribution of π^0, they have further [45] substantiated their conclusion. Similarly, Haguenauer et al. [46], examining the data obtained in UA7 & UA5 experiments by performing Monte Carlo simulation have observed that data from these two experiments indicate the validity of scaling in the fragmentation region at least up to energies of several hundred TeV in laboratory system. On the other hand, the earlier observations indicating the violation of scaling in the fragmentation region reported by the investigators of Brasil-Japan Emulsion Chamber Collaboration experiment at Mt. Chacaltaya [47] studying energy distribution of γ-rays in c-jets have further been supported by few other authors too, who have reported similar observations. Slavatinsky [48], analysing the experimental data of Pamir experiment on γ-quanta and hadrons obtained by means of X-ray emulsion chamber (XEC), have pointed out that inclusive spectrum of π^0, at x = 0.3 and primary energy $E_0 = 10^{14}$eV (x defined as E / E_0), turns out to be lower by 3-5 times when compared with the estimations of scaling model. Similarly, the authors in [49] and [50], from their investigation of hadrons with different energies have shown significant deviations of their

experimental observations from the calculations of scaling model. Furthermore, calculating the x-distribution [$d\sigma/(\sigma_{inel}\ dx)$] from the data of c-jets obtained in Chacaltaya emulsion chamber experiment and those from UA7 experiment, Belandi et al. [51] have pointed out that these two sets of data agree well with each other if p_t for gamma-rays is assumed to have same dependence on rapidity as p_t for pions and indicate breaking down of scaling considerably at $\sqrt{s}$= 500 GeV in the fragmentation region. Ohsawa [52] has reported similar observations about the consistency of the three different sets of data obtained in UA5, UA7 and Chacaltaya experiments and their indications of violation of scaling in both the central and fragmentation regions at energies 10^{14}-10^{15} eV.

The other important characteristic feature of QGS model has been its prediction of increase of inelasticity coefficient K with energy. In the calculations of QGS model, as pointed out by Vaskevich et al. [27], the inelasticity K not taken as a primary parameter of the model but calculated from the distribution of the secondaries, is observed to increase from 0.6 at 100 GeV to 0.75 at 10^5 GeV. But, some other authors like Wilk & Wlodarczyk [53 & 54] have argued that if direct contribution of gluon interactions are considered then the inelasticity should decrease as a consequence of gluon-gluon collisions. Moreover, Gershtein & Logunov [55] have pointed out that the cross-section of gluon interaction and hadron production via gluons increases with energy. And, Wlodarczyk [54] have shown that, if the hadron-nucleon interaction cross-section $\sigma^h(s)$ if represented by the sum of the constant Regge fraction σ_0^R and gluon fraction $\sigma_0^G(s)$ increasing with energy as suggested by Prokoshkin [56], then the inelasticity coefficients of leading hadrons interacting with air nuclei appear to decrease when energy increases, becoming K= 0.4 at energies 10^{17}- 10^{18} eV. And, Kalmykov et al. [38] have observed that calculations of model allowing for gluon interactions describes various EAS characteristics quite well and represent the experimental data at high energies even better than by that calculated with traditional QGS model where the contributions of gluon interactions are ignored. However, they have further pointed out that the same results can be obtained with QGS model by reducing the increase of hadron interaction cross-section with energy by keeping the value of model parameter Δ within 0.07 to 0.09.

Furthermore, it may be added here that several authors [48, 57, 58], reporting

the results of their analysis of Pamir and Tian-Shan experiments on gamma-hadron family have pointed out that the calculated predictions of the models showing increase of inelasticity K fit the experimental data well. Capdevielle et al. [58], by their comparative analysis of the data from Pamir and Tien-Shan experiments with the simulated results of three different Monte Carlo generators based on different models of hadron interactions, have shown that the predictions of the generator MQ based on QGS model with increasing K (0.68 at 100 GeV and 0.86 at 10^5 TeV) represent the experimental measurements of the gamma-hadron families better than the predictions of the other two, MCP and MSF generators based on, respectively, semi-empirical model proposed by Capdevielle [59] showing decrease of K from 0.53 at 100 GeV to 0.43 at 10^4 TeV and the model proposed by Mukhamedshin [60] in which K remains constant about 0.56.

Finally, the main results of the present experiment investigating the electron and muon components of the EAS of size 2.10^4 to 10^6 particles can be summarized as below:

1. The average values of age parameter of air showers are seen to decrease with their size when showers are grouped according to their sizes.

2. The lateral distribution of electrons up to the distances of (20-25)m in air showers of different sizes are seen to be well represented by the distribution function proposed by Hillas & Lapikens[1].

3. The shape of the lateral distribution and integral energy spectra of muons are seen to change very slowly with the size of air showers. However, the lateral distribuitons of muons are observed to have stronger dependence on the muon energy thresholds becoming steeper at higher energies.

4. The variation of muon densities with shower size for different muon energy thresholds is seen to depend on the radial distance from the shower core. If this variaion is represened by a functional form written as $\rho_\mu \sim Ne^\alpha$ then the value of exponent α is seen to decrease with the radial distance from the shower core.

5. The total number of muons (N_μ) for different muon energy thresholds ($\geq E_\mu$) is seen to increase smoothly with the size of the shower (Ne) and the value of exponent 'γ' in the relation $N_\mu \sim Ne^\gamma$, representing the variation is seen to remain

almost independent of the energy thresholds in the investigated shower size range.

6. The integral energy spectrum of the muons showing variation of total number of muons N_μ with the threshold energy E_μ in an EAS of fixed size is seen to be not representable by a function of power form for the whole range of muon threshold energies investigated (2.5 to 100 GeV). However, in the limited range of (10 to 100 GeV) it can be represented by such function writtten as $N_\mu \sim E_\mu^{-\delta}$ and the value of 'δ' is seen to be almost constant in the shower size range of 2.10^4 to 10^6 particles.

7. The measurements of the present experiment representing various features of the distribution of muons ($E_\mu \geq 10$ to 100GeV) in EAS of different sizes (5.10^4 to 10^6) such as lateral distribution, integral energy spectra and variation of N_μ with Ne, are seen to be fairly well represented by the theoretical results calculated with the QGS model of high energy particle interaction assuming normal mixed composition of primary cosmic ray.

REFERENCES

1. A. M. Hillas and J. Lapikens, *15th ICRC* (Plovdiv 1977), **8**, 466.
2. K. Asakimori, T. Hara, T. Maeda, K. Nishijima, Y. Toyoda, K. Kamamoto, M. Yoshida, T. Kameda and K. Mizushima, *17th ICRC* (Paris 1981) **11**, 301.
   K. Asakimori, T. Maeda, T. Kameda, K. Mizushima and Y. Misaki, *19th ICRC* (La Jolla 1985), **7**, 107.
3. K. Greisen, *Annu. Rev. Nucl.Sci.*, **10** (1960), 63.
4. B. A. Khrenov and J. Linsley, *17th ICRC* (Paris 1981), **10**, 354.
5. J. C. Earnshaw, K. K. Oxford, G. D. Rochester, K. E. Turver and A. B. Walton, *17th ICRC* (Paris 1981), **10**, 354.
6. J. Burger, E. Bohm and M. Suling, *14th ICRC* (Munich 1975), **8**, 2788.
7. W. S. Rada, A. C. Smith, T. R. Stewart, M. G. Thompson and M. W. Treasure, *IL Nuovo Cimento* **54A** (1979), 208
8. B. S. Acharya, M. V. S. Rao, K. Sivaprasad and B. V. Sreekantan, *18th ICRC* (Bangalore 1983), **9**, 191
9. G. B. Khristiansen, G. V. Kilikov, A. P. Lebedev, A. A., Silaev, V. I. Salovjeva, N. Sarodzev and S. M. Mukhmulov, *15th ICRC* (Plovdiv 1977), **8**, 148
10. N. V. Grishina, Yu. A. Fomin, A. P. Lebedev, N. N. Kalmykov, B. A. Khrenov, G. B. Khristiansen, G. V. Kilikov, S. M. Rozhdestvensky, A. A. Silaev, V. I. Salovjeva, A. P. Sulakov and Z. V. Varochkina, *17th ICRC* (Paris 1981), **6**, 3
11. V. B. Atrashkevich, G. G. Ermakov, Yu. A. Fomin, G. G. Garipov, N. P. Iljina N. N. Kalmykov, B.A.Khrenov, G.B.Khristiansen, G.V.Kilikov, A.P.Levedev, S.I.Matsenov, V. I. Nazarov, S. M. Rozdestvensky, V. P. Rukavichkin, A. V. Shkurenkov, V. S. Isaev, A. A. Sylaev, V. I. Solovjieva, V. P. Sulakov, V. V. Vashkevich, O. V. Vedeneev and Z. V. Yarochkina, *18th ICRC* (Bangalore 1983), **11**, 229
12. Y. N. Bazhutov, G. G. Ermakov, Yu. A. Fomin, V. S. Isaev, Z. V. Jarochkina, N. N. Kalmykov, B. A. Khrenov, G. B. Khristiansen, G. V. Kilikov, M. V. Motova, I. P. Proshkina, V. P. Rukavichkin, V. I. Solovjieva, V. P. Sulakov, V. Shkurenkova, A. V. Trubitsyn and V. V. Vashkevich, *19th ICRC* (La Jolla 1985), **7**, 151
13. V. V. Vaskevich, G. G. Ermakov, P. F. Ermolov, G. V. Kilikov, V. P. Rukavichkin, V. I. Solovjieva, V. P. Sulakov, Yu. A. Fomin, B. A. Khrenov, G. B. Khristiansen, A. V. Shkurenkov and Z. V. Yarochkina, *Sov. J. Nucl. Phys.*, **47** (1988), 672.
14. R. P. Feynman, *Phys. Rev. Lett.*, **23** (1969) 1415
15. T. K. Gaisser, R. J. Protheroe, K. E. Turver and T. J. L. McComb, *Rev. Mod. Phys.*, **50** (1978), 859.

16. S. Mikocki, A. Trzupek, J. Gress, J. Kochocki and J. Poirier, *Astrophysics* (1990), Physics Department, University of Notre Dame.
17. T. Cheung and P. K. MacKeown, *J. Phys. G: Nucl. Phys.*, **13** (1987), 687
18. J. Wdowczyk and A. W. Wolfendale, *J. Phys. G : Nucl. Phys.*, **10** (1984), 257
19. N. N. Kalmykov, G. B. Khristiansen and M. V. Motova, *19th ICRC* (La Jolla 1985), **7**, 44
20. N. N. Kalmykov, G. B. Khristiansen M. V. Motova and S. S. Ostapchenko, *22nd ICRC* (Dublin 1991), **4**, 217
21. J. N. Capdevielle, *J. Phys. G : Nucl. Part. Phys.*, **16** (1995), 1539.
22. J. Wdowczyk and A. W. Wolfendale, *IL Nuovo Cimento,* **54A**(1979), 433.
23. J. Wdowczyk and A. W. Wolfendale, *Nature* **306** (1983), 347
24. J. Wdowczyk and A. W. Wolfendale, *J. Phys. G : Nucl. Phys.*, **13** (1987), 411.
25. N. N. Kalmykov and G. B. Khristiansen, *JETP Lett.* **37** (1983), 294
26. N. N. Kalmykov, Yu. A. Fomin and G. B. Khristiansen, *Sov. J. Nucl. Phys.* **41** (1985), 608.
27. V. V. Vashkevich, P. F. Ermolov, N. N. Kalmykov, M. V. Motova, S. S. Ostapchenko, B. A. Khrenov and G. B. Khristiansen, *Sov. J. Nucl Phys.*, **48** (1988), 859
28. V. R. Sleptsova, N. N. Efimov, T. A. Egorov, M. I. Pravdin and N. N. Kalmykov, *22nd ICRC* (Dublin 1991), **4**, 343
29. V. B. Atrashkevich, Yu. A. Fomin, N. N. Kalmykov, G. B. Khristiansen, G. V. Kulikov, S. S. Ostapchenko, A. A. Silaev, V. I. Solovyeva, V. P. Solakov, A. V. Truvitsyn and O. V. Vedeneev, *23rd ICRC* (Calgary 1993), **2**, 116
30. A. B. Kaidalov, K. A. Ter-Martirosyan and Yu. M. Shabelskii, *Sov. J. Nucl Phys.*, **43** (1986), 822
31. Yu. M. Shabelskii, *Sov. J. Nucl Phys.*, **45** (1987), 143.
32. S. I. Syrovatskii, Yu. A. Fomin and G. B. Khristiansen, *Sov. J. Nucl Phys.*, **18** (1964), 1098
33. T. Hara, Y. Hatano, N. Hayashida, N. Jogo, K. Kamata, T. Kifune, Y. Mizumoto, M. Nagno, G. Tanahashi, Y. H. Tan, S. Kawaguchi, M. Diago and N. Hasebe, *17th ICRC* (Paris 1981), **11**, 52
34. B. S. Acharya, *Ph.D. Thesis* (1983), University of Bombay, India.
35. E. J. Fenyves, *Techniques in UHE γ-Ray Astronomy* (Edited by- R. J. Protheroe and S. A. Stephens), University of Adelaide (1985), 124.
36. Yu. A. Fomin, N. N. Kalmykov, G. B. Krhistiansen, M. V. Motova, S. S. Ostapchenko and O. V. Postylyakov, *20th ICRC*(Moscow 1987), **6**, 151
37. J. N. Capdevielle, P. Gabinski, J. Gawin and A. Kouider-Akil, *J. Phys. G: Nucl Phys* , **14** (1988), 1537

38. N. N. Kalmykov, G. B. Khristiansen, M. V. Motova and S. S. Ostapchenko, *21st ICRC* (Adelaide 1990), **9**, 240
39. N. N. Kalmykov, G. B. Khristiansen, M. V. Motova, S. S. Ostapchenko and V. V. Prosin, *23rd ICRC* (Calgary 1993), **4**, 239
40. N. N. Kalmykov, G. B. Khristiansen, S. S. Ostapchenko and A. I. Pavlov, *24th ICRC* (Rome 1995), **1**, 123
41. X. Campi et al, *Nucl. Phys.*, **A428** (1984), 327
42. UA5 Collaboration
    Phys. Lett., **107B** (1981), 315
    Z. Phys. C, **33** (1986), 1
    Nucl. Phys., **B291** (1987), 445
    Phys. Rep., No. **5** & **6** (1987), 247
43. CDF Collaboration
    Phys. Rev Lett., **61** (1988), 1819
    Phys. Rev. D, **41** (1990), 2330
44. M. Haguenauer et al. (UA7 Collaboration)
    21st ICRC (Adelaide 1990), **8**, 29
    20th ICRC (Moscow 1987), **5**, 23
45. E. Pare et al. (UA7 Collaboration)
    CERN-EP/89-181(1990)
    Phys. Lett., **B242** (1990), 531
46. M. Haguenauer, K. Kashara, Y. Nuraki, E. Pare and T. Yuda, *22nd ICRC* (Dublin 1991), **4**, 173
47. N. Arata, *Nucl. Phys.*, **B211** (1983), 189
    T. Tabuki, *Prog. Theo. Phys.*, Suppl. No.**76** (1983), 40
    J. A. Chinellato et al. (Chacaltaya Emulsion Chamber Collaboration), *Prog. Theo. Phys.*, Suppl. No.**76** (1983), 1
48. S. A. Slavatinsky, *22nd ICRC* (Dublin 1991), **4**, 121
49. S. K. Machavariani, S. I. Nikolsky and A. P. Chubenko, *19th ICRC* (La Jolla 1985), **6**, 232
50. Pamir Collaboration 4, *19th ICRC* (La Jolla 1985), **6**, 232
51. J. Belandi F. et al. (CEC Collaboration), *22nd ICRC* (Dublin 1991), **4**, 185
52. A. Ohsawa
    23rd ICRC (Calgary 1983), **4**, 25
    24th ICRC (Rome 1985), **1**, 127
53. G. Wilk and Z. Wlodarczyk, *22nd ICRC* (Dublin 1991), **4**, 165

54. Z. Wlodarczyk
20th ICRC (Moscow 1987) **5** 417
5th ISVHECRI, LODZ (1985), 16
55. S. S. Gershtein and A. A. Logunov, *Yad. Fiz.* **39** (1984), 1514
56. Yu. D. Prokoshkin, *Sov. Journal of Nucl. Phys.*, **40** (1984), 1579
57. A. S. Borisov et al. (Pamir Collaboration), *22nd ICRC* (Dublin 1991) **4** 129
58. J. N. Capdevielle, A. M. Dunaevsky, S. S. Karporova, N .P. Krutikova and S. A. Slavatinsky, *23rd ICRC* (Calgary 1993), **4** 68
59. J. N. Capdevielle, *J.Phys. G: Nucl. Phys.*, **15** (1989), 909
60. R. A. Mukhamedshin, *17th ICRC* (Munich 1975), **5** 343